Doctoral theses at NTNU, 2019:29

Nicholas Smith

Methods of Oxidation Inhibition for Al-Mg Alloys

ISBN 978-82-326-3664-8 (printed ver.)
ISBN 978-82-326-3665-5 (electronic ver.)
ISSN 1503-8181

NTNU
Norwegian University of
Science and Technology

NTNU
Norwegian University of Science and Technology
Thesis for the Degree of
Philosophiae Doctor
Faculty of Natural Sciences
Department of Materials Science and
Engineering

Doctoral theses at NTNU, 2019:29

NTNU
Norwegian University of
Science and Technology

Nicholas Smith

Methods of Oxidation Inhibition for Al-Mg Alloys

Thesis for the Degree of Philosophiae Doctor

Trondheim, January 2019

Norwegian University of Science and Technology
Faculty of Natural Sciences
Department of Materials Science and Engineering

NTNU
Norwegian University of
Science and Technology

NTNU
Norwegian University of Science and Technology

Thesis for the Degree of Philosophiae Doctor

Faculty of Natural Sciences
Department of Materials Science and Engineering

ISBN 978-82-326-3664-8 (printed ver.)
ISBN 978-82-326-3665-5 (electronic ver.)
ISSN 1503-8181

Doctoral theses at NTNU, 2019:29

Printed by NTNU Grafisk senter

Preface

This thesis is submitted to the Norwegian University of Science and Technology as partial fulfillment of the requirements for the degree of Doctor philosophiae. The work in this thesis was carried out at the Norwegian University of Science and Technology at the Department of Material Science and Engineering. This work was done as a part of the SFI Metal Production Center (Centre for Research-based Innovation, 237738). With financial support from the Research Council of Norway and the partners of the SFI Metal Production. A portion of the experimental work was carried out at the University of Pittsburgh in Pittsburgh, Pennsylvania USA.

The author has carried out all the experimental work described in this thesis. The XPS analysis was conducted with the help of Ingeborg-Helene Svenum (SINTEF) and Martin Sunding (SINTEF) and the TEM work was done with the help of Per Erik Vullum (SINTEF).

Acknowledgements

There are a number of people who I would like to thank for their help and guidance throughout this PhD. First and foremost, I would like to thank my supervisors Gabriella Tranell and Anne Kvithyld. You have both been of great help throughout this entire process, providing constant feedback and ideas. You both have taught me a lot about our field of study and scientific work in general. Your help in making sure I had all the resources required to complete my research cannot be overstated.

I would also like to thank the engineers in Bergbygget: Jonas Einan Gjøvik, Dmitry Slizovskiy, Ivar Andre Ødegård and Trygve Schanche for their assistance with the experimental work and making the labs enjoyable and efficient to work in. Also the staff of SINTEF: Per Erik Vullum for the training on the FIB, and help with the TEM analysis, Ingeborg-Helene Svenum and Martin Sunding for running the XPS analysis and helping to interpret the data.

I am thankful to Dr. Gleeson and his students at the University of Pittsburgh for welcoming me to his lab and helping with the initial set of oxidation experiments. What I learned there was of immense help throughout my entire PhD. Additionally, Dr. Gleeson's thoughts and feedback over these past years has improved the quality of the results and my understanding of them. Additionally, thank you to Dr. Saidi of the University of Pittsburgh for your DFT calculations and viewpoint on the effects of CO_2.

I am grateful to everyone in the SFI Metal Production Center for providing the support and resources to complete this work. As well as the industrial partners of Alcoa and Hydro for providing an industrial perspective and feedback.

Next, I would like to thank all the current and past members of the SiManTi group. The research environment that you all helped create was of great benefit. The meetings and discussions that were had provided a wonderful break from the daily work and helped to improve the quality of my work.

For providing thoughtful feedback and ideas I would like to thank Martin Syvertsen, Thorvald Engh and Christian Simensen especially for their valuable guidance during the first year of my PhD getting me on the right track.

I would like to thank my parents Randi and David for their constant support throughout my entire education. Finally, I have never made it through this PhD without the constant support of Veronika your positive support has made these three years possible.

Abstract

The oxidation of aluminum alloys plays a significant role in the aluminum casthouse. The oxidation of a liquid alloy during handling and processing is next to impossible to stop and in general, an oxide layer is desirable as it serves as protection against further oxidation of the melt. The oxidation can, however, become problematic if the generated oxide layer does not provide adequate protection for the melt. This is often the case for Al-Mg alloys where the magnesium will oxidize preferentially to the aluminum and form an MgO oxide layer on the alloy, and will result in a large increase in rate and extent of oxidation. This excessive oxidation can result in several problems for the aluminum industry. First, as the magnesium oxidizes preferentially the oxidation will result in a loss of magnesium from the melt and will impact the final alloy composition and metal yield. Second, and most important, an increase in oxidation results in an increase in the likelihood that oxide inclusions can become trapped in the melt. These inclusions can result in cracks in the final ingot and are detrimental to the final mechanical properties.

Several methods exist to aid in controlling the oxidation of Al-Mg alloys, the two methods discussed in detail in this thesis are beryllium additions and CO_2 cover gas. Both of these methods result in a notable inhibition of the oxidation. However, to date an understanding of the fundamental mechanisms behind how these inhibitors act, is lacking. The goal of this work is to examine and provide a greater understanding of these mechanisms. In the case of beryllium additions, the aluminum industry desires an alternative alloying element, due to the negative health consequences that are associated with its use which may be facilitated by an increased understanding of its interaction with Al-Mg alloys. To accomplish this, oxidation experiments were carried out in a horizontal tube furnace and TGA, followed by detailed characterization of the formed oxide layer in the FIB, SEM, XPS and TEM.

The studies on beryllium showed that on an Al-Mg alloy that was free of beryllium, the oxide layer consisted of two parts, a dense oxide layer adjacent to the metal and a granular oxide layer on the surface of the dense layer. This granular layer is believed to account for the majority of the oxidation in the liquid state. With the addition of beryllium it was found that the granular layer no longer formed on the dense oxide surface, and that a layer containing BeO forms at the metal-oxide interface. This BeO layer acts as a barrier to the oxidation by preventing the diffusion of

magnesium across the oxide-metal interface. This layer also separates the MgO oxide layer from the aluminum melt, forming a diffusion barrier to the formation of the $MgAl_2O_4$ spinel.

It was found that additions of 5-50 % CO_2 to air showed a similar effectiveness to beryllium additions, as it delayed the onset of breakaway oxidation of Al-5% Mg alloys compared to oxidation in pure air. Further, the effects of CO_2 were found to linger even after the CO_2 had been removed from the atmosphere. If the CO_2 was added to the atmosphere, after an initial period of oxidation in pure air, the CO_2 would rapidly act to inhibit the oxidation. The structure of the oxide layer after oxidation under a CO_2 containing atmosphere was similar to the samples that contained beryllium in that the formation of the granular layer had been reduced. From the XPS analysis across the oxide layer, it was concluded that the CO_2 had adsorbed onto the surface of the initial, dense MgO layer, and served to act as a "cap" that prevents the diffusion of magnesium vapor out through the oxide layer. The oxygen to carbon ratio decreased from the atmosphere-oxide interface towards the oxide-metal interface, indicating inward CO_2 diffusion and subsequent reduction by ascending magnesium vapor.

Based on the results discussed above, it was proposed that yttrium, erbium or strontium could serve as potential alternatives to beryllium. Unfortunately, tests of Al-Mg alloys containing 100 ppm of either of these elements did not show an increased oxidation resistance compared to an addition-free Al-Mg alloy. Erbium and strontium in fact decreased the overall oxidation resistance. It was proposed that an alternative alloying element must be able to: segregate to the oxide-metal interface, be stable in the melt (low vapor pressure) and form a solid layer at the oxide-metal interface.

List of Papers

Paper 1
Smith N, Gleeson B, Kvithyld A, Tranell G. *Effects of 2ppm Beryllium on the Oxidation of a 5XXX Aluminum Alloy at Temperatures between 500 and 750 °C.* Light Metals 2017 (pp 1465-1474) TMS annual meeting and exhibition 2017 DOI: 10.1007/978-3-319-51541-0_175

Statement of Contribution
Smith: Experimental work and oxide characterization, discussion of results, writing paper
Gleeson: Discussion of results, writing the paper
Kvithyld: Discussion of results, writing the paper
Tranell: Discussion of results, writing the paper

Paper 2
Smith N, Kvithyld A, Tranell G. *XPS Examination of the Oxide-Metal Interface of an Aluminum–Magnesium Alloy Containing Beryllium.* Light Metals 2018 (pp 913-919) TMS annual meeting and exhibition 2018 DOI: 10.1007/978-3-319-72284-9_119

Statement of Contribution
Smith: Experimental work and oxide characterization, discussion of results, writing paper
Kvithyld: Discussion of results, writing the paper
Tranell: Discussion of results, writing the paper

Paper 3
Smith N, Kvithyld A, Tranell G. *The Mechanism behind the Oxidation Protection of High Mg Al Alloys with Beryllium*. Metallurgical Transactions B (pp 913-919) 2018 DOI: 10.1007/s11663-018-1340-6

Statement of Contribution
Smith: Experimental work and oxide characterization, discussion of results, writing paper
Kvithyld: Discussion of results, writing the paper
Tranell: Discussion of results, writing the paper

Paper 4
Smith N, Gleeson B, Saidi W. Kvithyld A, Tranell G. *Mechanism behind the inhibiting effect of CO_2 on the oxidation of Al-Mg Alloys*, Submitted to Industrial and Engineering Chemistry September 2018

Statement of Contribution
Smith: Experimental work and oxide characterization, discussion of results, writing paper
Gleeson: Discussion of results, writing the paper

Saidi: DFT calculations, discussion of results, writing the paper
Kvithyld: Discussion of results, writing the paper
Tranell: Discussion of results, writing the paper

Paper 5
Smith N, Gleeson B, Saidi W. Kvithyld A, Tranell G. *Effects of CO_2 cover gas and yttrium additions on the oxidation of Al-Mg alloys*, Submitted Light Metals 2019, TMS annual meeting and exhibition 2019

Statement of Contribution
Smith: Experimental work and oxide characterization, discussion of results, writing paper
Gleeson: Discussion of results
Saidi: Discussion of results
Kvithyld: Discussion of results, writing the paper
Tranell: Discussion of results, writing the paper

Contents

List of Figures

List of Tables

List of Abbreviations and Symbols

Abbreviations

At %	atomic Percent
EDS	energy dispersive X-ray spectroscopy
EELS	electron energy loss spectroscopy
EPMA	electron probe microanalysis
FIB	focused ion beam
HSE	Health, Safety and Environment
ICP-MS	inductively coupled plasma mass spectroscopy
Lpm	liter per minute
PBR	Pilling Bedworth ratio
Ppm	parts per million
SEM	scanning electron microscope
SiC	silicon carbide
TEM	transmission electron microscope
TGA	thermogravimetric analysis
XRD	X-ray diffraction

Latin letters

K’	equilibrium constant
M	molar mass
V	volume
α	activity
γ	activity coefficient
ρ	density of metal or oxide
n	number of metal ions per oxide molecule
p	vapor partial pressure of an element over an alloy
p°	vapor partial pressure of a pure element
x	mole fraction

1. Introduction

The oxidation of aluminum alloys is a broad subject of study where the focus can range from the oxidation in aqueous environments at room temperature ("corrosion") to the oxidation of liquid aluminum in various atmospheres at temperatures well above the melting point. In this work the focus has been on the oxidation above the melting point with a focus on having similar oxidation conditions (time and temperature) to those that are experienced in the casthouse for industrial aluminum production. The oxidation of aluminum is typically not seen as problematic as the formed aluminum oxide is considered protective and the metal will quickly reach a limiting oxide thickness, however, for certain alloys, such as aluminum-magnesium (Al-Mg), and under certain processing conditions, this oxidation can become problematic.

In the casthouse the aluminum will oxidize to dross, which is a mixture of both oxide and metal, with a metal content of approximately 70 % (1). It is estimated that the formation of dross equates to approximately 2 % of the yearly ingot production in a casthouse (2). It has been estimated that a 0.1 % reduction in dross could result in a savings of 100,000 USD/year or more, for a hypothetical 250 ktpa aluminum smelter (3). For this reason the oxidation of aluminum alloys is of particular interest to the aluminum producing industry.

The oxidation of Al-Mg alloys typically occurs in three steps. The first stage, is known as the incubation stage and is characterized by a low oxidation rate. The second stage, is referred to as breakaway oxidation is characterized by a large increase in the oxidation rate due to a change in the structure of the oxide layer, caused by the formation of the $MgAl_2O_4$. The final stage occurs, once all the magnesium has been oxidized to the spinel phase, and the oxidation rate will be reduced to near zero resulting in a passivation of the oxide surface. The duration and chemical reactions that occur during each stage depend on a number of parameters including, but not limited to: alloy composition, atmosphere, and temperature. For casthouse operations, it is desired to remain in the incubation stage as breakaway oxidation results in an unacceptably large loss of metal to oxidation.

Al-Mg melts are subject to oxidation in the lauders, filter box and casting molds especially during operations that involve pouring of liquid aluminum, as the generated turbulence results in

increased oxidation compared to a static surface. The total amount of oxidation at these points is less than that occurring in the furnace, none the less the oxidation can still be problematic, especially if it occurs after the filter box. The rapid oxidation of alloys with a higher magnesium content can result in an increase oxide inclusions. If these inclusions become trapped in the melt they can result in defects and cracks in the final ingot. Beryllium additions have, historically, been the most effective way to control formation of these oxide inclusions. The use of beryllium is problematic due to the negative respiratory health effects associated with its use. CO_2 additions to the gas atmosphere have also been shown, primarily in academic publications, to limit the oxidation of Al-Mg alloys (4) (5).

The first goals of this work were to study and better understand the fundamentals of how beryllium additions and CO_2 cover gas inhibit the oxidation of Al-Mg melts. Beryllium additions have been known, since at least the 1930's, to reduce the oxidation rate of Al-Mg alloys (6). Owing to the small quantities used (< 10 ppm) and the difficulty of many spectroscopy methods to detect light elements, like beryllium, a lack of understanding exits for how beryllium actually inhibits the oxidation (4) (5). CO_2 cover gas was studied in the 1970's and it was found to be effective in inhibiting the oxidation. However, to the authors knowledge, its use was never widespread and the effectiveness is not well known among the aluminum industry. As with beryllium a fundamental understanding of how CO_2 inhibits the oxidation is lacking. As the aluminum industry desires new and alternative ways of oxidation control, the logical place to start was a fundamental investigation into the two known oxidation inhibiting mechanisms. The results of the studies on beryllium and CO_2 are presented in this thesis. Based on the results of the fundamental studies three alternative alloying elements of yttrium, erbium and strontium were proposed and tested to see if they may provide a similar protective effect to beryllium.

The experiments in this work consisted of two parts: thermal oxidation and oxide layer characterization. A thermogravimetric analysis balance (TGA) and horizontal tube furnace were used to conduct the oxidation tests. The mass change during oxidation was used to quantify the effects of selected variables on the oxidation rate. Oxide layer characterization was employed on the samples from the oxidation tests to determine the fundamental inhibiting mechanism. Multiple tools were used during characterization including Scanning Electron Microscope (SEM), Focused Ion Beam miller (FIB), Energy Dispersive X-ray Spectroscopy (EDS) and X-ray Photoelectron

Spectroscopy (XPS). Combined, these tools allowed both morphological and chemical characterizations to be carried out, yielding a better understanding of the oxidation inhibiting mechanisms.

This work has resulted in 5 papers which cover the body of work in this thesis. Chapter 2. covers the theoretical background and literature state of the art required to support the findings and conclusions of this work. Chapter 3. gives a detailed description of the experimental methods used. An overview of the results and relevant discussion are given in chapter 4. The conclusions and future work are given in chapter 5. Finally, copies of the 5 papers are provided as appendices to the thesis.

2. Theory

2.1 Introduction

The oxidation of aluminum and aluminum alloys has been extensively studied with published works tracing back over the past 100 years (7). The general principles behind aluminum oxidation are well described. However, aluminum oxidation is sensitive to many process parameters of which not all are well understood. Casthouse and furnace operations such as pouring, stirring and dross skimming will have a large effect on industrial oxidation losses, but will not be considered in detail here as they are difficult to quantify and test in a laboratory setting (8). The parameters that are generally assumed to play the largest roll in oxidation are:

- Alloy composition (5) (9) (10) (11)
- Temperature (12)
- Time (5) (13)
- Atmosphere (5) (14)
- Surfaces properties (15) (16) (17)

The effect of these parameters on the rate, extent and product of oxidation, is critically summarized in the following sections. Additionally, the published literature of the effects on oxidation of the specific alloying elements studied in this thesis (Be, Y, Er, and Sr) and CO_2 cover gas will be summarized.

2.2 General oxidation principles

2.2.1 Thermodynamics of oxidation

At temperatures above the melting point of aluminum, most metals will react exothermically with oxygen to form an oxide per Eq 2.1 where M is an arbitary metal. Oxygen will react preferentially with the metal that has the lowest Gibbs energy of oxide formation. The Ellingham diagram (18) shown in Figure 2-1clearly illustrates the relative stability of metal oxides by plotting the Gibbs energy of formation for a given metal oxide, per mole of oxygen reacted, as a function of

temperature. From this diagram it is clear that both aluminum and magnesium form very stable oxides with only a few elements oxidizing preferentially.

$$mM + \frac{n}{2}O_2 = M_mO_n \tag{2.1}$$

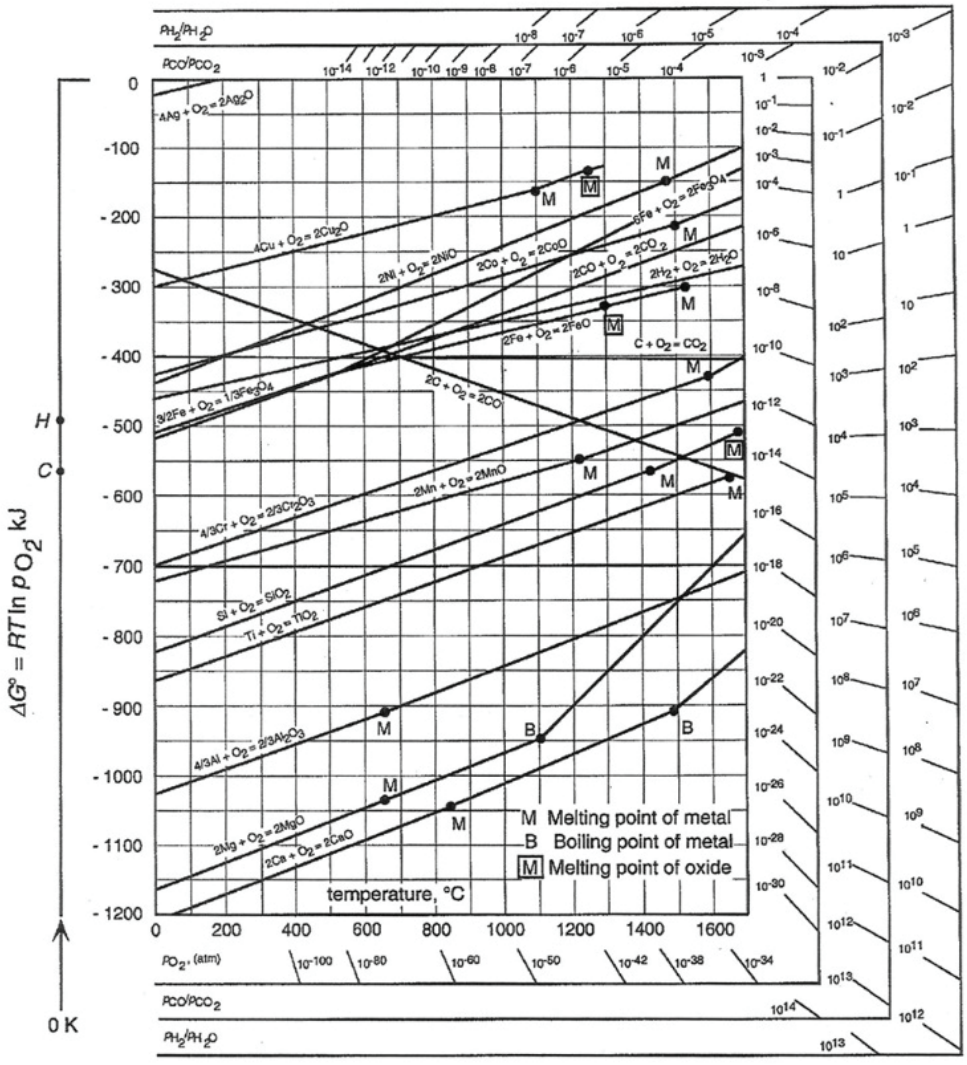

Figure 2-1 Ellingham diagram (18).

The standard Ellingham diagram shows only the simple binary oxide phases, whereas for alloy systems, more complex oxides can form. For example, with Al-Mg alloys the spinel phase ($MgAl_2O_4$) is often found after long oxidation times or low magnesium concentrations. If the activity of magnesium in the melt drops below 0.023 at 700 °C, the spinel phase will form. For activities above this level, the stable oxide phase will be MgO as will be discussed in detail later in section 2.5.1 (19).

2.2.2 Oxidation kinetics

From a kinetic viewpoint, there are two general oxidation modes: linear and parabolic. A linear oxidation rate is characterized by a constant oxidation rate with respect to time, whereas, a parabolic oxidation rate is characterized by an initially high oxidation rate which slows to near zero with time.

A linear oxidation rate is observed when the oxidation is controlled by the chemical reaction or the transport of one of the reactants occurs at a constant rate. For example, when the oxidizing gas species exists in dilute quantities and the transport from the bulk gas to the reaction site occurs at a constant rate. Alternatively, if the formed oxide layer is extremely porous or cracked, the oxide layer will not provide any significant barrier to the oxidation in which case the oxidation will continue at a constant rate (20).

Parabolic kinetics are generally seen when the oxidation rate is diffusion controlled. A typical parabolic curve will show initially high oxidation rates which slow as the thickness of the oxide layer increases. An increased oxide layer thickness results in a longer time for the reactants to diffuse to the reaction site, thus resulting in a decreasing oxidation rate with respect to time (20).

In addition to linear and parabolic kinetics, other rate laws such as logarithmic, paralinear, pseudo-logarithmic and pseudo-parabolic exist and have been used to describe the oxidation of Al-Mg alloys. These rate laws are the result of more complex or mixed rate kinetics, possibly involving two or more competing processes (15) (17) (21).

For the oxidation of aluminum and aluminum-magnesium alloys, the oxidation generally does not follow one given mode, but rather displays more complicated oxidation kinetics that include a parabolic incubation period that gives way to a rapidly increasing linear region followed by passivation as shown in an idealized form in Figure 2-2. This will be discussed in more detail later in section 2.3 (12).

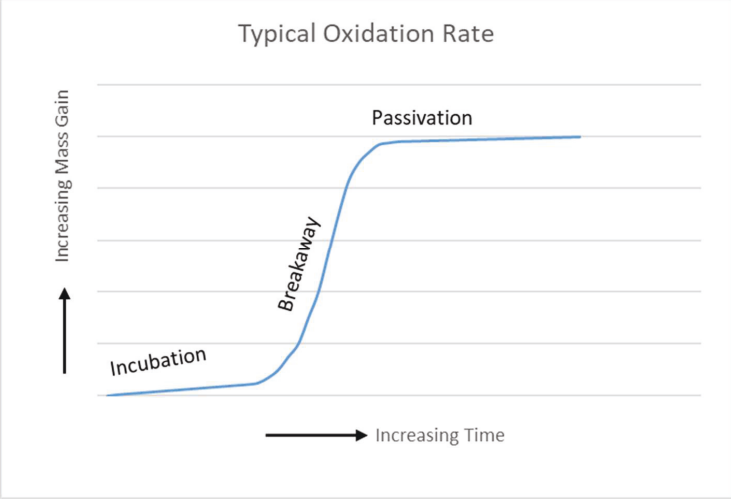

Figure 2-2 Idealized oxidation curve for aluminum and aluminum-magnesium alloys.

2.3 Factors that influence oxidation

To discuss the oxidation of Al-Mg alloys certain background information such as the effects of surface roughness, Pilling-Bedworth ratio (PBR) and oxide skin strength must be first defined.

2.3.1 Surface roughness

The surface of a sample has been found to have a significant effect on the oxidation of aluminum alloys with a higher surface roughness resulting in a larger amount of oxidation (15) (16) (17). The effect is attributed to an increased surface area on rougher samples giving a higher degree of oxidation. Cochran et al. tested various sample preparation techniques from chemically polishing to grinding and the difference between treatments resulted in up to an order of magnitude change in the mass gain due to oxidation as shown in Figure 2-3 (17).

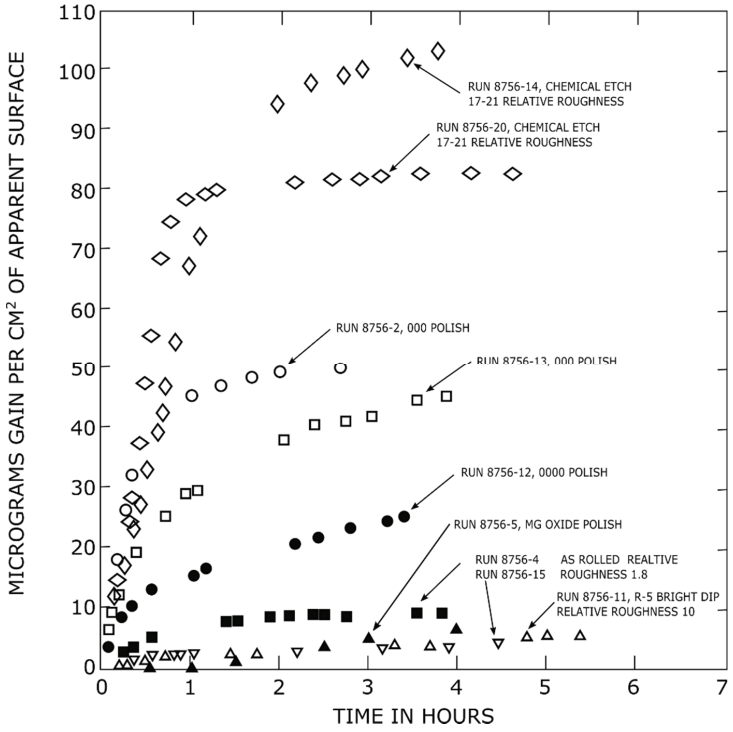

Figure 2-3 Effect of surface roughness on the oxidation of a pure aluminum sample at 525 °C, redrawn from Cochran et al. (17).

2.3.2 Pilling-Bedworth ratio

Once an oxide layer has formed the ability of said layer to inhibit further oxidation is of key importance. The Pilling-Bedworth ratio (PBR) is the most common measure used to quantify/characterize the protective effect of an oxide layer. PBR is defined in Eq 2.2.

$$PBR = \frac{V_{oxide}}{V_{metal}} = \frac{M_{oxide}\rho_{metal}}{nM_{metal}\rho_{oxide}} \tag{2.2}$$

Where V is the volume, M is the molar mass, ρ is the density and n is the number of metal atoms per oxide molecule. A PBR less than one means that the volume of the oxide is less than the metal resulting in a layer that is under tension and will crack or contain porosity. A PBR of one to two is generally desired as it indicates a continuous non-porous layer. If the PBR is over two the oxide

must expand significantly relative to the metal, which often causes poor adhesion and buckling of the oxide layer (7). The PBR for a number of common metals are given in Table 1.

Table 1 Pilling-Bedworth ratio of select metal oxide systems (22).

Metal	Oxide	PBR
Al	Gamma-Al_2O_3	1.31
Al	Alpha-Al_2O_3	1.28
Mg	MgO	0.80
Be	BeO	1.70
Y	Y_2O_3	1.13
Er	Er_2O_3	1.20
Sr	SrO	0.65
Fe	Fe_2O_3	2.15

While the PBR is commonly applied to the aluminum-magnesium system, caution should be taken with its use for two reasons. First, for alloys that contain magnesium, the formed oxide will be MgO or $MgAl_2O_4$. This means that there is not a constant metal volume that can be employed, as the volume of the metal is dependent on the diffusion of magnesium to the oxide-metal interface. Any magnesium that is lost to the oxide layer will be replaced by magnesium from the bulk. Secondly, when the oxidation occurs over a liquid alloy, the lack of atomic structure in the liquid alloy will prevent any variation in volume between the liquid and oxide from creating cracks or porosity in the oxide layer. However, cracks may still form due to flow in the melt, but these cracks are independent of the PBR.

2.3.3 Oxide skin strength

Kahl and Fromm found that a newly formed oxide skin accounts for 70 % of the overall strength of the oxide layer (23). This observation was confirmed by Syvertsen who showed that after the initial cracking of the oxide layer, it would break every 0.25 seconds with no significant drop in measured strength compared to an old oxide layer (24). Kahl and Fromm found that minor concentrations of elements such as beryllium, calcium and lithium had a larger impact on the

strength than the primary alloying elements. Figure 2-4 shows the effect of specific elements on the skin strength (23).

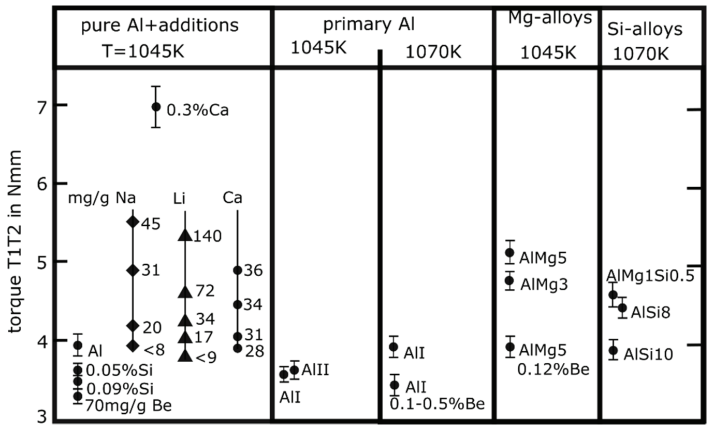

Figure 2-4 Effect of specific elements on the oxide skin strength. Note it is believe that figure contains an error in the units mg/g should be read as ppm redrawn from Kahl et al. (23).

Another observation from Kahl and Fromm's work was that some elements significantly decreased in concentration in the melt over the course of an experiment, whereas others remained constant. Figure 2-5 shows that the sodium, lithium and calcium content decreased with time, however, for beryllium, silicon and high calcium concentrations, the concentration in the melt remained nearly constant over the course of the experiment. In addition, a decrease in strontium content was seen in experiments with high silicon contents. The cause of the decrease was attributed to either evaporation or incorporation into the oxide skin, but the authors could not determine which as it will likely depend on the specific element. Either way, it is clear that minor elements are of key importance to the oxide strength (23). To date there has been no work to directly relate skin strength and oxidation rate, however, from Figure 2-4 it can be seen that sodium, lithium, calcium and magnesium which are all known to increase the oxidation rate, can be seen to increase the skin strength over pure aluminum, whereas beryllium additions cause a reduction in the skin strength. It is unclear from the previous work how skin strength is related to oxidation rate, or if any trends are purely coincidental. A stronger oxide layer will be less likely to crack, however, industrial practices such as stirring/mixing forces are likely to crack the oxide layer regardless of the strength.

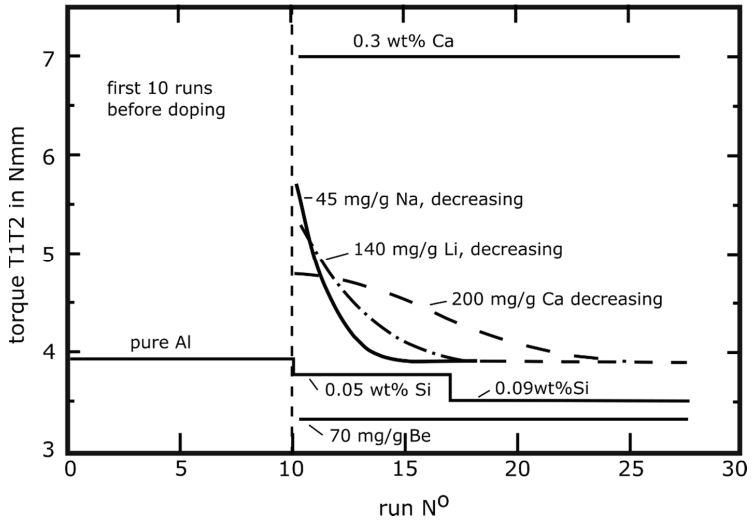

Figure 2-5 Oxide skin strength from redrawn from Kahl et al. (23).

2.4 Pure aluminum oxidation

The oxidation of solid and liquid aluminum has been the studied extensively since at least the 1920's and a significant amount of work was done in the 1950's and 1960's. The general principles are well agreed upon, however, many of the details are still open for debate. This includes the exact rate laws that govern the oxidation rate and the oxide phase transition temperatures as will be discussed below. In general, the oxidation mass gain versus time curve for aluminum and aluminum alloys shows a sigmodal shape that can be broken into three sections: incubation, breakaway and passivation with an idealized theoretical curve shown in Figure 2-2. The incubation stage of oxidation is characterized by a parabolic oxidation rate. The incubation stage often appears linear as the oxide will reach an initial limiting thickness rapidly (25). Breakaway oxidation is marked by a sudden and rapid increase in the oxidation rate and is triggered by a phase transformation of the oxide. Breakaway oxidation occurs after a time period ranging from a few minutes to hours depending on oxidation conditions such as temperature and composition. The final stage occurs once the phase transformation is complete, and is characterized by a reduction of the oxidation rate to near zero again (15).

As the formed alumina layer is considered protective, a limiting thickness for the oxide layer will be obtained. It has been shown that oxide thickness will not exceed 10-30 Å at room temperature, 200 Å at 300 °C and 2000 Å at 600 °C (26).

2.4.1 Forms of alumina

Alpha alumina is the only truly stable aluminum oxide phase that exists, however, six transition alumina polymorphs can form upon heating from room temperature, and these are: chi, kappa, gamma, theta, delta and eta, additionally an amorphous phase can exist at lower temperatures. The transformation from one transition alumina polymorph to another and the formation of alpha alumina is non-reversible; once alpha alumina has formed it cannot be transformed back into one of the transition polymorphs. For this reason, alpha alumina is considered to be the only truly stable alumina phase (27). However, for the purposes of this thesis, the transition aluminas will be treated as separate phases as gamma alumina exists and is stable over a large portion of the temperature range of interest in this work. With respect to the oxidation of aluminum at high temperatures both eta and gamma alumina have been reported in literature as the result of the recrystallization of amorphous alumina (15) (17) (26). The transitions forms of delta and theta have been shown to form as part of the transition from gamma to alpha alumina, however, these transition forms are often neglected in literature on the oxidation of aluminum (15) (17) (25). Chi and kappa are the result of the transformation of gibbsite to alpha alumina, and are not relevant to the transition from amorphous to alpha alumina that is typically seen with the oxidation of a pure aluminum sample (27).

2.4.2 Kinetics of solid state oxidation

Figure 2-6 shows the oxidation kinetics of pure aluminum from room temperature up to the melting point for aluminum. The oxide formed from room temperature up to 377-427 °C is amorphous. The growth of this amorphous oxide layer is stated to be controlled by the diffusion of aluminum ions out through the oxide which results in a parabolic oxidation rate (25) (28). Above this temperature any newly formed oxide will be in the form of gamma or eta. As gamma is more commonly reported in the literature, it will be used henceforth. The gamma alumina will form at the metal-oxide interface and grow out from there (28). The transition consists of two independent steps: one is the recrystallization of the amorphous alumina, the second is the growth of new

gamma alumina. Once gamma alumina begins to form, a shift in the oxidation kinetics to a linear rate law occurs. This shift is due to cracks in the oxide layer creating a short circuit in the diffusion path. The linear rate will continue until a limiting oxide thickness is reached. The transition from amorphous to crystalline oxide is slow and the amorphous phase may be present up to the melting point (15) (17) (25) (26) (28).

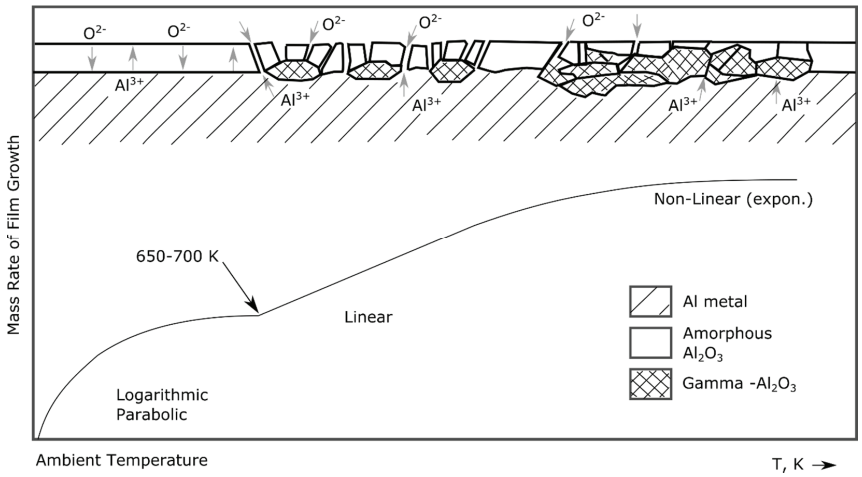

Figure 2-6 Effect of temperature on the oxidation of pure aluminum from room temperature up to the melting point redrawn from Bahk et al. (28).

The transformations of amorphous-to-gamma alumina and gamma-to-alpha alumina are associated with a notable reduction in volume of the oxide, with the PBR going from 1.31 to 1.28 for the gamma to alpha transition (22). This reduction in oxide volume results in cracks and a subsequent flux of oxygen into the oxidized metal. This cracking is responsible for the mass gain and changes in the oxidation rate (28).

Trunov studied the effects alumina phase transformations on the oxidation of aluminum particles as shown in Figure 2-7, which shows the mass gain as a function of temperature. It was found that by heating at a constant rate, sudden increases in the mass would occur. These increase were associated with the phase transformations of the aluminum oxide layer. A small mass increase was found with the transformation from the amorphous to gamma oxide phase followed by a large increase in mass with the transition from gamma to alpha. The reason for the mass gain is attributed

to the shrinkage of the oxide layer upon transformation from one polymorph to another resulting in cracks in the protective oxide layer similar to what was found for solid aluminum oxidation (29).

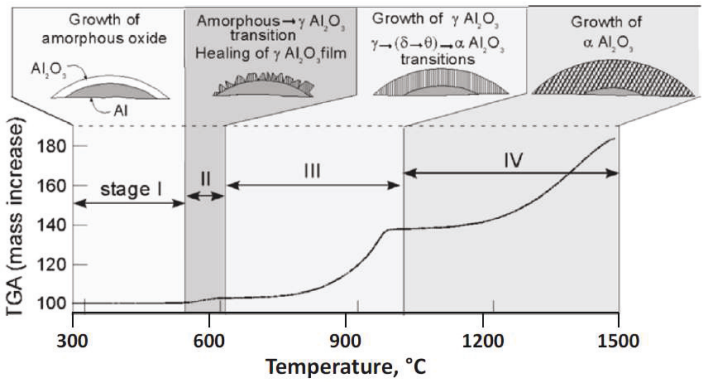

Figure 2-7 Phases formed during oxidation of pure aluminum from Trunov et al. (29).

2.4.3 Kinetics of molten aluminum oxidation

Sleppy (21) studied the oxidation of 99.99 % pure aluminum at temperatures over 670 °C. The results from the oxidation of as-rolled aluminum are shown in Figure 2-8. It was found that the oxidation followed a logarithmic rate up to 700 °C. Above this temperature, a modified parabolic rate was found to govern the oxidation. The modified parabolic oxidation rate is the result of diffusion of aluminum through the oxide layer plus a chemical reaction at the oxide-gas interface. For aluminum samples that were preoxidized for 1 hour at 600 °C before melting, oxidation was found to be dependent on the diffusion of aluminum out through the oxide layer, and therefore followed a parabolic rate law as shown in Figure 2-9.

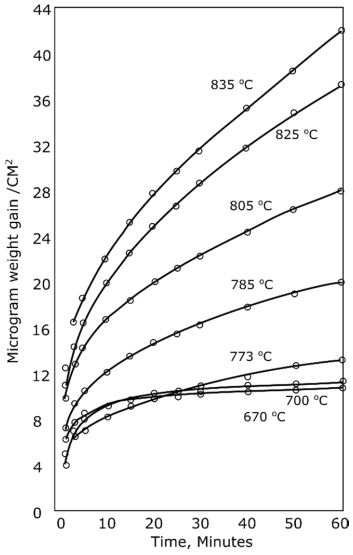

Figure 2-8 TGA results after oxidization in oxygen of the as rolled sample redrawn from Sleppy (21).

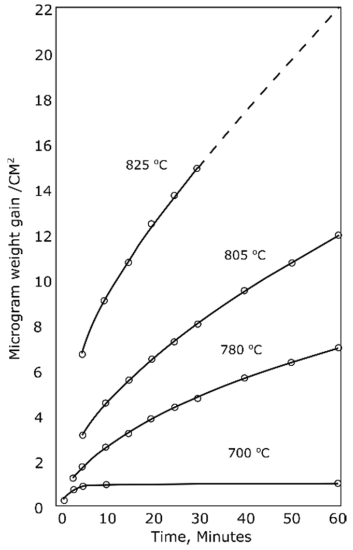

Figure 2-9 TGA curve for pure aluminum sample preoxidized for 1 hour at 600°C followed by oxidation in oxygen at higher temperatures redrawn from Sleppy (21).

Bergsmark et al. (30) were unable to find a single rate equation that described the oxidation of aluminum containing a very small amount of magnesium (50 ppm) over a longer oxidation time frame (60 hours) as the oxidation followed a sigmodal shaped oxidation curve. The oxide layer on the samples was found to be made up of 2 parts: an initial thin oxide layer and a MgO enriched oxide layer. The MgO enriched layer existed of either: crystals of Al_2O_3 with up to 35 % MgO if oxidation occurred in a dry atmosphere, or porous mounds if the oxidation occurred in an atmosphere that contained trace amounts of moisture. Significant amounts of MgO were found in the oxide layer, even though the magnesium content was very low, indicating that magnesium plays an important role in the oxidation even at low concentrations.

2.5 Aluminum-magnesium alloy oxidation

Oxidation of aluminum alloys containing magnesium are often treated separately from other aluminum alloys due to the large difference in oxidation behavior compared to pure aluminum. The oxidation of magnesium to MgO is one of the few reactions that has a lower Gibbs energy of oxide formation than the oxidation of aluminum, as seen on the Ellingham diagram in Figure 2-1. Additionally, the spinel phase $MgAl_2O_4$ can readily form in magnesium containing alloys. The formation of MgO and $MgAl_2O_4$ layers causes a significant shift in the protective properties of the oxide layer and results in an increase in both the rate and extent of oxidation unless extra measures are taken to control the oxidation (5) (12) (13).

2.5.1 MgO and $MgAl_2O_4$ formation and stability

The formation of MgO or $MgAl_2O_4$ on Al-Mg alloys is dependent on multiple factors, of which the most important is the magnesium activity. Figure 2-10 by Surla et al. shows the stability of the MgO, $MgAl_2O_4$ and Al_2O_3 phases over an aluminum-magnesium alloy at 700 °C, as a function of magnesium activity and oxygen partial pressure. It can be seen that the formation of pure Al_2O_3 is essentially not possible for any magnesium activity greater than zero. Further, extremely low oxygen partial pressures below 10^{-44} are required to maintain a surface free from oxide. The transition between the MgO and $MgAl_2O_4$ phase occurs at a magnesium activity of 0.023 at 700 °C, meaning that the MgO phase is only stable at magnesium activities above this. Once the magnesium activity drops below this point, the $MgAl_2O_4$ phase becomes stable and the MgO will transform to $MgAl_2O_4$. In a practical sense as the magnesium is oxidized from the melt the

magnesium content in proximity to the metal-oxide interface will be lowered. After a certain time, depending on the initial magnesium content and the oxidation conditions, the magnesium activity will drop below the 0.023 limit and the $MgAl_2O_4$ phase will begin to form (19).

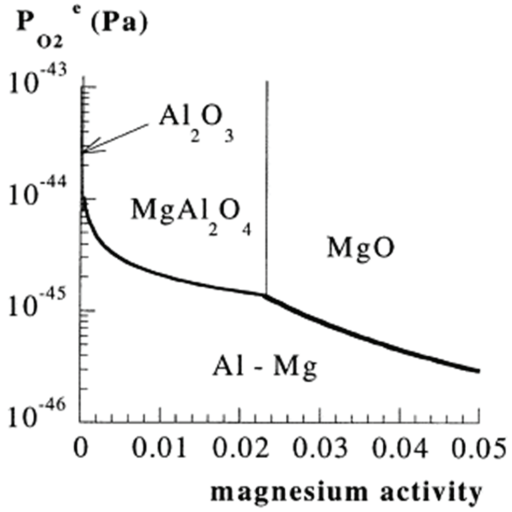

Figure 2-10 Thermodynamic repesentation of the oxide formed based on oxygen pressure and magnesium activity reprinted from Surla et al. (19).

2.5.2 Aluminum-magnesium system

For magnesium contents up to about 12 %, the aluminum-magnesium system is found to obey Henry's law with a slight negative deviation from ideal behavior as shown in Figure 2-11. For alloys at 800 °C, an activity coefficient of 0.88 can be used, yielding the expression below (31).

$$a_{Mg} = 0.88X_{Mg}$$

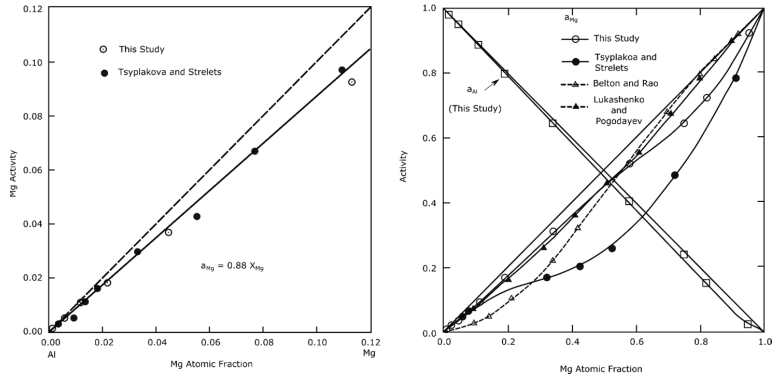

Figure 2-11 Magnesium shows a slight negative deviation from ideal behavior at 800 °C in aluminum redrawn from Tiwari (31).

The aluminum-magnesium phase diagram is shown in Figure 2-12 (32). It can be seen that addition of magnesium to pure aluminum metal will cause a decrease in the melting point. At temperatures as low as 450 °C, a large two phase solid-liquid zone exists. Further, this liquid zone will have an elevated magnesium content compared to the nominal composition. This elevated magnesium content is known to cause increased oxidation rates as shown by Cochran et al. (5).

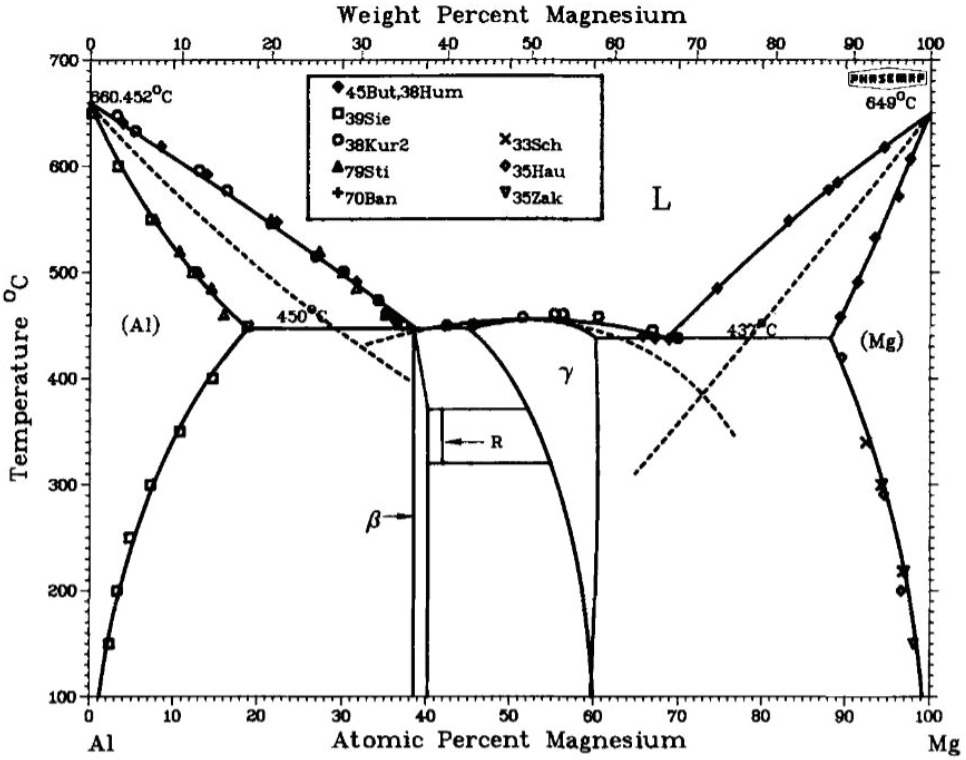

Figure 2-12 Aluminum-magnesium phase diagram (32).

2.5.3 Oxidation kinetics of solid Al-Mg alloys

Wefers proposed the oxidation behavior given in Figure 2-13 for the oxidation of an Al-Mg alloy below its melting point. At lower temperatures the oxide layer is made up of amorphous oxide and the rate is controlled by the diffusion through the oxide layer. As the temperature is increased, crystalline oxide begins to form at the oxide-metal interface, resulting in a cracking of the oxide layer and a change from a parabolic to linear oxidation rate. The oxidation rate will eventually slow as the cracks become filled with new oxide (33). This is similar to the oxidation of pure aluminum with the exception that the rate and extent for Al-Mg alloys is significantly higher.

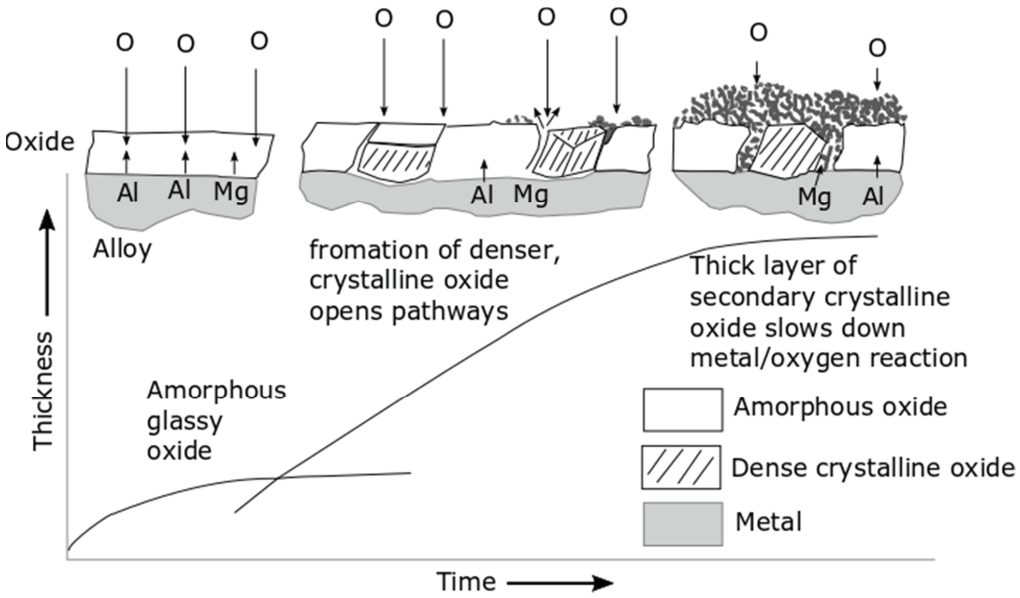

Figure 2-13 Schematic showing the solid state oxidation of Al-Mg alloys redrawn from Wefers (33).

Wefers proposed that four types of oxide layer could form depending on the temperature and magnesium content as shown in Figure 2-14. In a magnesium-free alloy below 400 °C, a uniform glassy layer of Al_2O_3 will exist. At temperatures above 400 °C, γ-Al_2O_3 will crystalize and grow at the oxide-metal interface. With the addition of less than 2 % magnesium, the MgO will form at the oxide-gas interface above γ-Al_2O_3. This is due to the cracks in the oxide layer caused by the formation of gamma alumina providing a short circuit for the diffusion of magnesium and oxygen. At magnesium contents over 2 % the entire surface becomes covered in MgO (33).

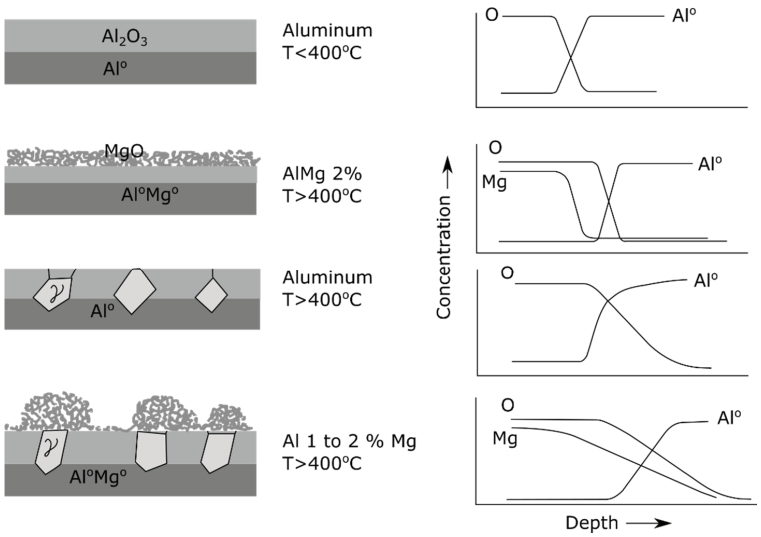

Figure 2-14 Effect of magnesium content and temperature on the oxide layer morphology and idealized concentration depth profiles for each of the alloy and temperature combinations where Mg indicates magnesium associated with MgO and Mg° indicates magnesium metal. Redrawn from Wefers (33).

2.5.4 Oxidation kinetics of molten Al-Mg alloys

The oxidation rate of magnesium containing alloys is dependent on the magnesium content, with a higher magnesium contents leading to an increase in both the rate and extent of oxidation. The effects of magnesium content on the oxidation can be seen in Figure 2-15 (34). Once all the magnesium in the alloy has been oxidized to $MgAl_2O_4$, the oxidation of aluminum to Al_2O_3 will continue. However, as aluminum oxidizes to a protective layer the oxidation will essentially stop once all the magnesium has been oxidized (12). As the total amount of magnesium in the melt is limited, an upper limit for the total mass gain that an alloy can reach can be calculated by finding the amount of oxygen uptake that corresponds first to complete oxidation of all the magnesium to MgO then further to $MgAl_2O_4$. (5). For a 5 % magnesium alloy this would correspond to a 3.3 % increase for oxidation to MgO and 13.3 % increase for $MgAl_2O_4$.

Cochran also reported that heating rate has an impact on the oxidation rate of Al-Mg alloys. If an Al-Mg alloy is heated slowly, the first phase to melt will be rich in magnesium. This magnesium-

rich liquid will oxidize at a higher rate than the aluminum-magnesium bulk alloy. This magnesium rich phase will act as a seed, causing increased overall oxidation. (5)

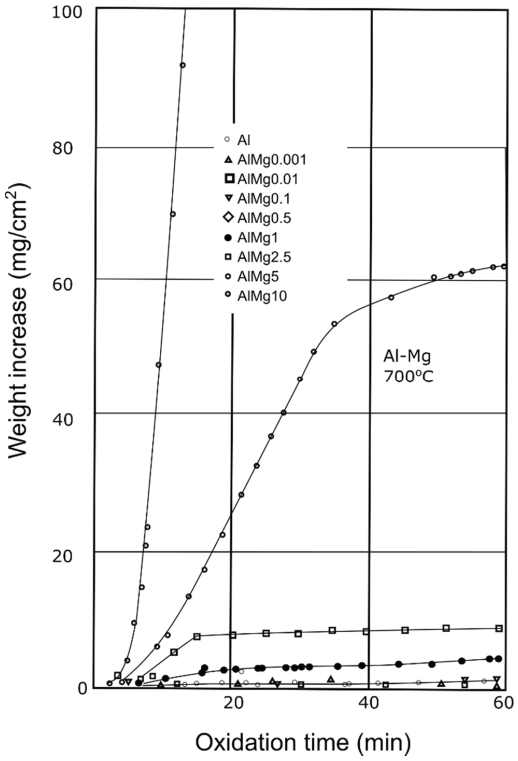

Figure 2-15 Effects of magnesium content on the oxidation, redrawn from Balicki (34).

The largest concern with Al-Mg alloys is breakaway oxidation. The idealized oxidation curve for aluminum shown in Figure 2-2 also applies to Al-Mg alloys, however the time for the onset of breakaway oxidation is significantly reduced and the rate and extent of oxidation is increased, compared to pure aluminum. As is seen with pure aluminum, breakaway oxidation is caused by a phase transformation resulting in a change in the structure and density of the oxide layer which exposes the melt to the atmosphere. Cochran proposed that breakaway oxidation could be delayed by adding beryllium, sodium or dusting with boron; adding CO_2 or N_2 to the atmosphere or by fast melting. The time for the onset of breakaway oxidation could be reduced by increasing the temperature or magnesium concentration; seeding with MgO or $MgAl_2O_4$ or slow melting.

It has been shown that breakaway oxidation can occur in two steps for Al-Mg alloys, with the first being the transformation of amorphous MgO to crystalline MgO and second by the transformation of MgO to $MgAl_2O_4$, as shown by the work of Haginoya and Fukusako in Figure 2-16 (12). The presence of two stages of breakaway oxidation is dependent on the temperature, and it is only possible for temperatures near the melting point. As the temperature increases, the oxidation rate increases and the two stages appear as a single stage, resulting in the formation of $MgAl_2O_4$ with MgO appearing only as an intermediate phase (12).

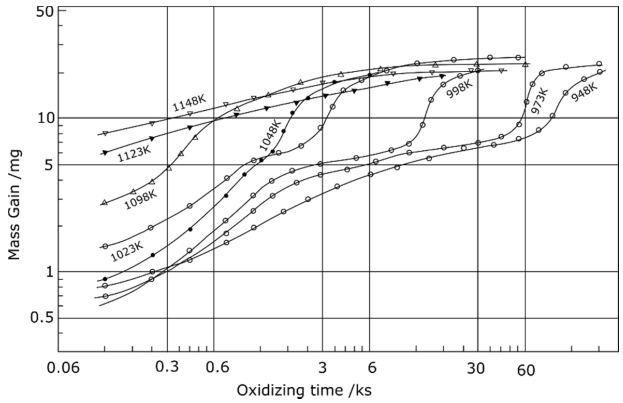

Figure 2-16 Two-step oxidation of Al-Mg alloy showing two stages of oxidation, redrawn from Haginoya et al. (12).

Cochran showed that it was the formation of the $MgAl_2O_4$ phase that initiates breakaway oxidation, by carrying out experiments in a TGA during which some of the samples where seeded with large or small crystals of $MgAl_2O_4$. These seeds were placed on top of a sample before melting. If the seeds were wetted by the melt, the time for breakaway oxidation to occur was significantly reduced compared to an unseeded melt, showing that $MgAl_2O_4$ will trigger breakaway oxidation (5).

Based on the above it can be seen that the magnesium concentration at the oxide-metal interface is important as once it drops below a critical value, the $MgAl_2O_4$ phase will form resulting in breakaway oxidation. Lea and Molinari showed there were two competing processes acting on the magnesium concentration at the oxide-metal interface. First, is the segregation of magnesium from the bulk metal to the interface. Second, is the loss of magnesium due to the oxidation and evaporation. If the oxidation/evaporation rate exceeds the segregation rate, the oxide-metal

interface will become depleted of magnesium. If segregation exceeds oxidation/evaporation, a buildup of magnesium will occur. The results of Lea and Molinari's work show that a magnesium depletion layer will exist at the oxide-metal interface when the oxidation occurs below the melting point (35). Lea and Molinari's work was carried out at solid state conditions, however, under liquid oxidation conditions, the flux of magnesium to the oxide-metal interface will be in competition with the oxidation and evaporation rate. This will in turn effect the length of the incubation period on the alloy.

2.6 Minor alloy additions

The alloying elements added to an aluminum melt will interact with the aluminum and as a result will impact the oxidation of an aluminum alloy. Through thermodynamic calculations, the distribution of a specific alloying/minor element between the aluminum melt, oxide phase and gas phase can be determined. The calculations below were carried out by Nakajima et al. (36) for typical concentrations of alloying elements in aluminum melts during remelting, and the results are given in Figure 2-17. The distribution of an element (M) between the metal and oxide is given by L' in Eq 2.3 where the equilibrium constant K' is defined by Eq 2.4. L' and K' are based on the general oxidation reaction given in Eq 2.1. The distribution of an element between the metal and gas phase is defined by L'' in Eq 2.5 and is based on the metal-gas equilibrium reaction shown in Eq 2.6. In these equations: x is defined as the mole fraction of the metal (M) or oxide (M_mO_n), γ is the activity coefficient, $p°$ is the partial pressure of the pure element (M), p is the partial pressure of M over the alloy and a is the activity of the metal or oxide.

$$L' = \frac{x_M}{x_{M_mO_n}} = \frac{\gamma_{M_mO_n}}{K'\gamma_M^m x_M^{m-1} p_{O_2}^{n/2}} \tag{2.3}$$

$$K' = exp\left(-\frac{\Delta G^\circ}{RT}\right) = \frac{a_{M_mO_n}}{a_M^m p_{O_2}^{n/2}} = \frac{\gamma_{M_mO_n} x_{M_mO_n}}{(\gamma_M x_M)^m p_{O_2}^{n/2}} \tag{2.4}$$

$$L'' = \frac{p_M}{P_{Al}} = \frac{\overset{\circ}{p}_M \gamma_M x_M}{p_{Al}} \tag{2.5}$$

$$M = M_{(g)} \tag{2.6}$$

Based on this work it can be seen that a majority of elements will remain in the aluminum alloy melt as alloying elements. Elements that will be distributed to the oxide layer will have an effect on the morphology and protective abilities of the oxide layer. Elements that have a tendency to vaporize can have an effect on the oxidation rate as they can cause porosity in the oxide layer if the vapor pressure is sufficiently high. This porosity will lead to a reduction in the protective properties of the oxide layer, by providing a shortcut for diffusion through the oxide layer. This is the case for selenium and sodium additions as stated by Thiele and translated by Agema (13) (37). It is important to note that the above is only a thermodynamic analysis and the rate that any specific element will be transported to the gas or oxide phase is not taken into account.

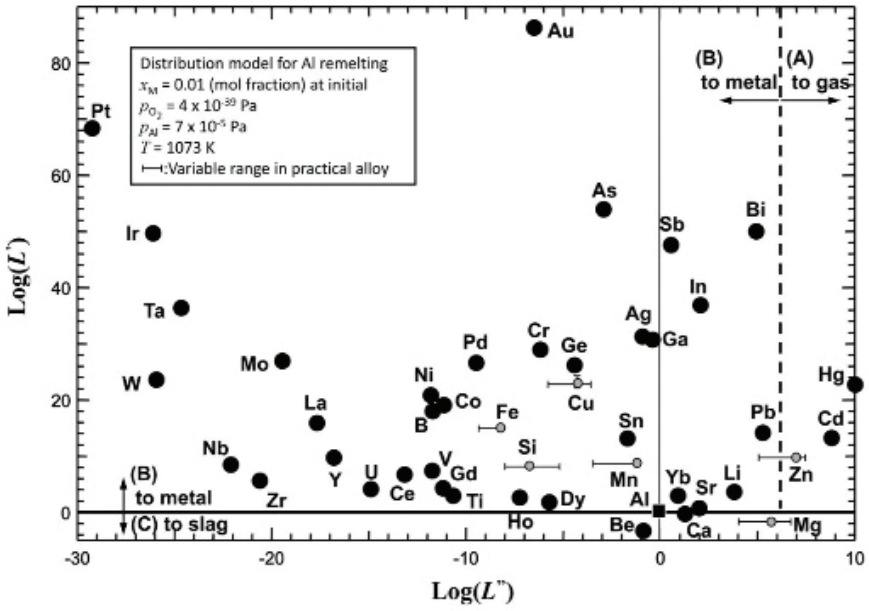

Figure 2-17 Thermodynamic distribution of elements adapted from Nakajima et al. (36).

Thiele carried out a number of experiments to study the effects a specific element will have on the oxidation rate of an aluminum melt, with the results shown in Figure 2-18. It can be seen that over long oxidation times (>20 hrs.), most common single alloying elements such as manganese, silicon and iron will cause an increase in the overall oxidation extent (38). This would seem contradictory to the results of Nakajima et al. who showed that these elements should remain in the melt (36).

The reason behind the effects of these elements is not readily known. Magnesium, sodium, selenium and calcium all cause a large and rapid increase in the oxidation an aluminum alloy (38). Select Al-Mg+ alloying element systems of interest to this work will be examined in detail below.

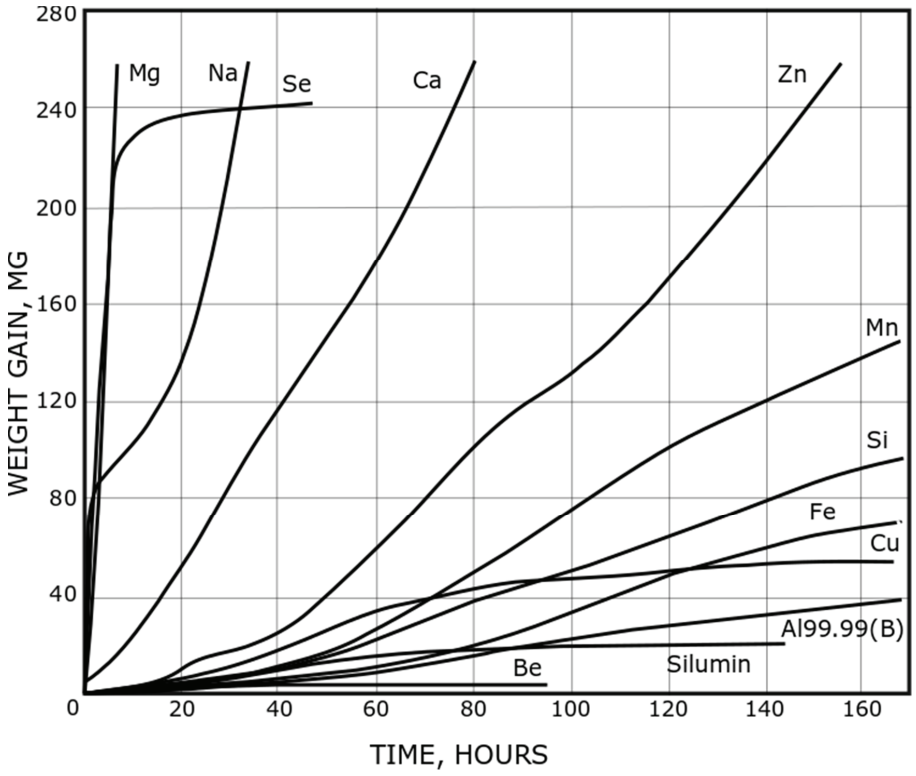

Figure 2-18 Effect of 1 wt. % additions to the oxidation of an aluminum alloy, redrawn from Thiele (38).

2.6.1 Beryllium

2.6.1.1 Oxidation of beryllium containing alloys

The effects of beryllium where first published by Gauthier in 1938 who found that as little as 0.02 % beryllium was required to protect an aluminum melt with 12 % magnesium during casting (6). The work by Balicki in 1958 and Thiele in 1962 showed in greater detail the effects of beryllium on the oxidation of aluminum alloys containing magnesium (13) (34). Figure 2-19 shows the results of Balicki's work on beryllium and the effect of increasing beryllium amounts on the

oxidation of a 5 % magnesium alloy. It can be seen that the addition of as little as 0.0005 % beryllium will result in a dramatic decrease in the amount of mass gain due to oxidation. Increasing the beryllium content above 0.0005 % will result in a further decrease in the mass gain due to oxidation (34).

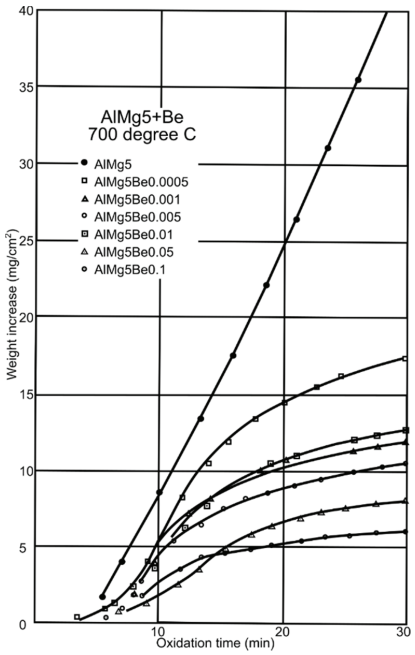

Figure 2-19 Results of different levels of beryllium additions on the oxidation of a 5 % magnesium alloy at 700°C redrawn from Balicki (34).

In 1962, Thiele published similar results showing the effects of beryllium on the oxidation as well as the effects of other alloy elements. Thiele's work focused on longer oxidation times and collaborated the results of Balicki as seen in Figure 2-20. Beryllium was shown to provide oxidation protection for atmospheric exposures up to 170 hours. Thiele proposed that the amount of beryllium required to protect a melt was directly dependent on the magnesium concentration in the melt and developed the expression shown in Eq 2.7 describing the amount of beryllium required to protect a melt from excessive oxidation based on the mass percent of magnesium (13). This would give a value of 15 ppm of beryllium to protect an alloy containing 5 % magnesium.

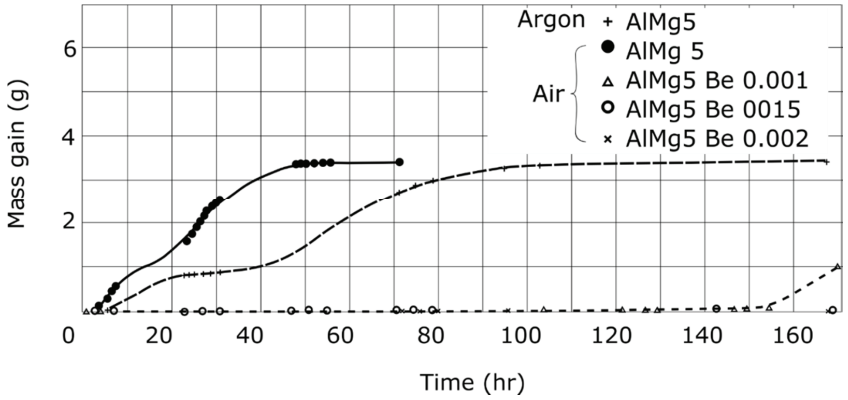

Figure 2-20 Protective effect of beryllium for longer times as shown by adapted and redrawn from Thiele (13).

$$Log(\%Be) = 85.7 \times 10^{-3} \times (\%Mg) - 3.26 \quad (2.7)$$

The work on beryllium was continued by Cochran in 1977 who found that 0.001 % beryllium could protect a 3.5 % magnesium alloy for up to 46 hours. Cochran proposed that the onset of breakaway oxidation was due to the formation of the $MgAl_2O_4$ spinel which disrupted the MgO layer and allowed a rapid diffusion between the atmosphere and melt. Beryllium additions were not effective in preventing breakaway oxidation in cases where the melt was seeded with crystalline $MgAl_2O_4$. The addition of the seeds had enough of a destructive effect on the oxide layer that beryllium was unable to inhibit the oxidation, showing that beryllium could delay the onset of breakaway oxidation, but is unable to stop it once it has been initiated. Holding the sample in a BeO crucible was found to have no impact on the oxidation, showing that beryllium must be added to the melt to have an impact on the oxidation (5).

2.6.1.2 Berylliums effect on skin strength

Kahl and Fromm studied the effect of beryllium on the strength of the oxide layer. It was found that additions of 70 ppm to pure aluminum and 0.012 % beryllium to an Al-Mg alloy caused a significant decrease in the oxide skin strength as shown in Figure 2-4. Furthermore, it was found that to get the same reduction in oxide skin strength in commercial primary aluminum (0.002 % Mg, 0.04 % Si) as was achieved in pure aluminum with 70 ppm of beryllium, 600 ppm of beryllium

was required. (23) It is interesting to note that this amount is approximately 60-300 times higher than the amount of beryllium used in industrial applications to achieve oxidation protection (8). Syvertsen tested the effects of 2 ppm of beryllium on an industrial 5XXX series alloy and found that the beryllium had no effect on the skin strength at such dilute concentrations (39).

2.6.1.3 The aluminum-beryllium system

The aluminum beryllium phase diagram can be seen in Figure 2-21 and Figure 2-22. Beryllium and aluminum have limited solubility in each other with a maximum solubility of 0.007 at % aluminum in beryllium and 0.3 at % beryllium in aluminum. There are no known stable intermetallic phases in the system (40). Given the small amounts of beryllium used by the aluminum industry, it can be assumed that any added beryllium will exist in dilute solution with the aluminum regardless of the temperature.

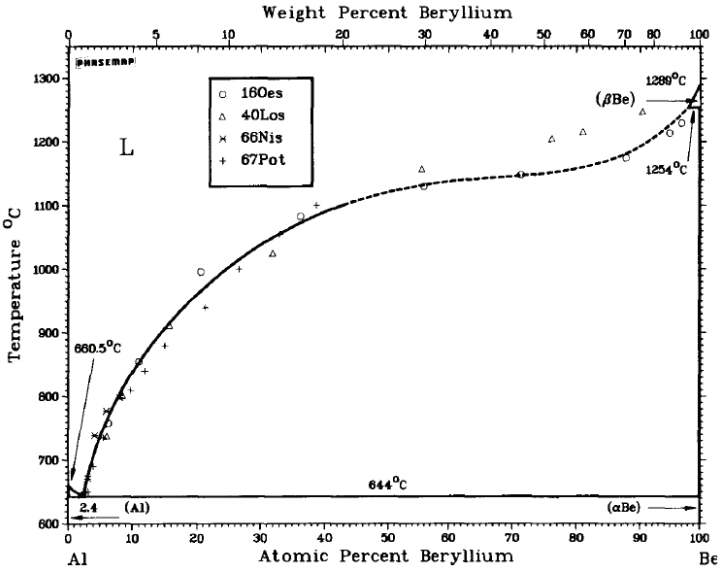

Figure 2-21 Aluminum-beryllium phase diagram (40).

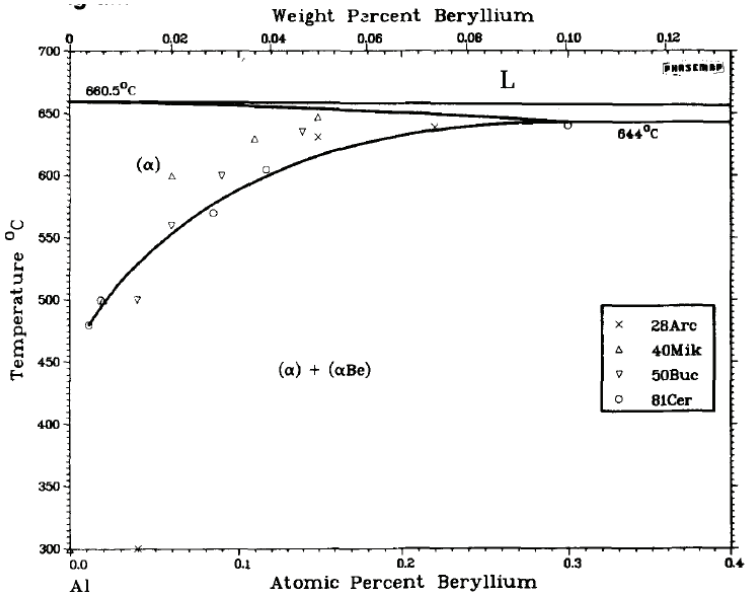

Figure 2-22 Enlarged aluminum rich section of the aluminum-beryllium phase diagram (40).

2.6.1.4 Al-Be-Mg-O system

With the introduction of oxygen to the aluminum-beryllium system, three oxides are generally considered to be stable: BeO, $BeAl_2O_4$ and Al_2O_3. The Gibbs energy of formation for these oxides and the corresponding aluminum-magnesium oxides are given below in Table 2, as calculated from FactSage7.1 with the FactPS, FTlite and Ftoxide databases.

Table 2 Gibbs energy of formation for beryllium, aluminum and magnesium oxides.

Oxide	Delta G (kJ/mol O)
BeO	-694.2
$BeAl_2O_4$	-656.3
Al_2O_3	-637.5
MgO	-676.9
$MgAl_2O_4$	-654.8

The BeO-MgO system has been studied by x-ray diffraction where it was found that no intermediate compounds form between BeO and MgO. No deviation in the lattice parameters of BeO was found indicating that there is little to no solubility of MgO in BeO. The eutectic point for the system was found to be at 1838 °C and sixty-nine mole percent BeO, which is well above the temperatures that are expected for the aluminum industry, meaning no liquid oxide phases are expected to form as shown in the BeO-MgO phase diagram in Figure 2-23 (41).

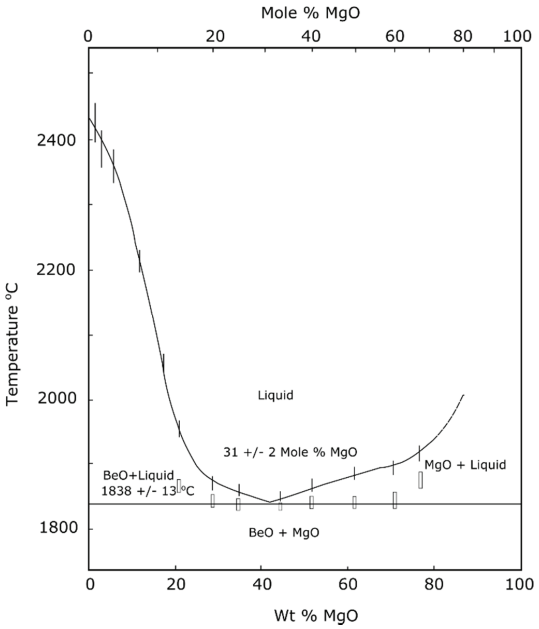

Figure 2-23 BeO-MgO phase diagram redrawn from Kordis (41).

2.6.1.5 Diffusion in beryllium alloys

The diffusion of gas species through any formed beryllium containing oxide layer are of critical importance to the protective properties of the oxide layer. Unfortunately, there is limited data available in regards to the diffusion of magnesium and aluminum through beryllium oxide. The diffusion coefficients of oxygen in MgO and BeO have been found by various authors and are shown in Table 2. It can be seen that the diffusion coefficient of oxygen through polycrystalline BeO is one to two orders of magnitude lower than the diffusion coefficient for polycrystalline MgO (42). This not taking into account the differences in temperature where the diffusion

coefficients are applicable, as the diffusion coefficients for BeO are applicable in the 1600-1900 °C range, whereas, the values for MgO are applicable in the 750-1150 °C range. The diffusion coefficient for BeO in the 750-1150 °C range would be even lower than the published numbers, resulting in an even larger difference. However, any porosity or cracks in the oxide layer would negate any differences in the diffusion coefficients as transport through these defects would be similar between BeO and MgO given a similar defect size. It is important to point out that breakaway oxidation occurs when the oxide layer is ruptured creating a shortcut for the diffusion through the oxide layer (43). Therefore, these variations in the diffusion coefficients are only relevant during the oxidation incubation period.

Table 3 Diffusion coefficient of oxygen in BeO and MgO (42).

Diffusing ion	**Oxide**	**Crystal type**	**Diffusion coefficient (cm^2/s)**	**Temperature range (°C)**
O^{18}	BeO	Poly	5.2×10^{-7}	1600-1900
O^{18}	BeO	Poly	5.2×10^{-6}	1600-1900
O^{18}	BeO	Single	2.95×10^{-5}	1560-1727
O^{18}	MgO	Single	2.5×10^{-6}	1300-1750
O^{18}	MgO	Poly	4.3×10^{-5}	750-1150

2.6.1.6 Segregation of beryllium in Al-Mg melts

Degreve carried out depth profiling of an Al-Mg-Zn (7075) alloy that contained beryllium after oxidation in air at 530 °C by employing a secondary ion microprobe and argon sputtering with the results shown in Figure 2-24. The focus of this work was the generation of an accurate depth profiles with a secondary ion microprobe, therefore the importance of the results themselves were secondary to the accuracy of the depth profile. As a result, a large portion of the relevant experimental data, such as exact alloy composition and oxidization time is lacking in the publication. Only the beryllium ion signal was plotted as a function of sputter depth and hence, a complete picture of the oxide layer composition is lacking. It was found that the beryllium was concentrated by a factor of 100 from the bulk composition with the highest concentration measured just below the metal-oxide interface. No analysis of the morphology was undertaken to relate any surface features to the composition (44). Despite the shortcomings of this study, this is the only known published depth profile through an oxide layer of an aluminum alloy with beryllium.

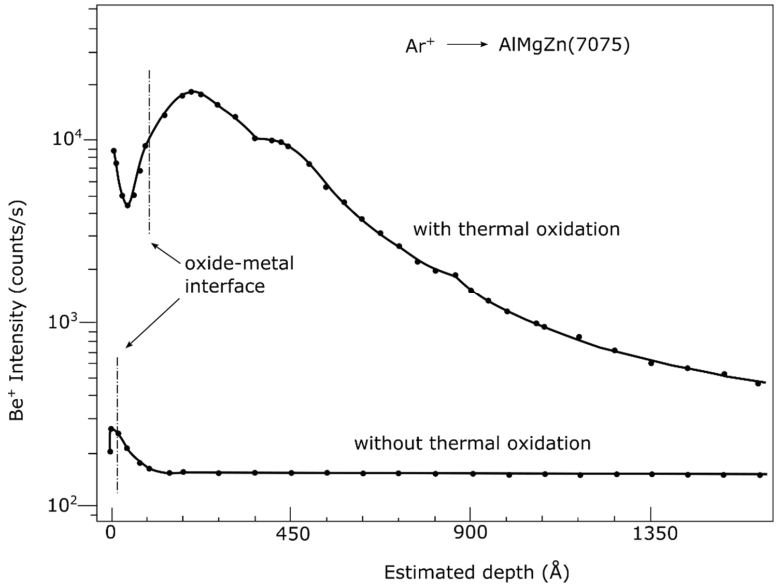

Figure 2-24 Beryllium depth profile from SIMS analysis redrawn from Degreve et al. (44).

2.6.1.7 Health risks of Beryllium

The use of beryllium is overshadowed by the severe health risks that are associated with exposure to beryllium and beryllium oxide, as such special handling is required for its use. Exposure to beryllium can result in one of three distinct conditions: beryllium sensitization, acute beryllium disease and chronic beryllium disease.

Beryllium sensitization occurs when the body develops a hypersensitivity to the exposure of beryllium and can result in redness and swelling (45).

Acute beryllium disease is defined as symptoms resulting from beryllium exposure that last less than one year, and include both respiratory and non-respiratory symptoms. The respiratory symptoms are generally the most severe with inflammation of the nasal passage, bronchitis and pneumonia all being possible with the first symptoms appearing 3-8 days after exposure to a large amount of beryllium. The non-respiratory conditions include beryllium ulcers and dermatitis. Acute beryllium disease is considered treatable and most make a full recovery (46).

Chronic beryllium disease involves long term symptoms that can occur years after exposure and will continue to worsen even after exposure to beryllium has stopped. The most common symptom is pneumonitis with a cough, chest pain and general weakness. In addition heart failure is often a result (46).

2.6.2 Strontium

Strontium is currently used by the aluminum industry, primarily to modify inclusions in silicon containing alloys (8). As one of the group II elements along with beryllium and magnesium, strontium is known to have a strong affinity for oxygen with the reaction of strontium to SrO having a Gibbs energy of formation of -676.1 kJ/mol of oxygen at 750 °C, which is nearly identical to that of magnesium at -676.9 kJ/mol of oxygen (from FactSage 7.1 with the FactPS, FTlite and FToxide databases). As one of the few elements to have as strong as affinity for oxygen as magnesium, strontium has previously seen interest from researches on its effects of oxidation.

2.6.2.1 Oxidation of strontium containing alloys

Unlike beryllium and magnesium which have a well agreed upon effect on the oxidation of aluminum alloys, debate remains about strontium's effects on the oxidation. Both positive and negative effects have been reported in literature with no conclusive answer or understanding yet achieved. Even amongst those that agree upon the effects of strontium, the mechanism is still debated. Miresmaeili tested the effects of strontium and magnesium additions to an Al 7%Si alloy weighing 47 grams. It was found that the strontium addition resulted in a larger oxidation mass gain than magnesium additions. Addition of both strontium and magnesium resulted in the largest mass gain as shown in Figure 2-19. The high oxidation rate and low strontium concentration resulted in a loss of more than 80 % of the strontium. Miresmaeili attributed the increase in oxidation to a low PBR of 0.65 for strontium oxide, failing to provide a protective oxide layer (11). This conclusion is seen as questionable as the PBR is not valid for the oxidation of minor elements in the liquid state. Miresmaeili also carried out experiments on larger melts of 2.5 kg, and found that the effect of strontium was reduced. It was concluded that the reactivity of strontium was significantly reduced as no evidence of strontium oxide was found at the surface after oxidation. However, strontium rich intermetallics were found near the surface. The differences between the large and small melts were attributed to the significantly higher surface area to volume of the small

melt (11). Emadi et al. found that additions of 0.02 wt. % of strontium to an Al 7%Si alloy resulted in a threefold increase in the oxidation mass gain. It was stated that $SrAl_2O_7$, $SrAl_2O_4$ and Al_2Si_2Sr phases were found by XRD analysis. No further details on a proposed mechanism by which oxidation is increased was proposed (47).

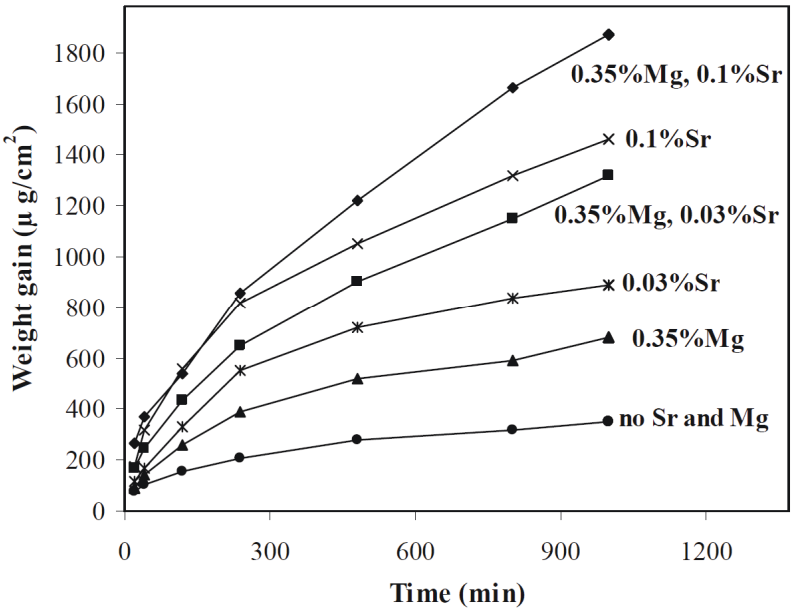

Figure 2-25 Effects of strontium and magnesium on a Al-7% Si alloy (11).

In contrast to the work by Miresmaeili and Emadi, the results of the Ozdemir et al. (48) and Yuen et al. (49) show a strong positive oxidation-reducing effect of strontium additions. Ozdemir found that a strontium addition of 0.1 % to a melt containing 0.5 or 1 % magnesium reduced oxidation by up to 98 %. An addition of strontium to a 5 % magnesium's alloy still showed a strong protective effect, but was less profound than seen on the low magnesium alloys, as illustrated by Figure 2-26 and Figure 2-27. A strontium rich layer, corresponding to $AlSr_4$, was found directly underneath the magnesium oxide layer and it was proposed that this layer was responsible for the protective effect of the strontium (48).

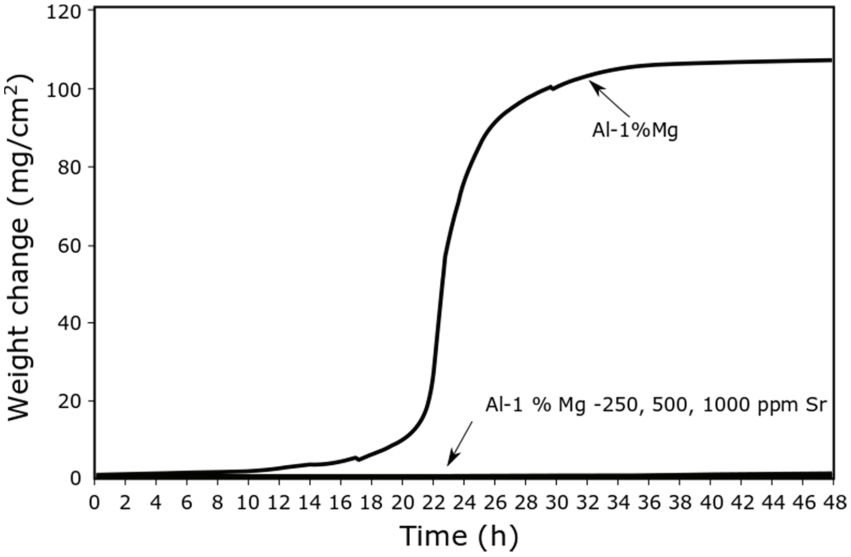

Figure 2-26 Effects of strontium on the oxidation mass gain of a 1 % magnesium alloy redrawn from Ozdemir et al. (48).

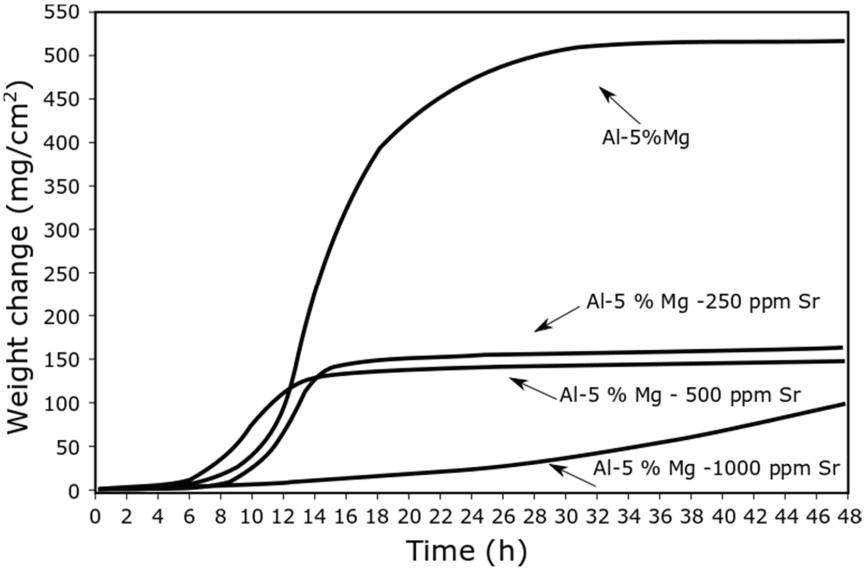

Figure 2-27 Effects of strontium on the oxidation mass gain of a 5 % magnesium alloy redrawn from Ozdemir et al. (48).

In the work by Yuen, it was found that the onset of breakaway oxidation could be delayed by 25 hours for a 5182 alloy with the addition of 0.025 % strontium as shown in Figure 2-28. For the low magnesium casting alloys A357 (0.52 % Mg, 6.7 % Si), changes in the overall oxidation kinetics from linear to a more logarithmic kinetics were found with strontium additions as seen in Figure 2-29. This would indicate a protective effect of strontium additions. A significant difference in the oxide layer on the A357 alloy was found with strontium additions. The typical cauliflower oxide growths associated with the oxidation of Al-Mg alloys were found on the samples without strontium, however these growths were absent on the strontium containing alloys. A similar oxide layer was found on the 5182 samples regardless of strontium content. However, all the samples were oxidized to passivation so it is not surprising that the oxide morphology is similar. Yuen attributed the protective effect to the formation of a $SrAl_4O_7$ layer on the 5182 and a $SrAl_4O_7$ or $SrSiO_3$ layer on the A357 alloys beneath the initial MgO layer which protected the melt from further oxidation (49).

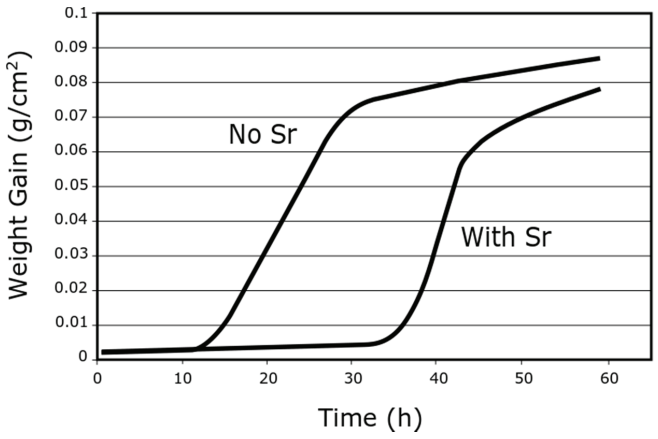

Figure 2-28 TGA curve showing the effect of strontium on the oxidation of a 5182 alloy at 750 °C redrawn from Yuen et al. (49).

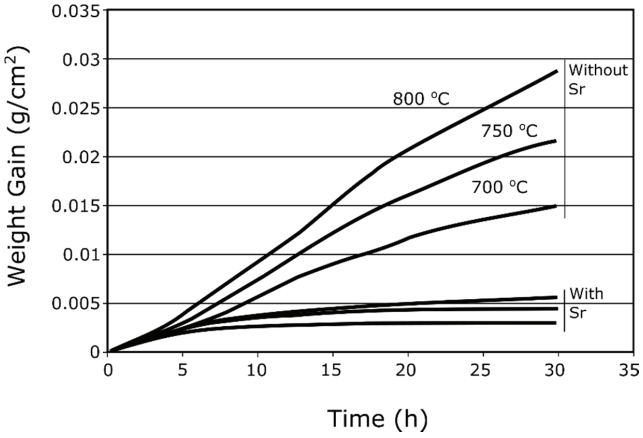

Figure 2-29 Effects of strontium on the oxidation of an A357 alloy redrawn from Yuen et al. (49).

Based on the large disagreement amongst the different authors on the effects of strontium it is logical to conclude that a yet unknown factor plays a key role in determining whether strontium will inhibit or promote the oxidation.

The work by Kahl and Fromm found that as strontium is readily oxidized and has a high vapor pressure, and subsequently the concentration in the melt will rapidly decrease. This was the possible explanation for the oxide skin strength results of silicon containing alloys where it was found that the skin strength decreased over time as shown in Figure 2-5. It was found that the silicon content remained constant, but the strontium content decreased with time, which would indicate that strontium has a large effect on the properties of the oxide layer (23).

2.6.2.2 The Sr-Al-O system

In contrast to the Be-Al and Mg-Al systems, the addition of strontium to aluminum results in the formation of several intermetallic compounds as seen in the aluminum-strontium phase diagram in Figure 2-30 (50). From the diagram, it can be seen that the formation of an Al_4Sr phase is possible with only a few percent of strontium. Other intermetallics phases are possible, but require additions of over 20 at % of strontium which far exceeds the amounts used by the aluminum industry. The formation of the Al_4Sr phase may play a large role in the oxidation if it forms at the oxide-metal interface as proposed by Ozdemir (48).

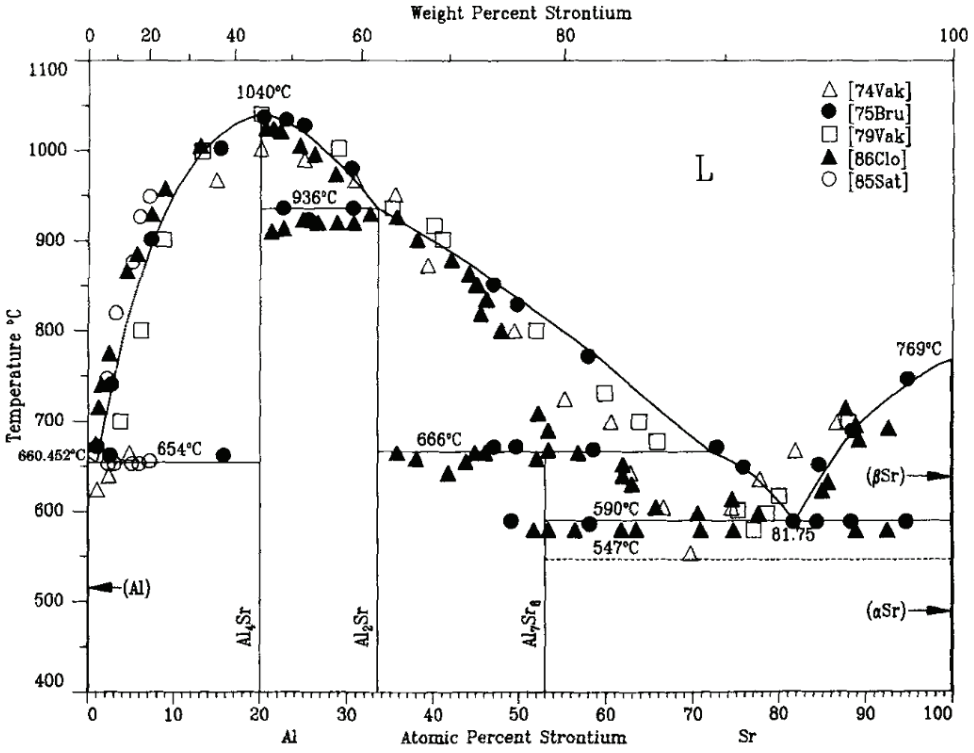

Figure 2-30 Aluminum-strontium phase diagram (50).

The addition of oxygen to the system results in the SrO-Al_2O_3 phase diagram as seen in the Figure 2-31 (51). Further, both SrO and SrO_2 exist as stable oxide phases (52). As such, there is potential for a variety of complex oxides to form. The protective effect of these oxides are unknown and could help to explain the large differences between the protective abilities found by different researchers, as all reported a different strontium containing compound formed after oxidation. $SrAl_4O_7$ was stated to be protective per Yuen (49), whereas, Miresmaeili stated that SrO was not (11).

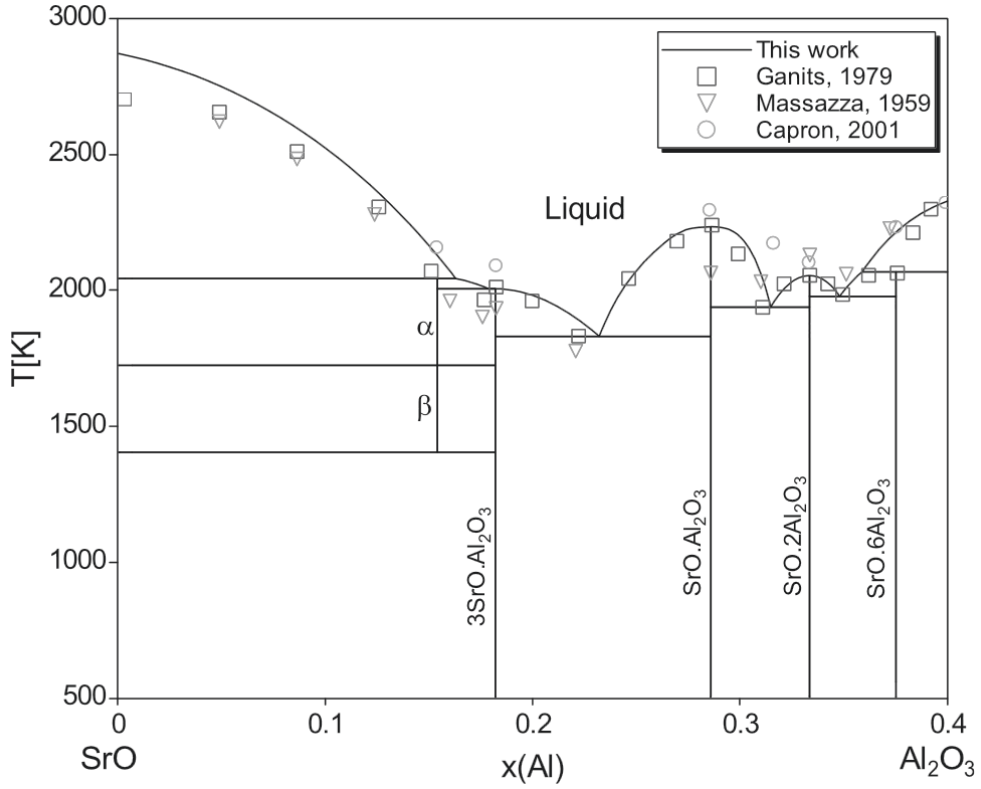

Figure 2-31 SrO-Al_2O_3 phase diagram (51).

2.6.3 Yttrium

The effects of yttrium on the oxidation of Al-Mg alloys is unknown, however, previous work by Ravi Kumar (53) has shown that yttrium can result in a decrease in the oxidation of magnesium alloys as observed in a study of the effects of yttrium on the ignition resistance of magnesium alloys. It was found that an alloy with 4 % yttrium did not begin to burn after heating up to 730 °C, whereas pure magnesium and a magnesium alloy with 9 % aluminum both began to burn below 650 °C. The ignition resistance of the yttrium containing alloy was attributed to the rapid formation of a protective Y_2O_3 layer at the cracks. Observations of the sample after the ignition test showed that cracks existed in the oxide layer. EDS analysis showed that these cracks had a higher yttrium content than the un-cracked oxide, meaning the formed Y_2O_3 prevented excessive oxidation (53).

Wang et al. conducted oxidation tests where the surface of a magnesium alloy was implanted with yttrium ions before being oxidized at 500 °C in oxygen for short times (90 minutes) and long times (96 hours). An improvement in the oxidation resistance was found with the implantation of yttrium ions on the surface as shown in Figure 2-32. This improvement in oxidation resistance was attributed to the presence of Y_2O_3 in the oxide layer as shown by Auger spectroscopy (54).

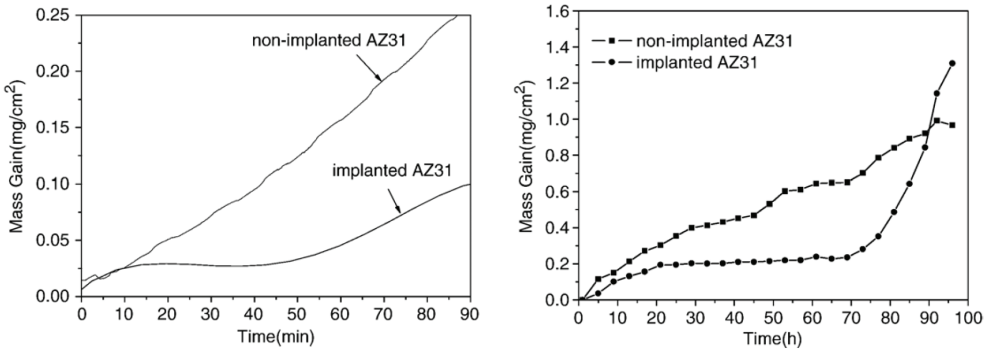

Figure 2-32 Effect of yttrium implantation on the oxidation of a magnesium alloy at 500 °C for short and long time periods redrawn from Wang et al. (54).

The aluminum-yttrium phase diagram is provided in Figure 2-33. It can readily be seen that with yttrium additions, five different intermetallic phases may form (55). Given that any added yttrium will likely have a concentration below 0.05 %, only the YAl_3 phase seem likely to form. For the YAl_3 phase to form at 750 °C, an yttrium concentration of 5.5 at % would be required. Given that the solubility of yttrium in aluminum at temperatures below 750 °C is less than 0.03 % (55), it is logical to assume that yttrium will have a tendency to segregate from the bulk. If the segregation to the surface can be promoted and reach a concentration of 5.5 %, a solid intermetallic phase could form at the surface.

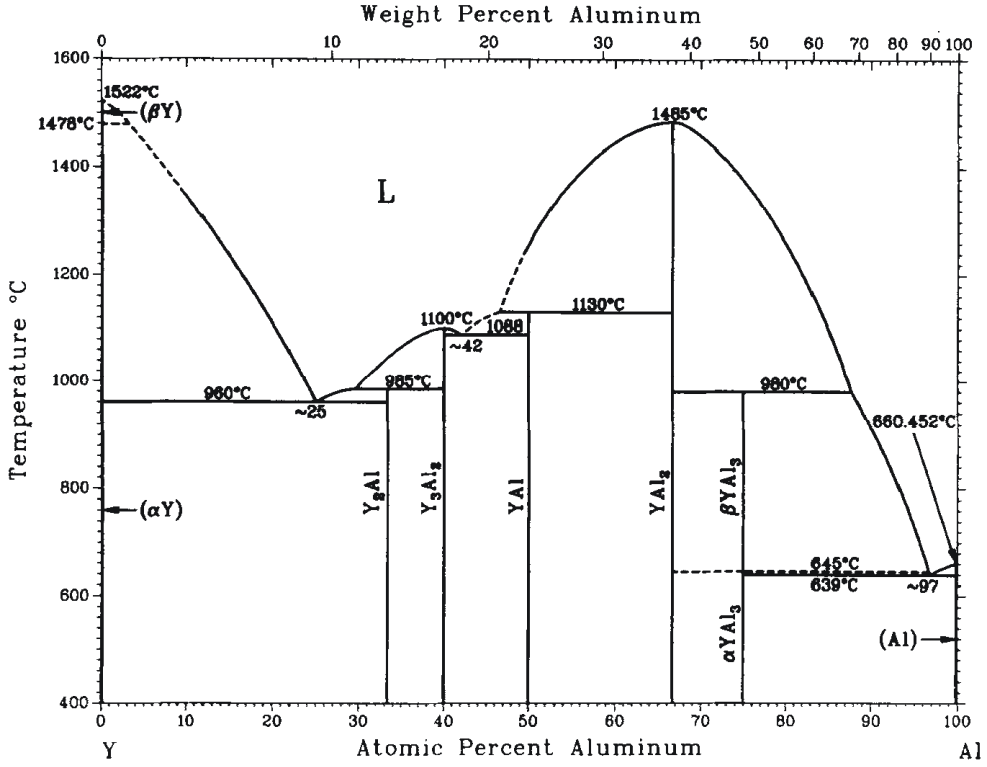

Figure 2-33 The aluminum-yttrium phase diagram (55).

2.6.4 Erbium

The aluminum-erbium system has not been previously studied in terms of oxidation. However, erbium has many similarities to yttrium. The aluminum-erbium phase diagram shown in Figure 2-34 shows that five intermetallic phases can form, with the $ErAl_3$ most likely due to the low initial erbium content (56). To form the $ErAl_3$ phase at 750 °C, 2.5 at % of erbium would be required. This is approximately half what is required to form an yttrium intermetallic meaning formation of a protective erbium layer may require a significantly lower bulk composition than would be required for yttrium.

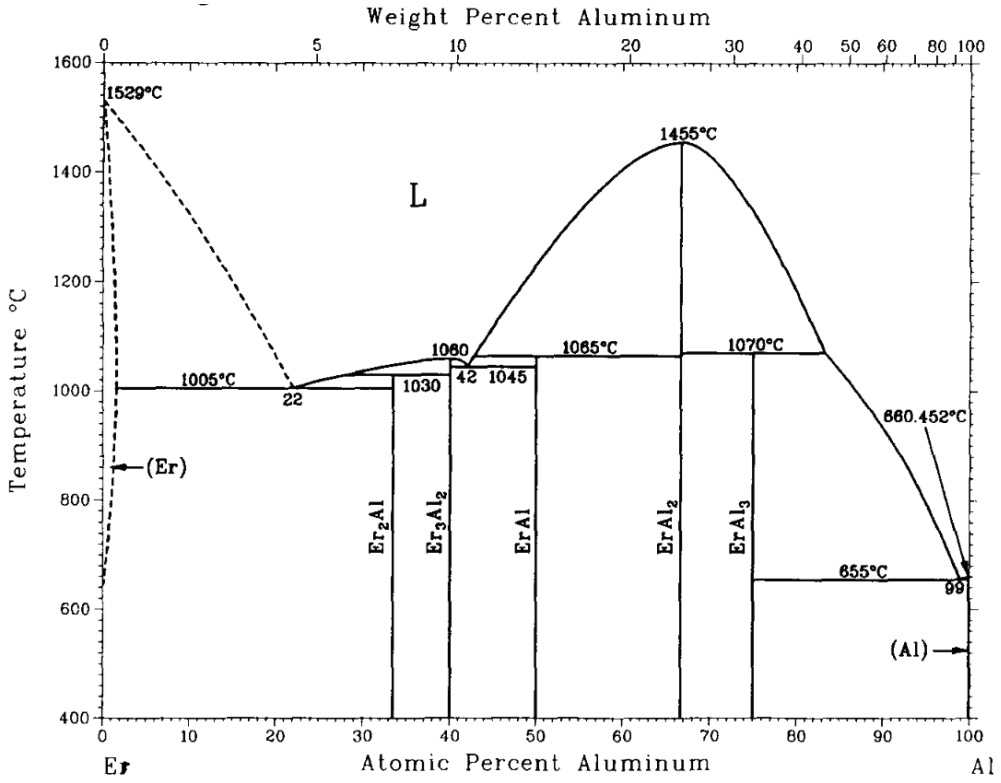

Figure 2-34 Aluminum-erbium phase diagram (56).

2.7 Atmosphere

The effect of different gas atmospheres on the oxidation of Al-Mg alloys has previously been studied by a number of authors. This is because the atmosphere is one of the major factors effecting the alloy's oxidation rate as supply of oxygen to the reaction site is critically important. Inside a gas-fired furnace, the atmosphere contains primarily CO_2 and H_2O with some CO as these are the primary products of combustion. If standard air fuel burners are used instead of oxy-fuel burners, a significant portion of nitrogen gas will also be present (57). A slight overpressure is often maintained inside the furnace to reduce the amount of air that is drawn into the furnace (58). Outside the furnace, the atmosphere is air, however, the humidity in the air can vary significantly as most casthouses have limited atmospheric control. This means that depending on the weather

and season (summer or winter) the amount of humidity will change. As CO_2 additions to the atmosphere is one of the main focuses of this work, it will be described in some detail.

2.7.1 CO_2 atmosphere

CO_2 has been shown to have a limited or enhancing effect on the oxidation of both anodized and non-anodized aluminum alloys without magnesium (14) (59) (60). In contrast, CO_2, has been shown to have a strong inhibiting effect on the oxidation of Al-Mg alloys (4) (5) (14) (61). Cochran found that the minimum amount of CO_2 required to protect an Al-Mg melt from excessive oxidation could be expressed as a function of the magnesium content as shown in Figure 2-35. It was found that the addition of 65 % CO_2 to air was able to delay the onset of breakaway oxidation of a 10 % magnesium alloy to more than 16 hours. Similar tests carried out with argon instead of CO_2 did not inhibit breakaway oxidation, showing that the addition of CO_2 reacts to inhibit the oxidation, not just reduce the oxygen partial pressure (5).

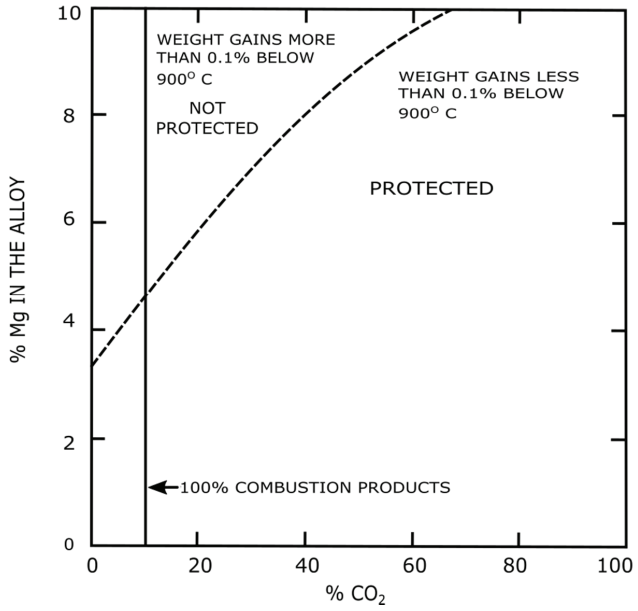

Figure 2-35 Amount of CO_2 required to protect an Al-Mg melt from excessive oxidation redrawn from Cochran et al. (5).

Haginoya et al. carried out a detailed study on the effects of CO_2 on the oxidation of an Al-Mg alloy; finding that additions of CO_2 to the atmosphere could slow the oxidation and delay breakaway oxidation. Higher CO_2 contents in air were found to enhance the inhibiting effect on a 10 % Mg alloy as can be seen in Figure 2-36 where 40 % CO_2 in air could delay the onset of breakaway oxidation by 300 minutes. Haginoya also found that the addition of CO_2 the atmosphere after an initial period of oxidation in a pure air atmosphere would result in the oxidation rate deceasing to near zero almost immediately as shown in Figure 2-37. This effect was found to occur as long as the CO_2 was added in the early stages of oxidation. The inhibiting effect would be significantly reduced if the CO_2 was added after more than 70 minutes of oxidation in air when the $MgAl_2O_4$ had begun to form. The addition of CO_2 must, therefore be done before the formation of the $MgAl_2O_4$ spinel as CO_2 was not effective in inhibiting the oxidation once it had formed. It was proposed that the inhibiting effect was the result of adsorption of CO_2 onto the MgO layer which prevented the inward diffusion of oxygen through the oxide layer, but conclusive proof of this was not found (4).

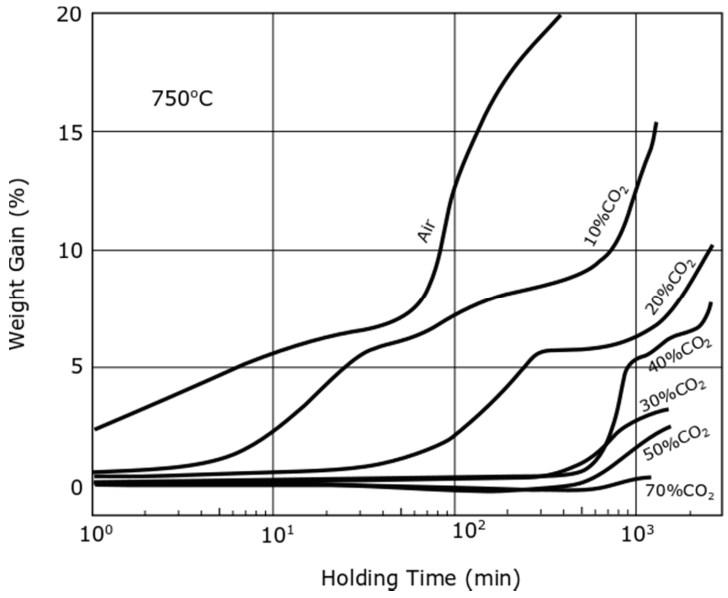

Figure 2-36 Effect of varying CO_2 contents in air on the oxidation of a 10 % magnesium alloy redrawn from Haginoya et al. (4).

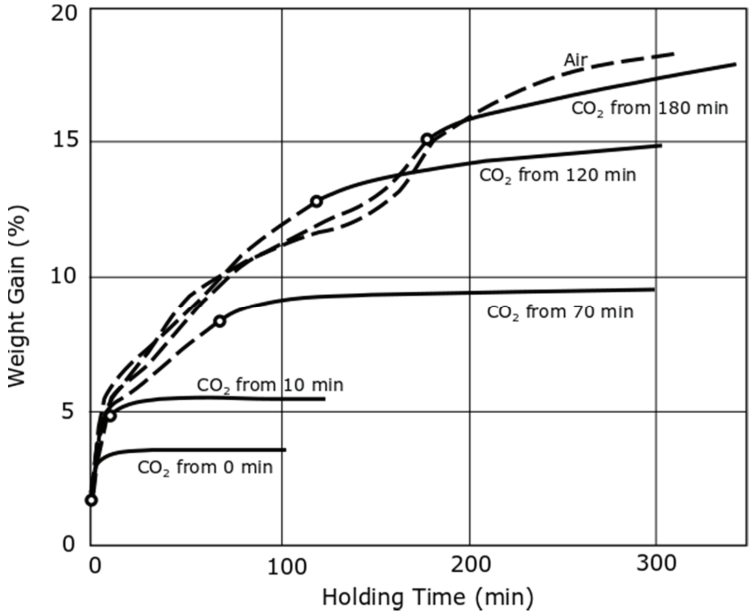

Figure 2-37 Effect of the addition of CO_2 to an air atmosphere on the oxidation redrawn from Haginoya et al. (4).

Bubbling CO_2 through an Al-Mg melt yielded similar results as a CO_2/air atmosphere. Wightman and Fray bubbled pure CO_2 through the melt and found that the CO_2 is first reduced to CO which is further reduced to carbon. The later reaction is dependent on the CO partial pressure. However, for low magnesium alloys, the CO_2 only reacted to CO. The reduction of CO_2 to CO was found to be controlled by the diffusion of magnesium through the oxide shell, whereas, the CO to carbon reaction is limited by the desorption of CO from the MgO.

2.7.1.1 Thermodynamic considerations

A theoretical study of the thermodynamics regarding the oxidation of Al-Mg alloys in CO_2/air can yield some interesting insights on how this system is expected to behave. From a thermodynamic viewpoint, the addition of CO_2 to an air atmosphere over an Al-Mg melt should not decrease the available oxidants in the system, as both magnesium and aluminum are able to reduce CO_2. With the CO_2 first being reduced to CO per Eqs. 2.8 or 2.10, the CO may also be further reduced to

carbon per Eqs. 2.9 or 2.11. Magnesium will oxidize preferentially to aluminum, however, once all magnesium has been oxidized to MgO, the alloy will continue to oxidize to $MgAl_2O_4$ (19).

$$\frac{1}{2}Mg + \frac{1}{2}CO_2 = \frac{1}{2}MgO + \frac{1}{2}CO \qquad \Delta G = -296.8 \text{ kJ/mol oxygen at } 750°C \qquad (2.8)$$

$$Mg + CO = MgO + C \qquad \Delta G = -288.4 \text{ kJ/mol oxygen at } 750°C \qquad (2.9)$$

$$\frac{1}{3}Al + \frac{1}{2}CO_2 = \frac{1}{6}Al_2O_3 + \frac{1}{2}CO \qquad \Delta G = -257.4 \text{ kJ/mol oxygen at } 750°C \qquad (2.10)$$

$$\frac{2}{3}Al + CO = \frac{1}{3}Al_2O_3 + C \qquad \Delta G = -249.0 \text{ kJ/mol oxygen at } 750°C \qquad (2.11)$$

In an atmosphere not containing any free oxygen, the maximum CO partial pressure in the system would be controlled by the Boudouard reaction given in Eq. 2.12. The equilibrium CO fraction ($CO/CO+CO_2$) is calculated to be 0.78 at 750 °C and will increase as the temperature increases. As CO is only generated from Eqs. 2.8 and 2.10, it will take time for the CO partial pressure to reach the level required for it to react in this system either by Eqs. 2.9, 2.11 or 2.12, unless the total amount of gas is limited in relation to the reactant surface area. Under a flowing gas the amount of CO build-up will be limited, which indicates that deposition of elemental carbon on the surface should not be expected. The addition of oxygen to the system will drive the CO partial pressure down as the CO will be oxidized back to CO_2 as shown in Eq 2.13.

$$CO = \frac{1}{2}C + \frac{1}{2}CO_2 \qquad (2.12)$$

$$\frac{1}{2}CO + \frac{1}{4}O_2 = \frac{1}{2}CO_2 \qquad \Delta G = -193.8 \text{ kJ/mol oxygen at } 750°C \qquad (2.13)$$

In a mixed CO_2-air atmosphere, any free oxygen in the system should react with the magnesium vapor to form MgO per Eq. 2.14 or, in the absence of magnesium, with aluminum per Eq. 2.15. The Gibbs energy of formation shows that this reaction is favorable compared to the with reaction with CO_2 or CO. Additionally, the flux of oxygen from the bulk gas to the oxide layer should also occur faster than CO_2 gas, based on Graham's law which states that the diffusion rate is inversely proportional to the square root of the molecular weight (62). Under a CO_2/air atmosphere, the sample will have a N_2 containing boundary layer through which O_2 and CO_2 will diffuse before

reacting at the oxide surface. Graham's law shows that the flux of O_2 from the bulk to the oxide surface will be 1.17 times higher than that of CO_2.

$$Mg + \frac{1}{2}O_2 = MgO \qquad \Delta G = -676.9 \text{ kJ/mol oxygen at } 750°C \qquad (2.14)$$

$$\frac{2}{3}Al + \frac{1}{2}O_2 = \frac{1}{3}Al_2O_3 \qquad \Delta G = -451.3 \text{ kJ/mol oxygen at } 750°C \qquad (2.15)$$

2.7.2 Alternative cover gases to CO_2

There exists potential of other gases than CO_2 to inhibit the oxidation of Al-Mg alloys. For example both SO_2 and H_2S have been shown to have a strong inhibiting effect on the oxidation of Al-Mg alloys (63). Further, fluorine containing gases such as SF_6 have been shown to have an oxidation inhibiting effect on magnesium (64). However, CO_2 gas would be preferable to SO_2, H_2S and SF_6 for HSE reasons as these gases can negatively impact human health and/or are strong greenhouse gases. CO_2 would, therefore be the logical choice for a cover gas, of those gases that are known to inhibit the oxidation, due to its minimal HSE concerns.

2.8 Summary

While a significant amount of work has been done on the oxidation of aluminum and aluminum-magnesium alloys over the past 100 years and a good general understanding of the oxidation behavior exists, many questions still remain. The effects of beryllium on the oxidation has been illustrated by Balicki (34), Thiele (13) and Cochran (5) showing conclusively that beryllium significantly reduces the oxidation rate and delays breakaway oxidation. In the works published by Cochran (5), Haginoya (4) and Wightman (14) the effects of CO_2 were shown to significantly delay the onset of breakaway oxidation. However, an in-depth understanding of the mechanisms behind how select minor elements and cover gases effect the oxidation of Al-Mg alloys is still largely lacking. Such understanding is key to alternative and improved approaches to melt protection.

3. Experimental

The experimental work carried out in this thesis focuses entirely on small scale (<5 grams) laboratory experiments, aimed at understanding the mechanisms behind observed protective effects of specific alloying elements or cover gases on the rate and extent of oxidation of Al-Mg based alloys. Such understanding may result in new paths for reducing problematic oxidation in the aluminum industry. While literature shows a significant body of prior work on the oxidation of aluminum primarily based on Thermogravimetric Analysis (TGA) what is often lacking is a detailed characterization of the generated oxide layer, giving a full understanding of the mechanisms behind known effects. As such, the focus of the experimental work in this thesis has been on the generation of suitable oxidized aluminum samples for subsequent advanced characterization.

This experimental section is divided into three main sections: alloy preparation, oxidation experiments, and characterization. In addition, the oxide stability and wettability and reactions between alloys and oxides were investigated to provide supplementary information, and are covered in a fourth section.

An overview of the different series of experiments with their objectives and methodology is presented in Table 4.

Table 4 Overview of experiments carried out in this thesis.

Experiment	Aim	Furnace and temperature	Analysis methods	Planned results
Oxidation and analysis of industrial alloy, 5182, 5182+2 ppm Be	Study and quantify the effects of beryllium on the oxidation of an Al-Mg alloy.	University of Pittsburgh horizontal tube furnace, 500-750 °C	Mass change, FIB	Mass change after 10, 30 and 120 minutes of oxidation over a range of temperatures. Morphological characterization of the generated oxide layer
Oxidation and analysis of model alloy: 100 ppm Be 5% Mg	Enhance the effects of the beryllium to determine the mechanism behind beryllium's, inhibiting effect.	NTNU horizontal tube furnace, 550-750 °C	FIB, XPS	Detailed chemical and morphological characterization of the generated oxide layer
Oxidation and analysis of model alloy: 5% Mg in CO_2 containing atmosphere	Test the effects of various CO_2 atmospheres on the oxidation, determine the mechanism behind the known inhibiting effect of CO_2.	NTNU horizontal tube furnace, TGA, 750 °C	TGA, FIB, XPS, TEM	TGA curves showing the effects of various CO_2 containing atmospheres. Chemical and morphological characterization of the generated oxide layer and the effects of CO_2 on the oxide layer.
Oxidation and analysis of model alloy: 5% Mg + Y, Er or Sr	Determine the effects of Y, Er, and Sr on the oxidation of Al-Mg alloys	NTNU horizontal tube furnace, TGA, 750 °C	TGA, FIB, SEM, EDS	TGA curves showing the effects on oxidation, morphological and chemical characterization of the oxide layer.
Oxide stability of MgO, BeO and Al_2O_3	Stability of Al_2O_3, MgO and BeO mixtures at an elevated temperature	NTNU TGA, 1100 °C	XRD	Understand the stability of Al_2O_3, MgO and BeO when heated and any formed intermediate phases.
Wettability and reactions between Al+0, 30, 60 ppm Be and Al_2O_3 and MgO	Stability and reactivity of AlBe with Al_2O_3 and MgO and the contact angle	NTNU Sessile drop furnace, 1100 °C	EPMA	Better understand how an AlBe drop will interact with a Al_2O_3 or MgO substrate.

3.1 Alloy preparation

Both industrially manufactured and laboratory made model alloys were used in the course of this work. The majority of the experimental work was carried out on model Al-Mg alloys containing approximately 5 % magnesium with additions of beryllium, yttrium, strontium or erbium. 5 % magnesium was chosen as it would give a similar result to the industrial alloy used in the initial work. Further, 5 % magnesium was sufficient to give a clear effect of the magnesium, however, was not too high that any protective effect of the minor elements or CO_2 would be overshadowed by the rapid magnesium oxidation.

3.1.1 Industrial alloys

Initial experiments were carried out on samples taken from industrial cast ingots with the alloy designation 5182. Two different 5182 alloys were used, one containing 2 ppm of beryllium and the other without beryllium. The compositions of the two alloys are given in Table 5 below.

Table 5 Composition of industrial 5182 alloys used for oxidation experiments.

Alloy 5182		
Element	**Be free**	**2ppm Be**
Si	0.05	0.05
Fe	0.18	0.17
Cu	<0.01	<0.01
Mn	0.42	0.45
Mg	4.70	4.79
Cr	0.06	0.06
Zn	<0.01	<0.01
Ti	0.030	0.029
Be	0.0000	0.0002
Ca	0.0003	0.0001
Li	0.0000	0.0000
Na	0.0000	0.0000
Pb	<0.01	<0.01
Sn	0.00	0.00
Zr	0.00	0.00
OT	0.01	0.01

3.1.2 Model alloys

Preparation of the model alloys was carried out according to the flowchart given in Figure 3-1.

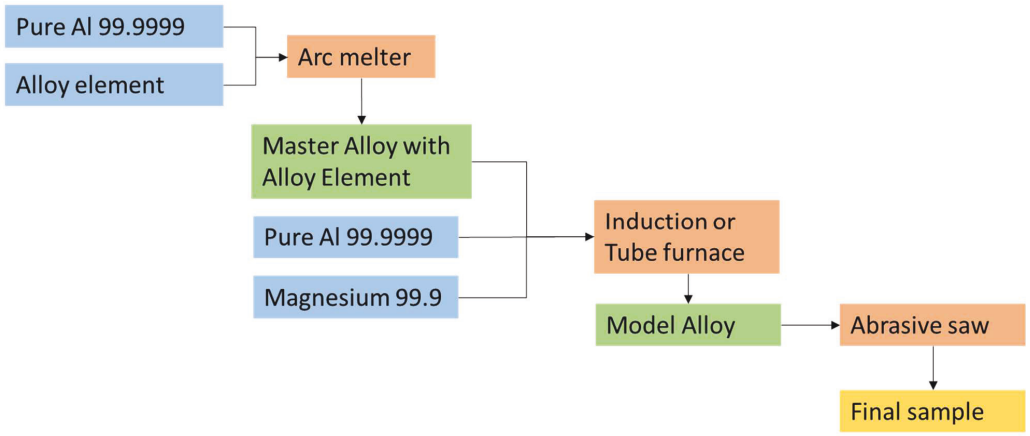

Figure 3-1 Flowchart describing the production of the model alloys.

This process was used to generate the following alloys with a target compositions of 4-5 % magnesium and 100 ppm of a select alloy element. A target of 100 ppm of the alloy element was selected based of the results of the first series of experiments on the industrial alloys containing beryllium, where it was found that while 2 ppm of beryllium had a clear protective effect, the analytical methods available were unable to detect a beryllium containing phase at such low concentrations. By increasing the concentration to 100 ppm, the likelihood of detecting any specific phases that contain the alloy elements was increased, but the increased concentration should not affect the overall oxidation mechanism as the solubility and phases formed are similar between 2 and 100 ppm for these alloys as was discussed in detail in the theory section.

3.1.2.1 Starting materials

The starting materials for the alloys were:

- 99.999 % aluminum-hemispherical pellets 4-8 mm in diameter from Alfa Aesar.
- 99.9 % magnesium chips from Sigma Aldrich
- 99 % beryllium wire from Alfa Aesar

- 99.9 % yttrium pieces Alfa Aesar
- 99 % strontium pieces from Sigma Aldrich
- 99.9 % erbium pieces from Alfa Aesar

The lower purity of the minor elements was acceptable as with a target composition of 100 ppm a 99 % purity level would result in a total of 1 ppm of impurities into the sample from the minor element. This is well below the level of impurities that would enter the sample through the 99.999 % aluminum.

3.1.2.2 Master alloy

The first step in producing the alloy was to produce a 5 % master alloy that contained 5 % of one of the alloying elements in aluminum. An Edmund Buhler table-top tungsten electrode arc-melter capable of melting up to 20 g charges under an argon atmosphere was employed for this. The arc-melter consists of a tungsten electrode and a copper plate-casting form as shown in Figure 3-2 and schematically Figure 3-3. An electrical current is passed from the electrode through the sample and into the copper plate melting, melting the sample in the process. The copper plate is water cooled allowing the sample to be rapidly solidify once the electrical current is shut off and prevents the copper plate from melting. The copper plate also contains a slot where the sample can be cast into a rectangular shaped mold measuring 25 x 10 x 1.5 mm shown in Figure 3-4, giving a sample weighing approximately 1 gram. Casting is accomplished with the aid of a vacuum system, which when turned on will cause the sample to be sucked into the mold. The water cooling in the casting mold is sufficient to cool the sample in a fraction of a second. The rapid cooling rate minimize the amount of segregation that can occur resulting in a homogenous master alloy. The downside to using this method is lack of temperature control when melting the alloy. The temperature of the arc is dependent a number of variables including: arc current, sample composition, shape, contact area with the copper plate the result is an arc temperature up to 3500 °C. While the current being passed through the electrode can be controlled it is not possible to maintain a specific temperature. This is especially problematic for metals that have a high vapor pressure, as the high arc temperature can cause significant evaporation of the metal. For this reason, magnesium containing alloys cannot be produced in the arc-melter.

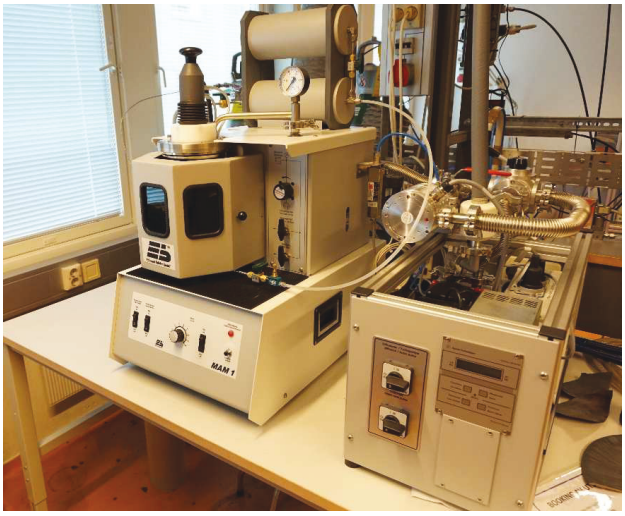

Figure 3-2 Arc-melter used to make master alloys.

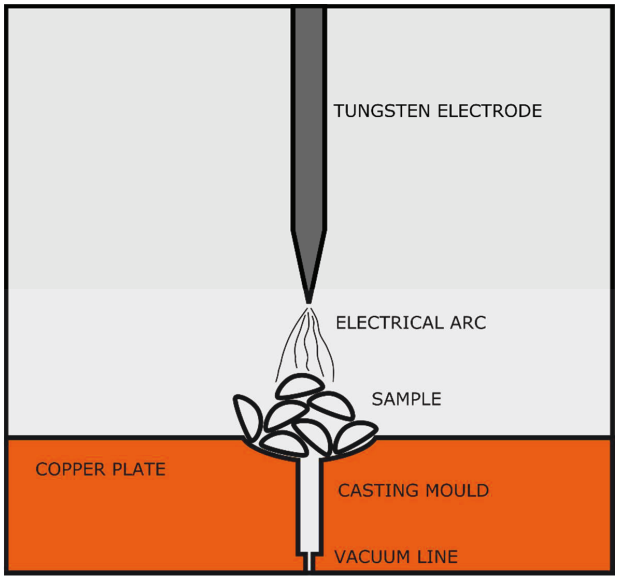

Figure 3-3 Schematic of the arc melter chamber.

Figure 3-4 Casting mold used in the arc-melter to make master alloys

3.1.2.3 Dilution to model alloy

To create the 5 % magnesium and 100 ppm beryllium-5 % magnesium alloys, the Al-Be master alloy from the arc-melter was combined with the aluminum and magnesium in an alumina crucible to give a final ingot of approximately 100 grams, which was in turn placed in a graphite crucible. When charging the alumina crucible, care was taken to ensure that the entire top surface was aluminum pellets to minimize the loss of the magnesium or minor element to evaporation or oxidation during melting. The crucible was then placed in an induction furnace. The furnace was evacuated and refilled with argon 3 times and heated to 850 °C in 30 minutes at which point it was held for 15 minutes. After the required holding time had passed the furnace power was switched off and let cool. Once cooled to room temperature the alloy was removed from the crucible.

The alloy did not wet the alumina crucible and was easily removed after it had cooled down. The alloy was then sectioned in to oxidation samples with a SiC abrasive saw. Sample size was determined by the furnace used for the oxidation. Upon sectioning, a number of pores under 0.5 mm in size were found on the samples as shown in Figure 3-5, these were attributed to shrinkage during solidification.

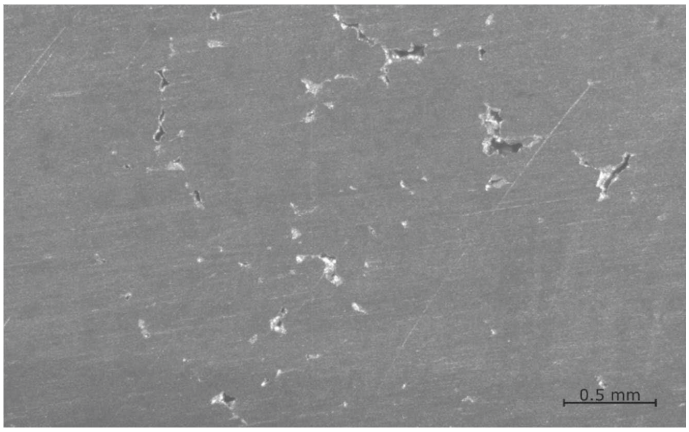

Figure 3-5 Shrinkage pores in Al-Mg alloy due to solidification with pore size under 0.5 mm.

A similar procedure was used to produce the yttrium, erbium and strontium alloys, the only difference being that the final alloys were made in a preheated horizontal tube furnace (NTNU furnace) at 850 °C under argon. This furnace is equipped with a sample loading system that allows the sample to be slid quickly in and out of the preheated furnace, therefore the melting time was significantly reduced compared to the induction furnace and the cooling rate was similarly reduced. An alumina boat was used instead of the crucible used for the magnesium and beryllium alloys. As a result, limited shrinkage porosity was found on these alloys.

3.1.2.4 Analysis and composition of model alloy

To confirm the composition of the alloys produced, Inductively Coupled Plasma Mass Spectroscopy (ICP-MS) was carried out on the 5 % Mg and 100 ppm-5 % Mg alloys with the composition coming back as:

- 4.7 % Mg
- 4.7 % Mg 102 ppm Be

The ICP-MS showed that the main impurities were calcium and copper. The calcium was found to be the main impurity in the aluminum and the copper contamination was likely picked up during the production of the master alloys in the arc-melter. Both impurities measured in the ppm range and should not impact the oxidation.

3.2 Oxidation experiments setup

The bulk of the experimental work carried out in this thesis were laboratory scale oxidation experiments that took place in either a horizontal resistance–heated tube furnace or a small scale TGA setup. Both these furnaces have a long history of use in the study of oxidation.

The horizontal tube furnace is a simple furnace setup that allows oxidation of a sample under a controlled atmosphere for a specific time. The variables that can be easily controlled in this furnace are: oxidation time, temperature and atmosphere. The basic method used was to preheat the furnace and establish the desired atmosphere, slide the sample into the hot zone of the furnace and hold it for a specified time before removing. The mass of the sample was taken before and after oxidation to determine the mass change during oxidation

The TGA allows a continuous mass curve to be generated as a function of oxidation time. In the TGA, the sample is placed on a micro balance which continually records the mass of the sample. The sample is placed in the furnace at room temperature and heated under a specified heating program. The atmosphere can be changed during the course of the oxidation experiment allowing a specific oxidation time period. Afterwards, the mass gain vs time curve can be analyzed for the effects of atmosphere and temperature.

For both experimental setups attempts were made to maintain a similar level of humidity across all experiments. This was done in several ways. First, all gases that were used for oxidation were bottled gases supplied Matheson (Pittsburgh) or by AGA (NTNU). The gas flow rates were low enough that a single bottle of each air and CO_2 were used for all the experiments at NTNU, and a single bottle of synthetic air was used for the work in Pittsburgh. Second, before a heating/oxidation cycle began the furnace was purged of ambient air either by a vacuum/purge cycle or by flowing the process gas through the furnace for at least 30 minutes. While the humidity levels were not measured it is assumed that they were similar across an experimental series.

3.2.1 Horizontal tube furnace Pittsburgh

A Mellen furnace at the University of Pittsburgh was used for initial experiments on the industrial 5182 alloys. This furnace is shown in Figure 3-6 and schematically in Figure 3-7. The furnace tube

and sample loader were made of glass with a tube measuring approximately 50 mm diameter. The hot zone of the furnace was lined with an alumina tube to minimize any contamination from the glass tube. The sample loading system allowed the furnace to be preheated to the required temperature and the desired atmosphere established, at which point an alumina boat with the sample in it could be slid into the center of the hot zone. After a set time the sample could be removed from the furnace and allowed to solidify under the controlled atmosphere (air). Solidification occurred within 10 seconds of removal from the hot zone. Within 5 minutes the sample had cooled to room temperature and was removed from the furnace. This setup minimized the heating and cooling cycle time, thus reducing the amount of oxidation that could occur during these times. Synthetic air was constantly blown through the furnace at a rate of 0.05 lpm.

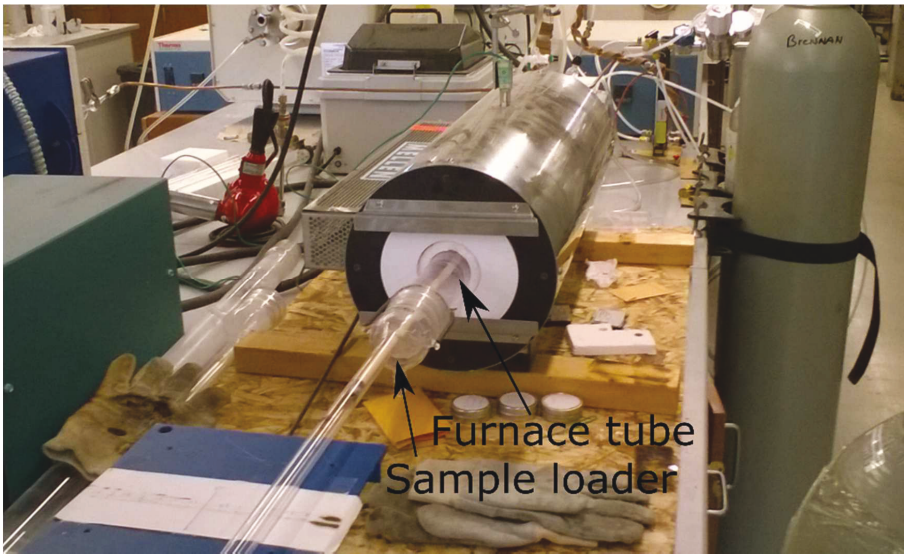

Figure 3-6 Mellen furnace used at University of Pittsburgh.

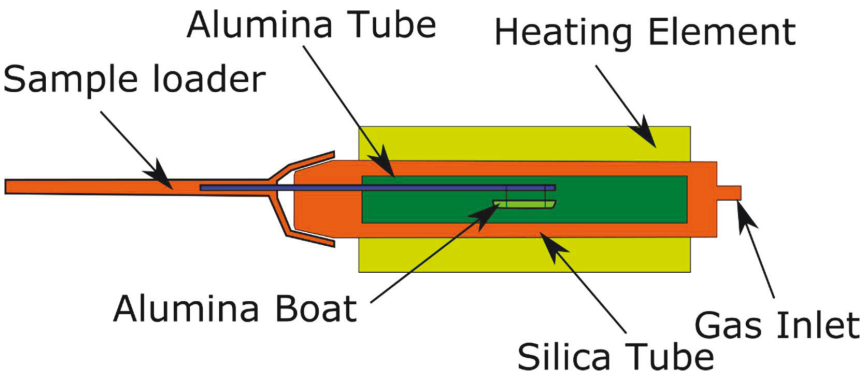

Figure 3-7 Schematic of Mellen tube furnace used for experiments on industrial alloys.

Both the beryllium-containing and beryllium free industrial alloys were tested in this furnace to understand the effects of beryllium on the formation and growth of the oxide layer. By testing two similar alloys oxidized under the same conditions, any differences in the oxide layer will help to elucidate beryllium's impact on the oxidation. The mass before and after oxidation was recorded primarily allow comparison to previous TGA work carried out by others such as Cochran (5) and Thiele (13).

Oxidation samples were cut to 13.5 x 25.0 x 1.5 mm using a SiC abrasive saw, then ground to a 22 µm (800 grit) finish on SiC paper and washed in ethanol. The mass of the sample was recorded on a Mettler Toledo balance with 0.01 mg precision. Table 5 shows the times and temperatures used for these experiments. The time was selected to study the oxidation during the incubation period as this period is of the most interest for controlling oxidation of Al-Mg alloys.

Table 6 Exposure times and temperatures used for experiments carried out on the industrial sample. X indicates a single experiment was done at the specific time and temperature, XX indicates two experiments were done at the specific time and temperature.

Alloy	**5182**				**5182+Be**		
Time	**10 Min**	**30 Min**	**120 min**		**10 min**	**30 min**	**120 min**
500 °C	X	XX	X		X	XX	X
550 °C	X	X	X		X	X	X
625 °C	X	XX	X		X	XX	X
700 °C	X	X	XX		XX	X	X
750 °C	X	X	XX		X	X	X

3.2.2 Horizontal tube furnace NTNU

The second tube furnace was used to test the oxidation of the model alloys that contained 100 ppm beryllium. The Nabertherm horizontal tube furnace used is shown in Figure 3-8 and schematically Figure 3-9. The setup and sample loading system were similar to the tube furnace in Pittsburgh, with the exception that the glass tube is replaced with an alumina tube with water cooled steel end flanges and the tube diameter increased to 75 mm. The sample preparation was carried out in a similar fashion; however, the samples were polished to a 1 µm finish with a water-based diamond suspension, then rinsed in ethanol. This was done to give a smoother surface after oxidation to allow a more accurate composition depth profile to be generated. As the effects of the beryllium had been confirmed by the industrial samples, the focus of the tests on the 100 ppm beryllium samples was to understand the mechanism behind the protective effect. The oxidation times and temperatures were selected to enable detailed characterization and are given in Table 7 below. While the primary interest was the effects of beryllium on the oxidation in the liquid state, a number of experiments were carried out below the melting point of the Al-Mg alloy, as the oxide layer was significantly distorted during oxidation of the liquid samples. This uneven surface made detailed analysis of the oxide layer difficult hence, it was decided to carry out the oxidation in both the solid and liquid state and relate the detailed analysis results from the solid state to the liquid state.

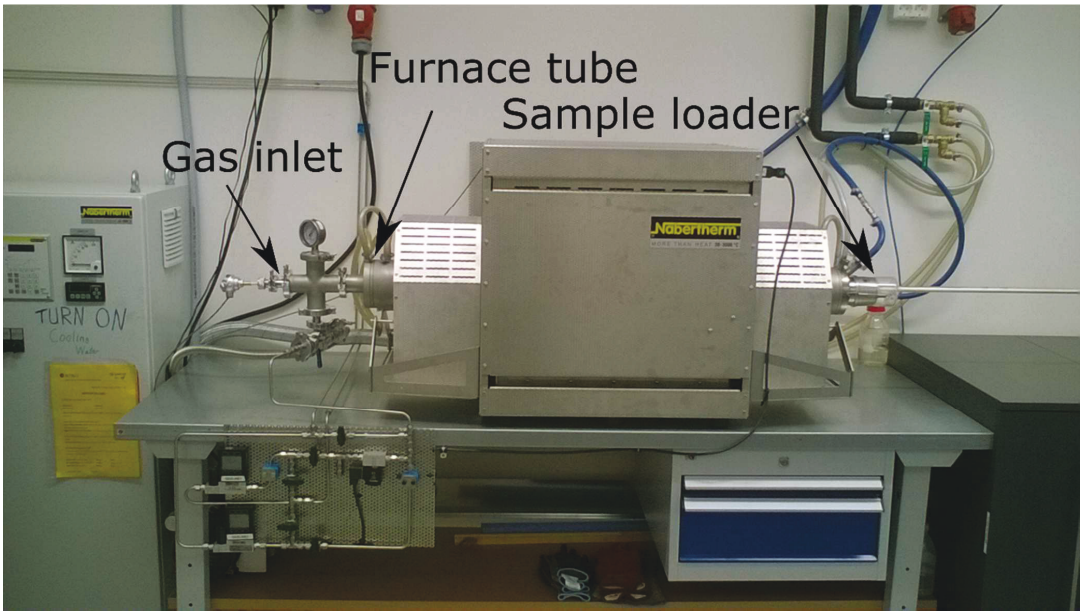

Figure 3-8 NTNU tube furnace from Nabertherm use for oxidization experiments.

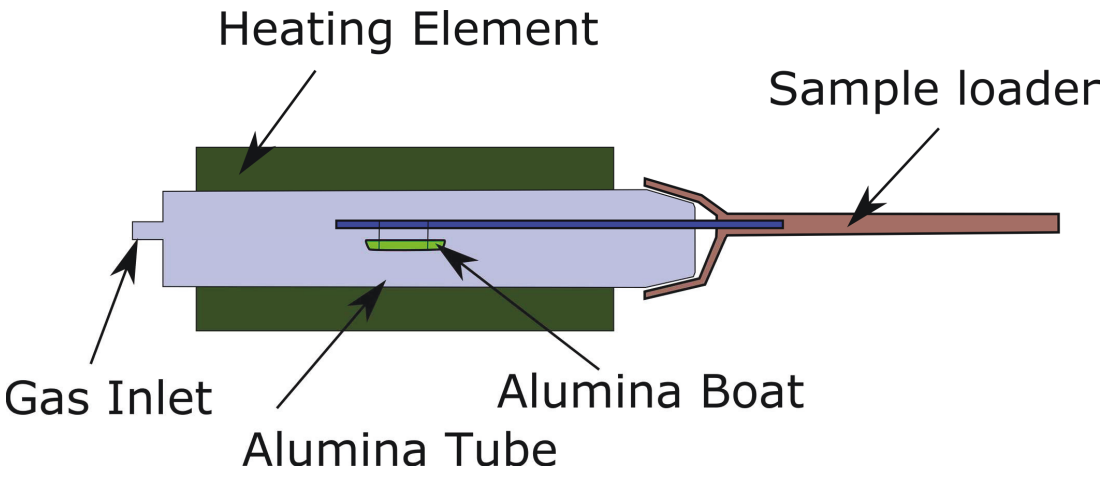

Figure 3-9 Schematic of Nabertherm tube furnace at NTNU.

Table 7 Experimental matrix horizontal tube furnace experiments on the 100 ppm beryllium samples.

Time (min)	30	45	60	90	240	360
550 °C	X	X	X	X	X	X
700 °C	X					X

3.2.3 6063 series experiments

A series of supplementary CO_2/CO experiments in the NTNU tube furnace were carried out on an industrial 6063 alloy containing 0.72 % Mg and 0.52 % Si. Samples of the 6063 alloy were polished to 1 µm finish and place in the preheated furnace at 500 and 550 °C. The samples were then exposed to 5%CO_2/Ar, 5%CO/Ar or 100%Ar for 30 or 90 minutes. The surface of the samples was then characterized in the SEM to highlight the effects of CO_2 compared to CO and argon.

3.2.4 Thermogravimetric analysis

To study the effects of CO_2 and yttrium, erbium and strontium additions on the oxidation rate and mass gain, a Linseis PT 2400 TGA was used as shown in Figure 3-10 and schematically in Figure 3-11. This TGA uses graphite resistance heating elements to heat the sample to a maximum of 1740 °C. The sample and balance are isolated from the heating elements via a sealed alumina tube. The alumina crucible with the sample is placed on an alumina rod, containing a type-B thermocouple that is directly connected to a balance with an accuracy of 10 µg. The mass of the sample was recorded every second, however, for analysis sampling every 2 seconds gave sufficient resolution in the data to see any trends or changes.

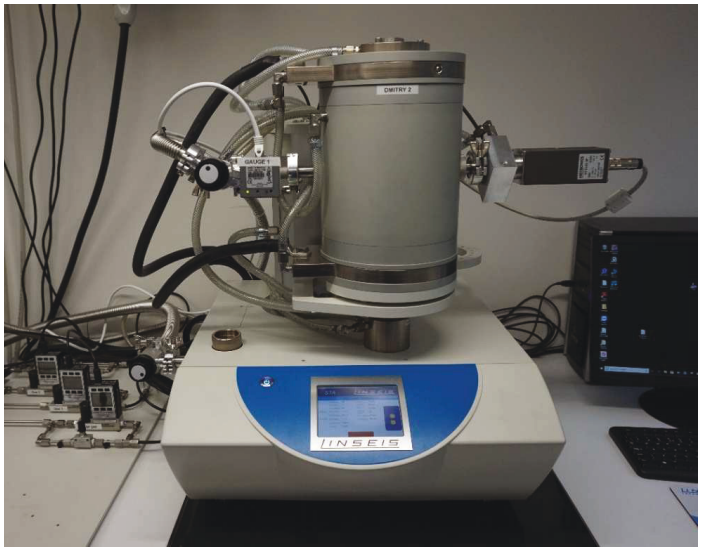

Figure 3-10 Linseis TGA used for CO_2 and alternate alloy experiments.

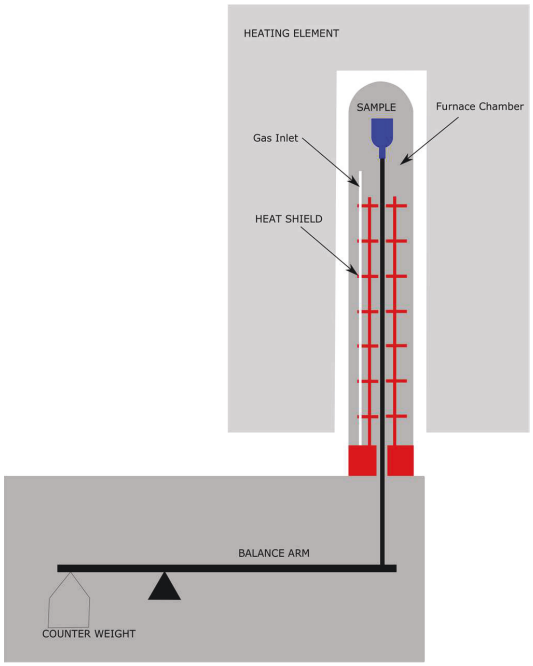

Figure 3-11 Schematic of Linseis TGA used for CO_2 experiments and alternative alloy experiments.

3.2.4.1 CO_2 atmosphere

For the experiments investigating the effects of CO_2 additions to the atmosphere on the oxidation rate, the model 5 % magnesium alloy (without beryllium) was used for all the experiments. Samples measuring 1.5 mm thick and 10 mm in diameter were polished to a 1 µm finish on the top side and a 22 µm finish on the bottom side. After polishing, the sample was rinsed and stored in ethanol to minimize oxidation in ambient air. The sample was placed in an alumina crucible and loaded into the TGA. Generally speaking, the sample did not wet the crucible after oxidation and could be easily picked up out of the crucible after the experiment. As a result, each crucible was used for multiple experiments.

After the sample was charged into the TGA the furnace chamber was evacuated to a vacuum of at least 5.9 $x10^{-2}$ mBar and refilled with the specific gas to be used for the experiment. Several different gas programs were used. For the majority of the experiments, the furnace was refilled with 5.0 purity argon. The argon atmosphere was maintained until 750 °C was achieved at which point the process gas (Air, CO_2 and Argon mixtures) was introduced for the course of the isothermal period. After the isothermal period, the process gas was switched off and argon flushing begun. In certain cases, the process gas was added from the start of heating not just during the isothermal period. A gas flow rate of 0.2 lpm was used for all experiments. Table 8 show the experimental matrix covering the experiments completed for the study on the effects of CO_2 atmospheres.

Table 8 Experimental matrix for CO_2 experiments done at 750 °C, heating and cooling was done under argon with gas 1 and gas 2 flow starting once the isothermal period had been reached, unless otherwise noted.

	Stage 1			Stage 2			Notes
EXP #	**Gas 1**	**Gas 2**	**time**	**Gas 3**	**Gas 4**	**time**	
1	100 Air		420				
2							
3	20 CO	80 Ar	420				
4	5 CO_2	95 air	420				
5	20 CO_2	80 air	420				
6							
7	50 CO_2	50 air	420				
8	20 CO_2	80 Ar	420				
9	20 CO_2	80 air	30	100 air		390	
10							
11	20 CO_2	80 air	60	100 air		360	
12	100 air		60	20 CO_2	80 air	360	
13	100 air		till breakaway	20 CO_2	80 air		
14							
15							
16	20 CO_2	80 air	420				from start
17	20 CO_2	80 air	420				Not flowing
18							
19	20 CO_2	80 Ar	420				Not flowing
20							

For experiments 17-20, 20%CO_2/80%air or 20%CO_2/80%Ar was flushed through the furnace from the start of heating. At the start of the isothermal period the gas flow was shut off and held static in the furnace for the entire isothermal period of 420 minutes. This allowed any gas reaction products to remain in the furnace longer than they would under flowing gas conditions.

A standard heating program was set for all the experiments in which the sample was heated at 50 °C/min from room temperature to 500 °C then at 10 °C/min to 750 °C. A slower heating rate for the last 250 degrees was used to prevent the temperature from overshooting the 750°C set point.

Once 750 °C was achieved the sample was held for a maximum of 420 minutes before it was cooled as fast as the furnace would allow. The sample cooled to under 500 °C within 5 minutes and down to room temperature within 60 minutes. Shorter isothermal hold times were also employed to give characterization samples of the oxide layer from intermediate times.

3.2.4.2 Alternate alloy additions

The experiments to test the effects of yttrium, erbium and strontium on the oxidation were carried out in a similar method as those for the CO_2 atmosphere with a few notable exceptions. First, the top surface of the sample was only ground to a 5 µm finish with SiC paper. Removing the diamond polish stage, previously used, was done to reduce the risk of surface contamination from the diamond suspension. Second, a flow rate of 0.05 lpm was used to minimize noise in the balance system caused by higher flow rates. For the alternate minor elements each of the three elements were run with multiple parallels for each alloy element at 750 °C and compared to Al-Mg and Al-Mg+Be baselines.

3.3 Characterization methods

The mass change of a sample can only give a limited amount of information about the protective mechanism at work. To gain a full understanding of the different protective mechanisms, detailed characterization of the oxide layer, oxide-atmosphere interface and oxide-metal interface was required. A variety of methods were employed to characterize the sample after oxidation. These methods can be split up into two categories: morphological and compositional and are summarized in Table 9. None of the methods could provide a complete understanding alone, but by combining multiple methods an understanding of the protective mechanism could be obtained.

Table 9 Characterization methods used in this work and desired outcome result from use of the method.

Method	Signal	Primary purpose	Resolution	Analysis area	Analysis depth	Desired result
FIB	Electrons	Morphological	1nm			Images of both surface and cross-section of the oxide layer and how process parameters effect the morphology of the layer
SEM	Electrons	Morphological	2nm			Effect of process parameters on the surface morphology of the samples
TEM	Electrons	Morphological	<1nm			Detailed understanding of the structure of the oxide layer
EDS	X-rays	Composition		1µm	1µm	General composition of the oxide layer and any phases within it
XPS	Electrons	Composition		100 µm	under 5 nm	Depth profile through the oxide layer showing how the ratio of each phase changes with depth
XRD	X-rays	Composition		>1 mm		Oxide phases present in powder samples
EELS (TEM)	Electrons	Composition		0.5 nm	Sample thickness	Composition of any second phase in the oxide layer

3.3.1 FIB

The main use of the Focused Ion Beam miller (FIB) for this work was to characterize the morphology of the oxide layer as it can be used to image both the surface and cross-section of the oxide layer. A cut was made perpendicular to the sample surface through the oxide layer into the base metal with the gallium ion gun. The sample can then be imaged via the electron gun (SEM). By using this method, many issues with the standard method of mounting and polishing samples can be avoided as the ion beam is significantly less destructive than grinding and polishing, and avoids edge rounding which is critical for examination of thin oxide layers. Several samples were mounted in epoxy and polished in the traditional way of grinding with SiC paper and polishing with 1µm diamond suspension, but it was found that this resulted in edge rounding and a loss of a significant portion of the oxide layer.

A FEI Helios NanoLab DualBeam FIB was used to analyze the morphology of the oxide layer, but provided limited chemical composition information. Chemical composition could be gathered via a standard EDS system, however, the accuracy was limited especially for the alloy elements in trace quantities. The FIB has 2 separate columns: an ion gun and an electron gun. The electron gun is mounted vertically, and the ion gun is tilted at 52° from the vertical axis. The ion gun employed gallium ions and was used to mill the sample surface to create a cross-section of the oxide layer as shown in Figure 3-12. Additionally, there is a platinum gas injection needle that can be used to deposit platinum on the surface. Imaging was done with an in-lens detector that employed secondary electrons that were generated by the electron gun that operates on the same principles as a SEM with a maximum resolution of 0.9 nm. Imaging with the ion gun was possible, however, the resolution was low and caused minor damage to the sample surface.

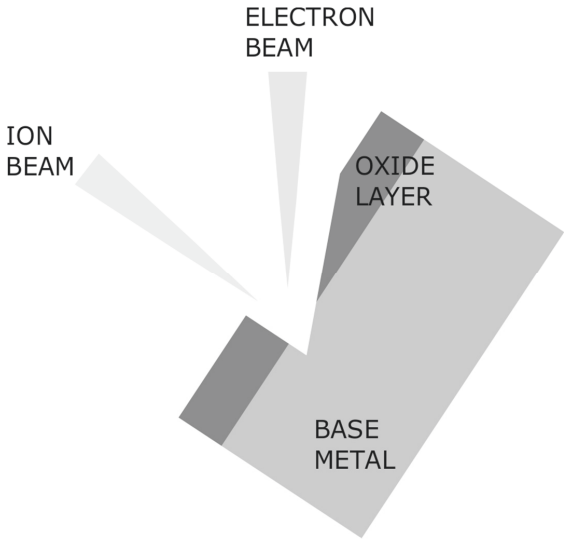

Figure 3-12 Schematic showing how the cross-section was made to characterize the oxide layer in the FIB.

The oxide layer on the samples is non-conductive and prone to charging depending on the thickness. The thickness generally became problematic if the oxide layer exceeded 750 nm. For the samples from Pittsburgh, the samples were first sputter-coated with a thin layer of platinum/palladium. This was done to make the surface of the sample conductive thus reducing charging and improving the resolution of the images. A Cressington 208 HR B sputter coater was set to give a 30 nm thick coating, however, the final coating thickness was significantly smaller. The requirement to coat the sample before analysis is one of the main downsides of the FIB, as the coating effects the overall sample cleanliness and could affect other analysis methods. For this reason, coating was excluded on later samples as acceptable resolution was obtained without.

Once the sample was loaded into the FIB, an area that was representative of the entire sample was selected after scanning the entire sample surface at a low magnification. Care was taken to ensure that any topography in the sample did not cause issues during milling or tilting the sample. Once the area was selected, a series of surface images were taken ranging from 100-50000x magnification. After these images had been collected, the platinum injection needle was used to coat an area 5x40 µm in size and at least 1 µm thick. The purpose of this coating was to protect

the surface during ion milling. The deposition will cause minor damage to the top nanometers of the surface of the oxide layer, therefore, any information that is required from this layer must be gathered from the surface analysis before the cross-section in made.

The cross-section was cut using the gallium ion gun until it extended through the oxide layer and into the base metal as shown in Figure 3-12. Initially, a high beam current was used to allow fast sputtering, the current was reduced in the end to give a final cross-section with a minimal amount of damage. The morphology and thickness of the oxide layer could then be studied.

3.3.2 SEM

A Zeiss Supra 55 Scanning Electron Microscope (SEM) was used to analyze the surface of the oxidized samples. The images gathered from the SEM were of similar quality to those taken in the FIB. However, the absence of an ion gun means only images from the top surface were obtained.

The SEM was equipped with an Ametek Octane Pro-A Energy-Dispersive X-ray Spectroscopy (EDS) system that can be used to gather chemical data. The EDS system had a limited use in analysis of the oxide layer, primarily due to the large analysis volume in comparison to the oxide layer thickness. The chemical composition signal for the EDS comes from a depth of up to 1 μm. This thickness was several times larger than the oxide layer thickness on many of the samples, meaning a significant portion of the analysis volume will be aluminum metal not the oxide layer. Additionally, the EDS system cannot accurately detect light elements such as beryllium or carbon.

3.3.3 TEM

A Joel JEM ARM200F Transmission Electron Microscope (TEM) was used to analyze the oxide layer on select samples tested under a CO_2 atmosphere. The TEM was used to get detailed morphological understanding of the structure of the oxide layer and identify any carbon containing layer. In addition, the composition of the oxide layer was confirmed. TEM samples were prepared by milling in the FIB. Additionally, the TEM was capable of carrying out Electron Energy Loss Spectroscopy (EELS) to analyze the chemical composition of select phases with a resolution of 0.5 nm.

3.3.4 XPS

X-ray Photoelectron Spectroscopy (XPS) was the primary method used to obtain a chemical composition analysis through the oxide layer and down into the bulk metal. The XPS is a surface sensitive quantitative technique that analyzes the top nanometers of a surface with a surface analysis area of approximately 100 µm x 100 µm. The XPS is equipped with an argon sputter gun that allows the surface layer in the analysis area to be sputtered away after which a new XPS spectrum can be generated. By repeating this cycle, a depth profile through the oxide layer can be generated. The amount of material removed in each sputter cycle can be varied by changing the sputter time. For the samples investigated, a target of 10 nm/cycle was set. A target of 10 nm/cycle will give a good resolution and limited the chances of sputtering through any thin layers.

An XPS spectrum gives the binding energy of any atoms present in the analysis area. The binding energy is useful for the analysis of an oxide layer as it gives information about the oxidation state of an element. This e.g. allows magnesium that is present as a metal to be distinguished from magnesium present as MgO. This allowed an accurate determination of the amount of magnesium metal in the oxide layer.

For the work in this thesis 3 different XPS's were employed, as two of the instruments had periods of long down time due to maintenance and repairs. The three XPSs are as follow:

1. Kratos Analytical AxisUltra^{DLD} using monochromatic Al Kα with a 110 µm diameter analysis area. Argon sputtering at 4 kV. (Oslo instrument)
2. Thermo Scientific Thetaprobe XP spectrometer using monochromatic Al Kα with up to a 400 µm diameter analysis area. Argon sputtering at 4 kV. (Oslo instrument)
3. Kratos Analytical AxisUltra^{DLD} using monochromatic Al Kα with a 100 µm diameter analysis area. Argon sputtering at 4 kV. (Trondheim instrument)

3.4 Supplementary experiments

To give supplementary information to the oxidation experiments, two sets of experiments were carried out and are described in detail below.

3.4.1 Oxide stability

As little information in respect to the phase stability of the MgO-BeO-Al_2O_3 ternary system is available a series, of oxide stability experiments were undertaken. In these experiments the three oxide powders were mixed in either a 1:1:1 or 1:1:2 (MgO:BeO:Al_2O_3) ratio and heated to 1100 °C and held for 7 hours in a tungsten crucible. For HSE reasons, the samples were heated in the TGA as the sealed alumina tube in the furnace would contain any BeO powders that may escape the crucible and allow easy cleaning of the contaminated tube afterwards. The following powders were used:

- 99.9 % γ Al_2O_3
- 99.998 % MgO
- 99.95 % BeO

The primary goal of the experiments was to see if the $BeAl_2O_3$ or the $MgAl_2O_3$ phase would form. To determine if any new phases formed after holding at 1100 °C, the samples were examined with powder X-Ray Diffraction (XRD). A D8 Focus with Cu kα radiation and a Lynxeye detector was used with data processing done in the Diffrac.Eva XRD software from Bruker, utilizing the Crystallography Open Database. After removal from the crucible, the powders were crushed by hand as a minor amount of sintering of the small particles had occurred. The powder was then placed in a standard XRD sample holder and covered with Kapton film to prevent the BeO powder from escaping and contaminating the lab.

3.4.2 Wettability and reactions between alloys and oxides

To examine the reaction between Al-Be alloys and Al_2O_3 and MgO, tests were carried out in a sessile drop furnace shown in Figure 3-13. Use of this furnace allowed the reaction between the metal and oxide to be examined including the phase contact angles. As aluminum is readily oxidized, a several nm thick layer of oxide will exist on an aluminum surface upon exposure to any oxygen. To study the interaction between the metal and oxide, this native oxide layer must be removed. As an oxygen partial pressure below 4×10^{-32} is thermodynamically required to avoid the oxidation of aluminum at 1100 °C, extra steps must be taken to produce a sample without an oxide layer. The simplest method to achieve a metal sample with-out an oxide layer is to employ

both a high temperature and high vacuum. At temperatures over 1000 °C and a vacuum greater than 10^{-5} mBar, the oxide layer will evaporate as the flux of oxygen away as AlO gas exceeds the flux of oxygen to the surface (65).

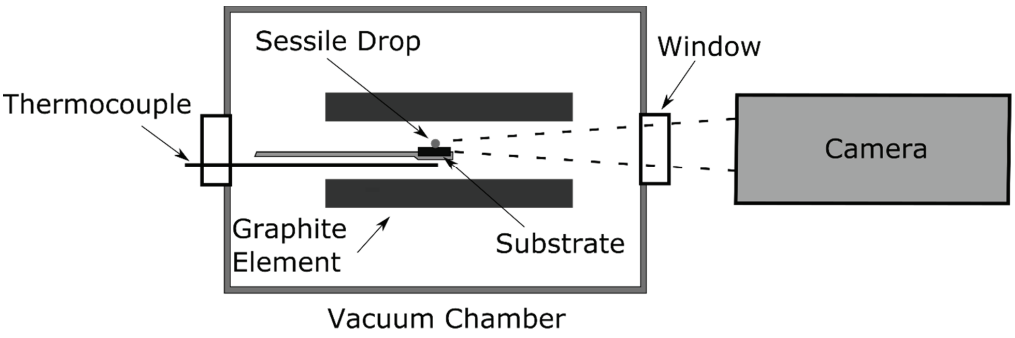

Figure 3-13 Sessile drop furnace used to study reaction between Al-Be and Al_2O_3 and MgO substrate.

A 99.7 % pure Al_2O_3 substrate and 98 % pure MgO substrate were used along with pure aluminum (99.999 %) and aluminum doped with 30 or 60 ppm of beryllium. The MgO was yttrium stabilized, and therefore contained 2 % Y_2O_3. It was decided to test the samples at temperatures over 1100 °C and a vacuum of 10^{-5} mBar to allow the oxygen layer to be quickly removed. The sample was heated at 713 °C/min to 950 °C and 50 °C/min to 1100 °C and held for 2 hours. This heating program was based on previous work carried out by Bao (65) that showed that after 2 hours, the entire oxide layer had been removed and a stable contact angle had been achieved.

After reaction, the samples were mounted in epoxy and cut in half to allow the interface between the metal and substrate to be examined. Maps of the metal-substrate interface were made with Electron Probe Microanalysis (EPMA), which allowed any changes in the composition of the substrate to be noted and if the addition of beryllium to the metal had any impact on the interface reaction. The contact angle between the metal and substrate was also measured.

4. Results and Discussion

Beryllium additions and CO_2 cover gas have been shown to have a marked inhibiting effect on the oxidation of Al-Mg alloys. The goal of this work has been to obtain a better understanding of their inhibiting mechanisms, to be able to propose alternate methods to beryllium additions to protect Al-Mg melts from excessive oxidation. These oxidation inhibiting mechanisms have been discussed in detail in the published papers, but are presented briefly here and summarized in Table 10. General conclusions that are drawn from the specific inhibiting mechanisms at play with beryllium and CO_2 will be developed and discussed. These conclusions will be discussed next to the results from the work on the proposed alternate alloying elements of yttrium, erbium and strontium to provide thoughts on a route forward to protecting Al-Mg melts from excessive oxidation that avoids the current health risks associated with beryllium.

Table 10 Summary of results from experimental work

Experiment	Furnace and temperature	Analysis methods	Results	Published
Oxidation and analysis of industrial alloy, 5182, 5182+2ppm Be	University of Pittsburg horizontal tube furnace, 500-750 °C	Mass change, FIB	Addition of Be to 5182 alloy resulted in up to a tenfold reduction in oxidation. Be addition slowed transport of Mg through the oxide.	Light Metals 2017 (paper 1) and Met Trans B (paper 3)
Oxidation and analysis of model alloy: 100 ppm Be 5% Mg	NTNU, horizontal tube furnace	FIB, XPS	Be addition resulted in the formation of a BeO-$BeAl_2O_4$ layer at the oxide-metal interface.	Light Metals 2018 (paper 2) and Met Trans B (paper 3)
Oxidation and analysis of model alloy: 5% Mg in CO_2 containing atmosphere	NTNU horizontal tube furnace, TGA	TGA, FIB, XPS, TEM	CO_2 can inhibit the oxidation of Al-Mg alloys. Protective effects of CO_2 will linger for a period after CO_2 is removed. CO_2 addition at the onset of breakaway oxidation can slow the oxidation rate and stop breakaway. CO_2 adsorbs onto the initial MgO oxide layer and acts as a "cap" to reduce the transport of Mg vapor through the oxide layer.	Submitted to Industry & Engineering Chemistry Research (Paper 4)
Oxidation and analysis of model alloy: 5% Mg + Y, Er or Sr	NTNU horizontal tube furnace, TGA	TGA, FIB, SEM	Er and Sr reduced the time for breakaway oxidation to occur, yttrium had limited effect. Segregation to the surface was found and the formation of discrete particles below the MgO layer observed.	Submitted to Light Metals 2019 (paper 5)
Oxide stability of MgO, BeO and Al_2O_3	NTNU TGA, 1100 °C	XRD	Both $BeAl_2O_4$ and $MgAl_2O_4$ can form simultaneously in a mixture of Al_2O_3, MgO and BeO.	Met Trans B (paper 3)
Wettability and reactions between Al+0, 30, 60 ppm Be and Al_2O_3 and MgO	NTNU Sessile drop furnace, 1100 °C	EPMA	Addition of Be has little effect on the contact angle between Al and Al_2O_3. Al and MgO not stable under a vacuum at 1100 °C as the formation of $MgAl_2O_4$ is rapid resulting in significant Mg vapor formation.	Met Trans B (paper 3)

4.1 Effects of beryllium

Historically, beryllium is well known to inhibit the oxidation of Al-Mg alloys. The effects of beryllium were conclusively shown in paper 1, where up to a tenfold decrease in the mass gain due to oxidation was found. The effect was shown in both the solid and liquid state and can be seen in Figure 4-1 and Figure 4-2 which show the mass gain curves from 10, 30 and 120 minutes of holding time in a tube furnace for the 5182 and 5182+2 ppm Be alloys.

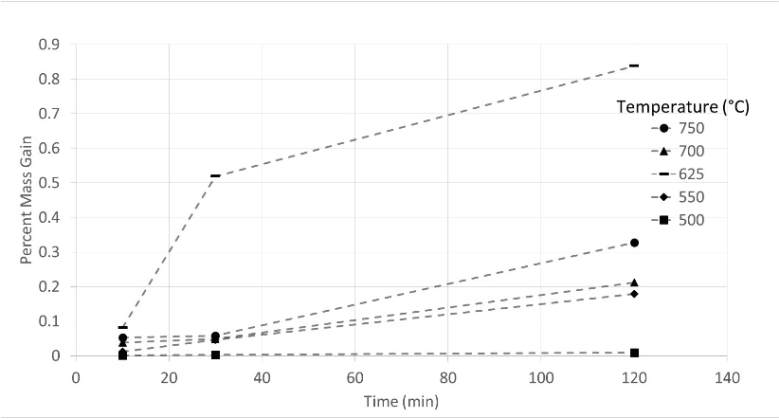

Figure 4-1 Percent mass gain of 5182 sample without beryllium after oxidation in a horizontal tube furnace.

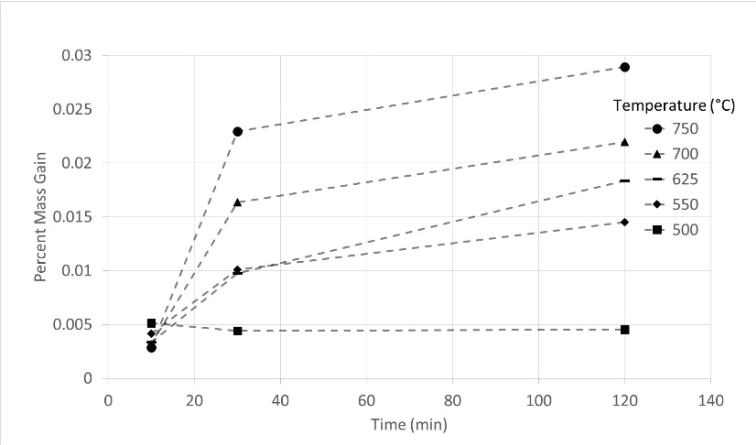

Figure 4-2 Percent mass gain of 5182 sample with 2 ppm beryllium after oxidation in a horizontal tube furnace.

For the beryllium free samples tested at 625 °C the mass gain was about three times higher than the mass gain at 750°C. 625 °C is in the middle of the mushy zone for this alloy, where both solid and liquid phase exist with the liquid phase having a magnesium content of 7 %. This high magnesium content in the liquid phase resulted in an increase in the oxidation rate. The addition of 2 ppm beryllium was enough to suppress this high oxidation in the mushy zone. While the oxide layer on the samples oxidized in both the solid and liquid state appeared to grow outwards with a clear and well defined oxide-metal interface, the oxide layer on the 625 °C sample lacked this clear interface and appeared to grow inwards as seen in paper 1. The inward growth on the sample from 625 °C is likely due to the oxide sinking due to its higher density. The oxide did not sink on the samples from above the melting point due to surface tension holding the layer on the top surface.

For the beryllium free samples, the oxide layer was found to be made up of two layers: a dense MgO layer adjacent to the metal surface and a granular MgO layer on top of the dense layer. It was found that the addition of 2 ppm of beryllium resulted in a large reduction in the granular layer thickness as shown in Figure 4-3 where both the surface and cross-section of the samples from 120 minutes of oxidation at 700 °C are shown. It can be seen that the granular layer covering the beryllium free sample, only exists as a few small granules on the 2 ppm beryllium alloy.

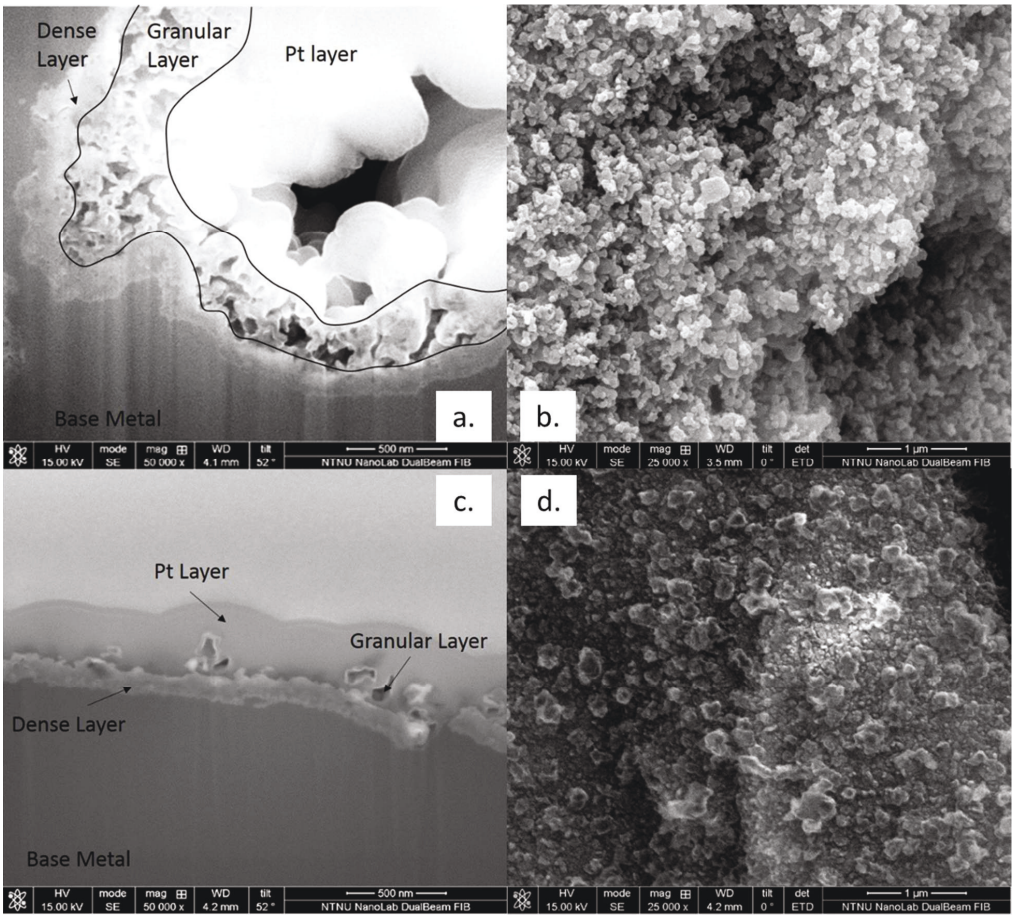

Figure 4-3 Beryllium and beryllium free 5182 samples oxidized for 120 minutes in air at 700 °C. a). Cross-section of beryllium free sample b). Surface beryllium free sample c). Cross-section of sample with 2 ppm beryllium d). Surface of sample with 2 ppm of beryllium.

The XPS depth profiles that are discussed in paper 2 and 3 clearly show that a layer of BeO-$BeAl_2O_4$ forms at the dense (MgO) oxide-metal interface. In the samples oxidized below the melting point the BeO-$BeAl_2O_4$ phase existed at discrete points just below an MgO layer rather than as the uniform layer that was found on the sample oxidized above the melting point. It is believed that at temperatures below the melting point, the beryllium will react at the point with the largest potential for oxidation, resulting in oxide growths on the surface. As the beryllium oxidizes at the points with the highest potential for oxidation, the oxidation of the magnesium is therefore

inhibited, resulting in a reduction of the overall oxidation rate. Longer oxidation times appeared to primarily impact the BeO to $BeAl_2O_4$ ratio, with increasing time resulting in an increase in the amount of BeO. The increased amount of BeO with time is due to the increased segregation of beryllium to the oxide-metal interface with longer times. For the samples above the melting point, no XPS depth profile could be made due to the sample topography, however, a uniform layer was found to exist between at the oxide-metal interface as shown in Figure 4-4. This layer had many similarities to the BeO-$BeAl_2O_4$ layer found on the solid state samples. It was therefore concluded that the BeO-$BeAl_2O_4$ growths found after oxidation in the solid state exits as a uniform layer at the oxide-metal interface above the melting point.

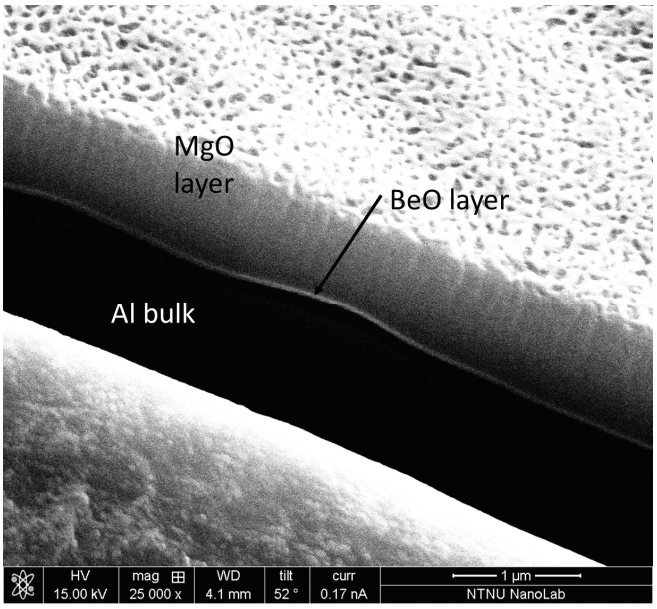

Figure 4-4 Thin BeO-$BeAl_2O_4$ layer at the oxide metal interface of 100 ppm beryllium sample after oxidation at 700 °C

The theoretical amount of beryllium required to protect a melt was calculated from Eq 2.7, proposed by Thiele (13). For an alloy with 5 % magnesium, 15 ppm of beryllium was stated to be required. If the magnesium content is increased to 7 %, as was the case for the liquid phase in the 625 °C samples, 22 ppm of beryllium would be required. In paper 1, it was shown that 2 ppm beryllium was sufficient to protect an industrial 5182 alloy. One possible explanation for the

discrepancy between this study and Thiele's work is that Thiele work tested the protective ability over long periods, up to 160 hours, and a lower beryllium content may only be able to protect the alloy for a shorter time period such as was tested in this work. As the 5182+2 ppm beryllium alloy was provided by an industrial partner, the protective properties of a 2 ppm alloy should be considered sufficient to protect a melt during industrial processing.

Based on the experimental and characterization results, a protective mechanism has been proposed for beryllium on Al-Mg alloys, shown schematically in Figure 4-5. The protective mechanism was found to be the formation of a layer of BeO-$BeAl_2O_4$ at the oxide-metal interface. This layer has a twofold effect in reducing the oxidation. First, as a barrier to slow the transport of magnesium vapor out through the oxide and second, as a barrier separating the aluminum in the alloy from the oxide layer. Oxidation will begin as the alloy is heated from room temperature. A dense, primarily MgO layer will form, due to the high magnesium content compared to beryllium; meaning the probability of an oxygen ion interacting with magnesium is higher. With increasing time, beryllium will segregate to the oxide-metal interface where it will be oxidized to BeO or $BeAl_2O_4$, The BeO-$BeAl_2O_4$ layer will continue to grow until it forms a uniform layer covering the entire oxide-metal interface, at which point further oxidation is significantly inhibited by the BeO-$BeAl_2O_4$ layer.

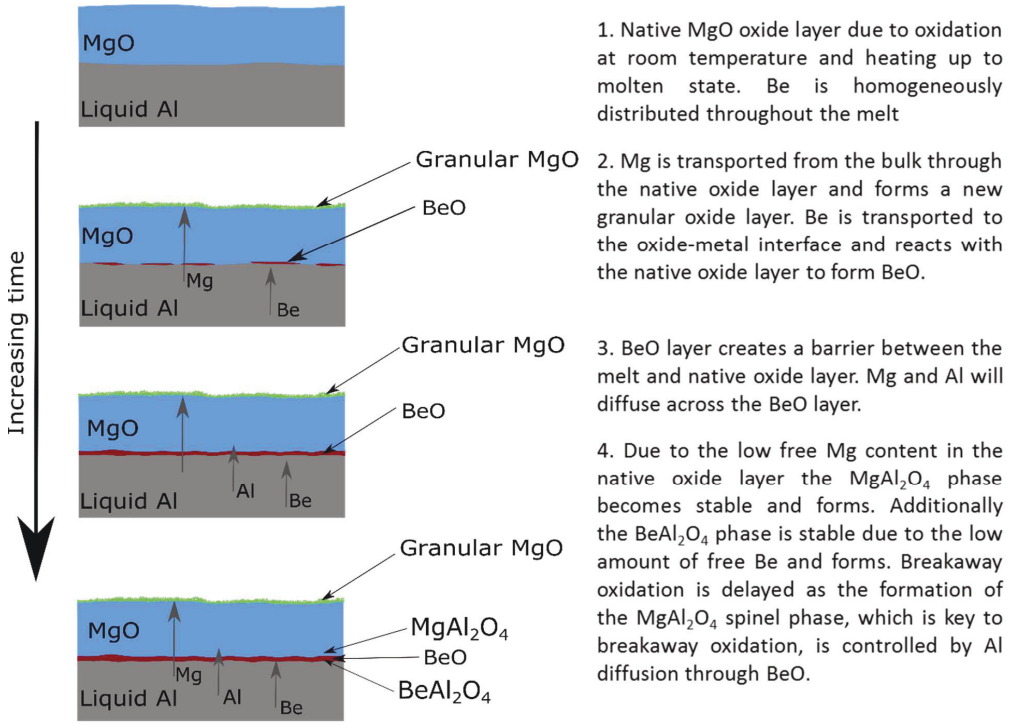

Figure 4-5 Oxidation inhibiting mechanism on Al-Mg alloys provided by beryllium additions.

As was discussed in the theory section, the transformation of MgO to the $MgAl_2O_4$ spinel phase is believed to initiate breakaway oxidation. For the spinel phase to form, the aluminum must be in contact with MgO. The addition of the BeO-$BeAl_2O_4$ layer separates the MgO and aluminum, altering the transformation of MgO to $MgAl_2O_4$ into a diffusion controlled process, which significantly reduces the rate at which the spinel phase can form, thus increasing the time for breakaway oxidation to occur.

4.1.1 Formation of a BeO-$BeAl_2O_4$ layer

Given that the concentration of beryllium in the melt is on the order of a few ppm, the formation of a coherent BeO layer is of interest. For a coherent layer to form from such a low initial concentration, segregation of beryllium to the interface must be significant. On the industrial samples containing 2 ppm of beryllium, a BeO layer could not be detected, however, on the model

alloy containing 100 ppm of beryllium, a BeO-$BeAl_2O_4$ layer averaging 40 nm thick was found after oxidation at 700 °C. A 40 nm thick layer would equate to 16 % of the of the total beryllium content in the sample. This indicates that a significant portion of the beryllium in the sample had been oxidized. The picture is slightly different for the oxidation in an industrial furnace where the volume to surface area ratio is several orders of magnitude larger. The formation of a nanometer thick oxide layer in this case would account for only a small portion of the total beryllium content.

Without an efficient short-term casthouse alternative to beryllium additions to reduce Al-Mg alloy oxidation, a more efficient method for delivering beryllium to the melt could be utilized. As additions of beryllium result in segregation to the surface, a method that added beryllium directly to the oxide-metal interface during casting could allow the overall amount of beryllium added to the melt to be reduced to a more acceptable level. This solution would not serve to eliminate beryllium from the casthouse, but could reduce the beryllium concentration in the final ingot to acceptably low levels.

4.2 Effects of CO_2

As earlier reported, this study also showed that additions of CO_2 to an air atmosphere has a marked effect on the oxidation of an Al-Mg alloy as discussed in detail in paper 4. The addition resulted in a delay in the onset of breakaway oxidation at 750 °C to beyond 420 minutes, whereas, the same alloy in a pure air atmosphere underwent breakaway oxidation after only 210 minutes on average as shown in Figure 4-6. It was found that CO_2 additions to air ranging from 5-50 % protected the melt equally well. As discussed in the literature review, the addition of CO_2 should have little to no effect on the direct oxidation of the alloy as oxygen is plentiful in the gas atmosphere and will preferentially react with the metal as compared with CO_2. Another mechanism is hence at play in the observed reduction of the oxidation rate where CO_2 interacts with the system.

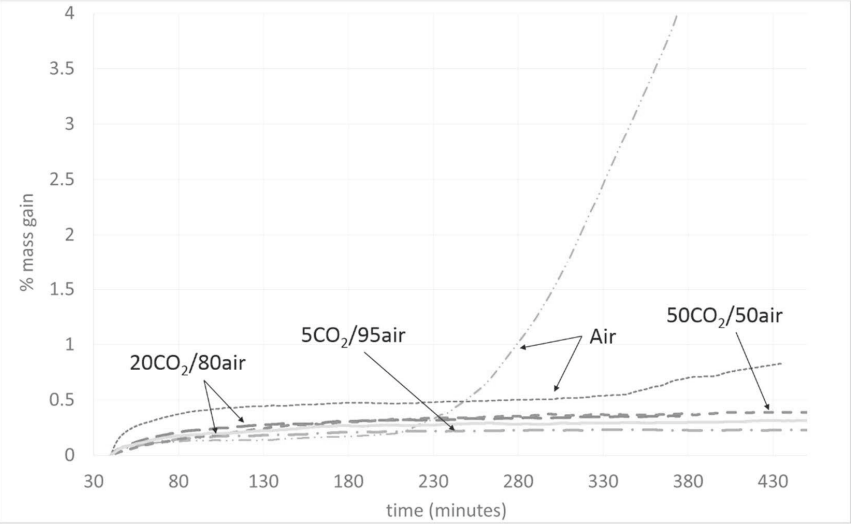

Figure 4-6 Effects of CO_2 additions to air on a 5 % magnesium alloy.

The XPS examination of a sample oxidized in CO_2 is discussed in paper 4. It was shown that a carbon-containing layer existed at the initially formed oxide (MgO)-gas interface. The oxygen and carbon signals from the XPS depth profile are shown in Figure 4-7. Multiple carbon signals were found, with a signal from 286.4 eV being associated with oxygen (labeled C-O bond in Figure 4-7). It was found that the ratio of oxygen (O 1s) to carbon (C-O bond) was 2:1 on the top surface and was reduced to 1:1 as the depth increased. This would correspond to an initial layer of adsorbed CO_2 on the surface which is reduced to other carbonaceous species inside the oxide layer as the oxygen partial pressure is reduced towards the oxide-metal interface (equilibrium pO_2 at 10^{-35} atm for Mg-MgO at 750 °C). Additionally, two unidentified carbon peaks and a carbonate peak were found. The carbonate peak is attributed to a reaction during cooling.

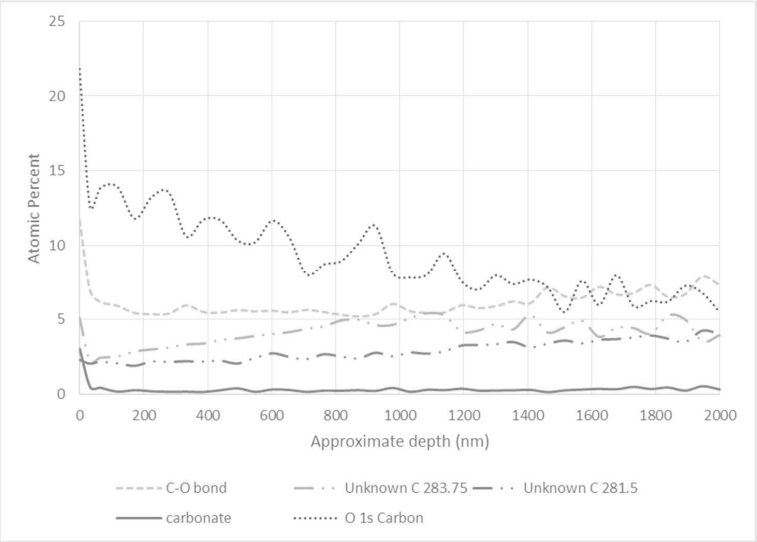

Figure 4-7 Carbon and oxygen signals from the XPS depth profile. Carbon that is bonded with oxygen is termed C-O bond and had an initial ratio of 2:1 (O:C) with the O 1s signal, this ration decreases to 1:1 as the depth increases.

The proposed mechanism by which CO_2 protects an Al-Mg alloy is described below and shown in Figure 4-8. A dense MgO layer is initially formed (as described for the beryllium containing alloys) through reaction between magnesium in the alloy and oxygen. Once CO_2 is introduced, the CO_2 will adsorb onto the oxide surface. The adsorption of CO_2 on the oxide surface does not completely stop the oxidation from occurring as the presence of CO further into the MgO layer indicates that the MgO layer continues to grow around the adsorbed CO_2. Due to the reduced oxygen partial pressure in the oxide layer, the adsorbed CO_2 is reduced to CO and forming Mg-C-O bonds. This reaction acts to modify the structure of the oxide layer, the modified structure acts as a "cap" on the oxide layer acting to slow the transport of magnesium vapor. By trapping the magnesium vapor in oxide layer the activity of the magnesium remains above the critical limit required for the formation of the spinel phase and subsequently the onset of breakaway oxidation is delayed.

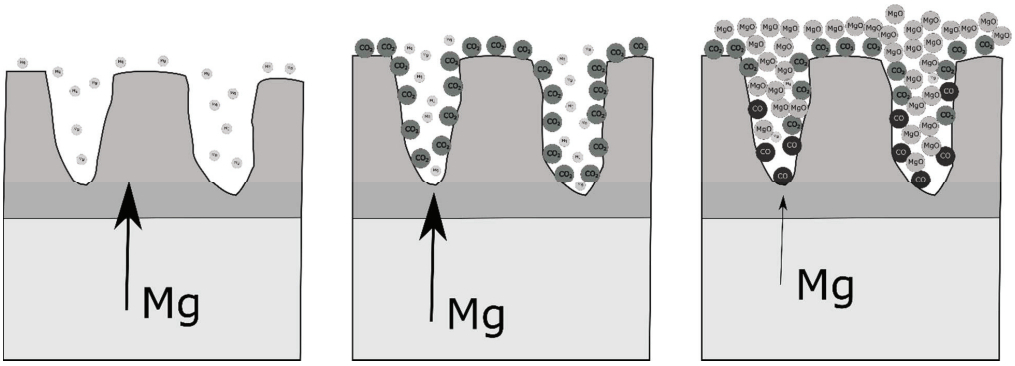

Figure 4-8 Proposed CO_2 inhibiting mechanism for Al-Mg alloys.

4.3 CO_2 as a replacement for beryllium

The addition of beryllium is only seen as a negative due to the negative health impacts beryllium has on the human body. The addition of a specific element at ppm levels to control the oxidation is a relatively easy method to implement from an industrial viewpoint, as alloy additions to the melt are a regular occurrence in the casthouse. Altering the gas composition in the furnace, launders or casting pit would require at least minor retrofitting of the casthouse to install a gas distribution system. The amount of retrofitting and cost would depend significantly on the casthouse in question. However, since CO_2 had a similar effectiveness in inhibiting the oxidation of Al-Mg alloys as beryllium, additions of CO_2 should be considered as a potential replacement for beryllium.

One of the largest advantages of CO_2 is that 100 % coverage in respect to both time and composition is not required to protect the melt from excessive oxidation. The critical step in the use of CO_2 gases for oxidation control is the exposure of the MgO oxide layer to CO_2 gas for a sufficient period of time to allow sufficient CO_2 adsorption to form a protective carbon-containing layer. The CO_2 exposure time required to protect the melt would depend greatly on both magnesium content and the protection time required. For example in the laboratory experiments, it was found that, thirty minutes of 20 % CO_2 in air was sufficient to protect a static 5 % magnesium melt for 300 minutes, however, if the melt was to be held for 420 minutes, more than sixty minutes of 20 % CO_2 in air would be required. Exact exposure times and an optimal concentration of CO_2

would require testing in the casthouse. The effects of CO_2 on dynamic, flowing melts should also be further tested.

As gas-fired furnaces are used in most casthouses, the atmosphere inside the furnace will already contain a notable CO_2 partial pressure as a reaction product from the gas burners. As CO_2 will preferentially adsorb on MgO, it is logical to assume that the dross already has an adsorbed CO_2 layer. This layer could already be inhibiting the oxidation in the furnace compared to a furnace that does not have gas-fired burners. In this situation, increasing the CO_2 content in the furnace could have minimal effect. Potential reductions in oxidation could be had if the CO_2 is added to the launders, filter box or casting mold as the atmosphere at these points is primarily air and the addition of CO_2 would have a notable impact on the amount of oxidation at these points. This may result in a reduction in the number of oxide inclusions in the melt. In this regard, CO_2 would have a similar effect as beryllium, which is often added right before casing to limit oxidation during the casting process.

4.4 Practical considerations and safety concerns with CO_2

The higher density of CO_2 means it would act to replace air, and therefore caution would be required to ensure that a sufficient oxygen level exists at low points in the casthouse before personnel enter an area. Gas detectors and proper working procedures could mitigate most of these health risks. As opposed to beryllium, the health risks of CO_2 are not transferable in that the dross generated under a CO_2 cover gas requires no special handling practices, which is not the case for drosses that contain beryllium and must be treated separately from beryllium free dross.

An advantage of CO_2 being denser than air is that the CO_2 will have a tendency to remain trapped in low points such as casting molds or lauders making it easier to maintain the CO_2 environment and not have it immediately lost to the atmosphere.

The addition of CO_2 gas is extremely effective and the effects of the CO_2 were shown to remain even after the CO_2 had been removed from the atmosphere. This would indicate that establishing a CO_2 atmosphere at the start is more important than maintaining it throughout the casting process. However, CO_2 must adsorb onto the oxide layer, meaning that if a protective atmosphere is established at a specific point in the casting process it will likely have little to no effect on the

oxidation at points further downstream. This is because the oxide formed at points downstream will be a fresh oxide, this fresh oxide will not contain any adsorbed CO_2, it would, therefore be necessary to add CO_2 along the entire casting process to maintain a protective effect at points where oxidation is problematic.

As described above, CO_2 is one of the reaction products from the gas-fired burners used in many casthouses. Cochran tested the effectiveness of the flue gas from the furnace and found it was significantly less effective than CO_2 (5) as the off-gas from the burners contains significant portions of water vapor, which may enhance oxidation.

4.5 Alternate minor alloying elements

The effects of yttrium on the oxidation were touched upon in paper 5, whereas, the results of erbium and strontium were not. The results of the alternate alloying addition that were tried are, therefore, presented in more detail in the following section.

4.5.1 TGA curves

The summarized results from the TGA experiments are given in Table 11 with representative mass gain curves for the yttrium, erbium and strontium containing alloys, shown in Figure 4-9. For comparison, the results of a reference 5 % magnesium alloy with no other additions is also included. As the primary interest in this work is to delay the onset of breakaway oxidation, the time for breakaway oxidation to begin after the isothermal period had been reached was calculated to determine the effectiveness compared to the reference 5 % magnesium alloy. The onset of breakaway oxidation was determined by the criterion below, set to determine at which point the mass change over 1 minute departed significantly a from linear relationship.

$$mass_t(\text{mg}) - mass_{t-1min}(\text{mg}) > 0.02$$

Yttrium additions had a limited impact on the oxidation compared to the reference. Significant variation was found amongst the samples as shown in Figure 4-10. The yttrium samples all broke away and oxidized until all magnesium in the sample was oxidized to $MgAl_2O_4$, with the exception of one sample that did not oxidize to completion. The total percent mass gain an alloy can

experience is determined by the magnesium content. As the total percent mass gain varied from sample to sample it would indicate the magnesium content in the samples varied, perhaps due to alloy inhomogeneity. However, this did not seem to effect the breakaway time significantly as Y2 had a higher magnesium content than Y4 yet it broke away later.

For the erbium alloys, a slight decrease in the time for breakaway oxidation to occur was found with breakaway oxidation occurring at 121 minutes rather than 209 minutes for the 5 % magnesium alloy as shown in Figure 4-11. Breakaway for the strontium alloys occurred shortly after the flow of air began with the average time for breakaway oxidation being 28 minutes, however, one sample broke away immediately upon the introduction of air to the TGA as shown in Figure 4-12.

Table 11 Mass gain and breakaway time for oxidation tests.

Test	Mass Gain (mg)	%Mass Gain	Breakaway Time
Y1	43.7	15.6	328
Y2	42.2	15.6	186
Y3	-	-	452
Y4	31.2	12.9	170
Sr1	29.3	13.3	56
Sr2	29.8	12.5	0
Er1	35.5	14.1	178
Er2	35.08	14.0	78
Er3	35.2	13.4	108
Mg Ref	30.5	13.6	209

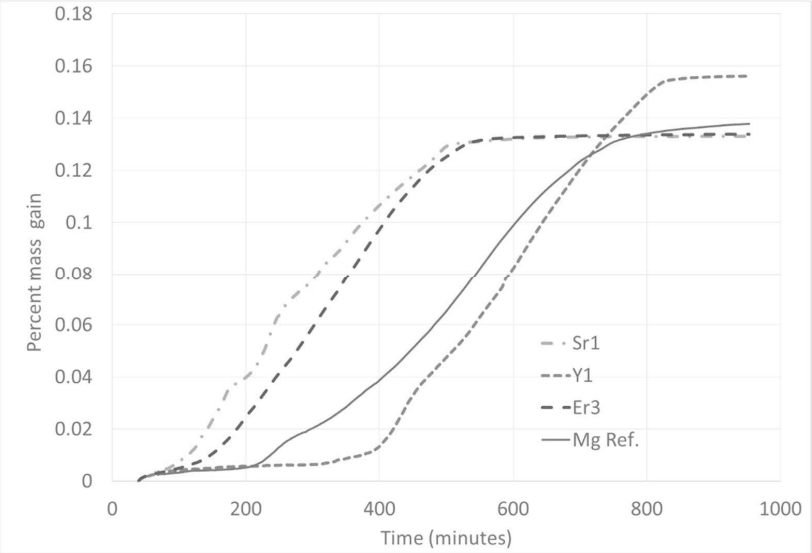

Figure 4-9 Average mass gains of 5 % magnesium alloys containing yttrium, erbium and strontium as compared to the mass gain of an addition-free 5 % magnesium alloy after oxidation at 750 °C.

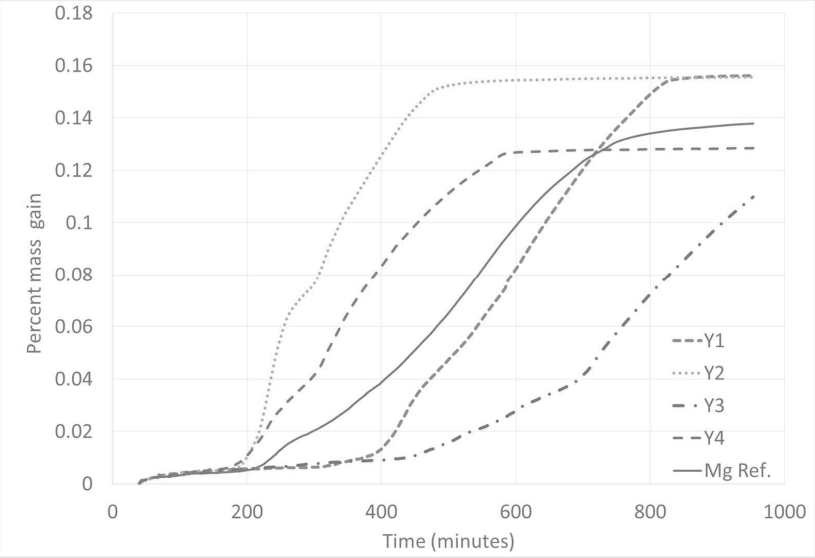

Figure 4-10 TGA curves for yttrium containing alloy oxidized in air at 750 °C showing a large variation between breakaway times and magnesium content.

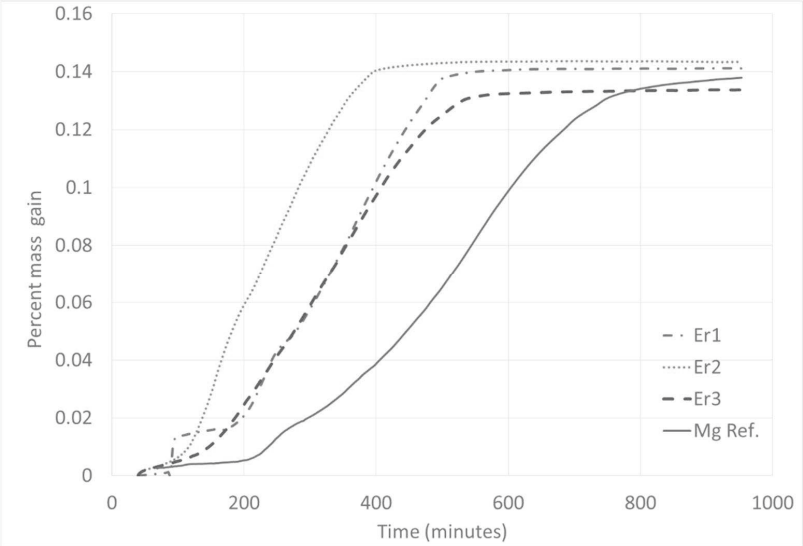

Figure 4-11 TGA curves for erbium containing alloy oxidized in air at 750 °C showing a decrease in time for the onset of breakaway oxidation.

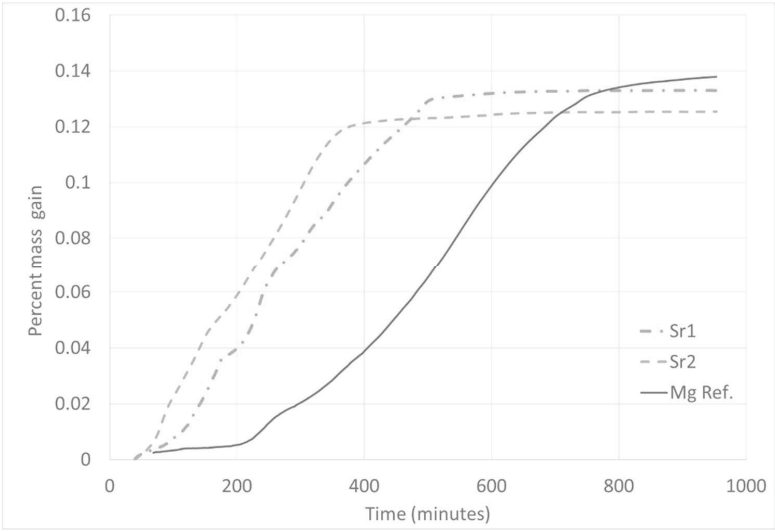

Figure 4-12 TGA curves for strontium containing alloy oxidized in air at 750 °C showing a decrease in time for the onset of breakaway oxidation.

4.5.2 Morphology and composition

The samples were found to be significantly distorted from their original disk shape and were covered in a black oxide layer after oxidation in air for 16 hours. A cross-sectional image of the 5 % magnesium reference without any additions, is shown in Figure 4-13, with the dashed rectangle showing the outline of the original sample shape (10 mm dia. x 1.5 mm). EDS scans showed that the samples were covered in a thick layer of $MgAl_2O_4$ spinel. The presence of the spinel phase was determined from the Mg:O ratio, where a 1:1 ratio indicated MgO and a 1:4 ratio indicated $MgAl_2O_4$. Towards the center of the sample, un-oxidized aluminum was found. Aluminum metal was found inside the $MgAl_2O_4$ layer giving a mixed region of metal and spinel as shown in Figure 4-15.

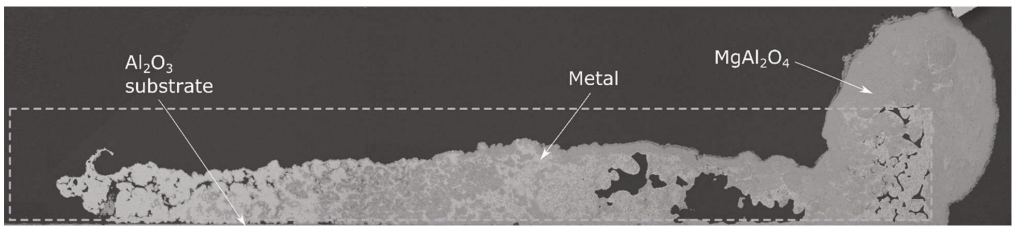

Figure 4-13 Cross-section of reference 5 % magnesium sample oxidized at 750 °C for 16 hours in air (dashed line shows the original sample shape of 10x1.5mm).

4.5.2.1 Yttrium

An overview of the yttrium containing sample oxidized for 16 hours is shown in Figure 4-14, the oxide phase was found to be $MgAl_2O_4$ with no traces of yttrium. An yttrium containing phase was found in the aluminum metal where the yttrium had segregated out into a second phase where the primary component was aluminum as shown in Figure 4-15. This phase existed as discrete particles spread throughout the aluminum. The exact composition of the yttrium phase was not determined as the particle size is less than the analysis volume of the EDS system of the SEM. The measured yttrium content was found to be between 3-5 at %. Given that the yttrium content in the second phase was less than 5 at % it is likely that it was the YAl_3 phase as it is the known phase with the lowest Y:Al ratio as can be seen in the Al-Y phase diagram in Figure 2-33.

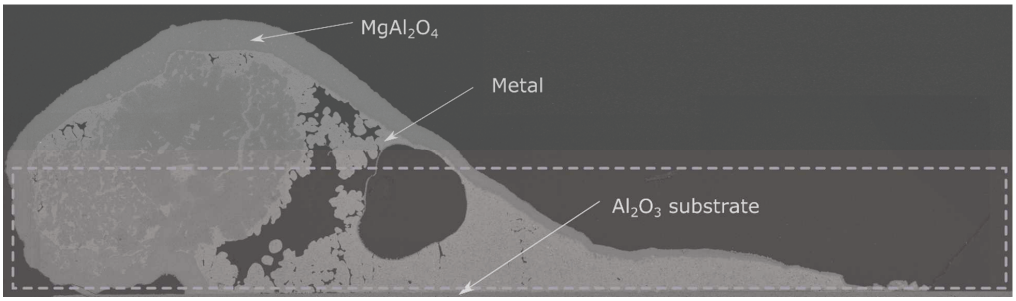

Figure 4-14 Cross-section of 5 % magnesium+yttrium sample oxidized at 750 °C for 16 hours in air (dashed line shows the original sample shape of 10x1.5mm).

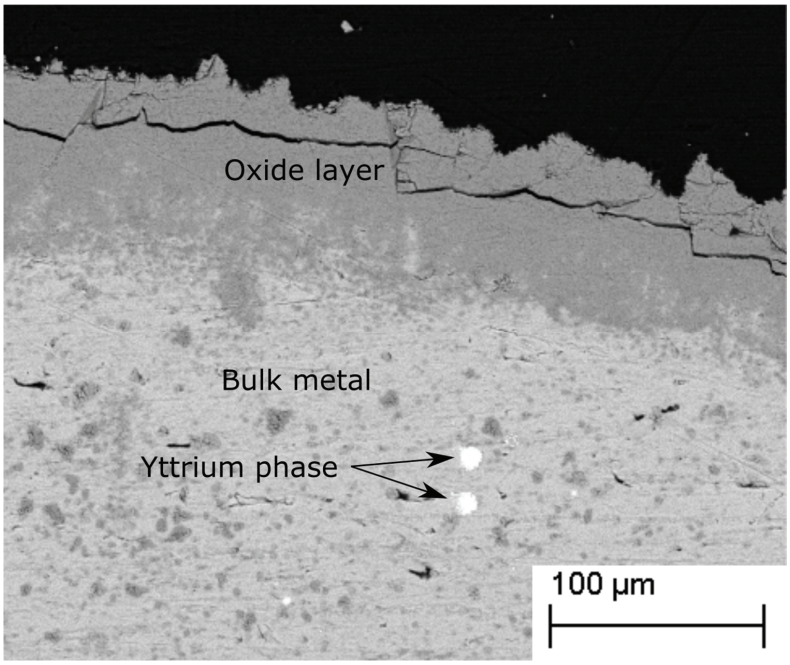

Figure 4-15 Cross-section of sample containg yttrium showing yttrium containing phase after oxidation at 750 °C for 16 hours. In additon the precensce of aluminum metal in the oxide phase can be seen.

Investigation of the yttrium containing sample oxidized for thirty minutes in the tube furnace showed that the yttrium had segregated to the oxide-metal interface as discrete particles, shown in Figure 4-16. The oxide layer was found to be a thin layer of MgO measuring between 130-600 nm

thick, but commonly between 200-470 nm thick. No variation in the Mg:O ratio was seen between the regions containing yttrium and those without, indicating that the yttrium was in the un-oxidized state just below the MgO oxide layer. After 90 minutes of oxidation, the yttrium phase was no longer visible with the backscatter detector on the SEM, but was still detectable with EDS, likely due to a thickening of the MgO layer.

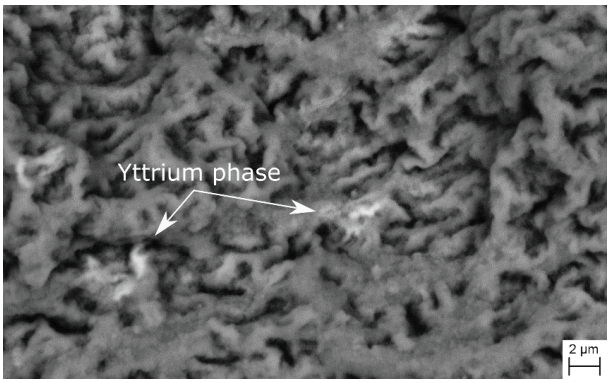

Figure 4-16 Yttrium containing sample oxidized for 30 minutes at 750 °C showing yttrium phase near the surface of the MgO oxide layer.

The lack of a clear protective effect such as was seen on the ignition proof magnesium alloy could be the result of insufficient yttrium to form a protective layer. The Y:Mg ratio was only 1:500 as opposed to the 1:25 seen in the ignition proof magnesium alloy reported by Ravi Kumar (53) it is possible that higher yttrium concentrations could inhibit oxidation.

4.5.2.2 Erbium

A cross-section of the erbium sample after oxidation for 16 hours at 750 °C is shown in Figure 4-17. Erbium was found to exist in the un-oxidized state, but unlike yttrium it was found in close proximity to both the $MgAl_2O_4$ and metal phase as shown in Figure 4-18. This would indicate that erbium had a stronger tendency to segregate to the oxide layer than yttrium. Overall, the total amount of erbium appeared diminished compared to the yttrium sample as fewer erbium containing phases could be found. This indicated that the erbium segregated to the oxide layer and was lost from the sample. While erbium was found in proximity to both the metal and oxide, there

was no indication that the erbium existed in the oxidized state, rather as un-oxidized metal within the oxide.

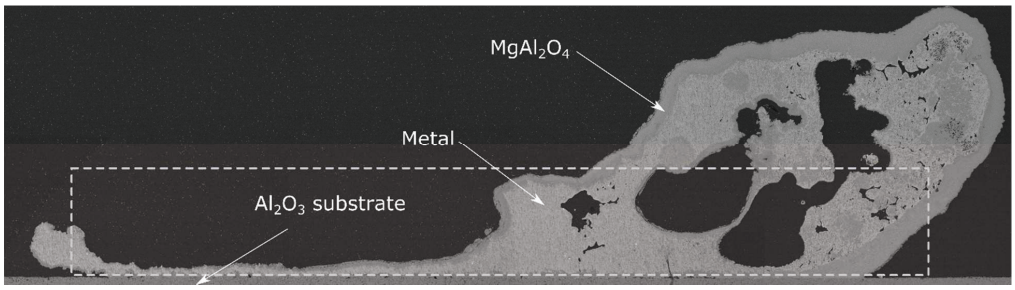

Figure 4-17 Cross-section of 5 % magnesium+erbium sample oxidized at 750 °C for 16 hours in air (dashed line shows the original sample shape of 10x1.5mm).

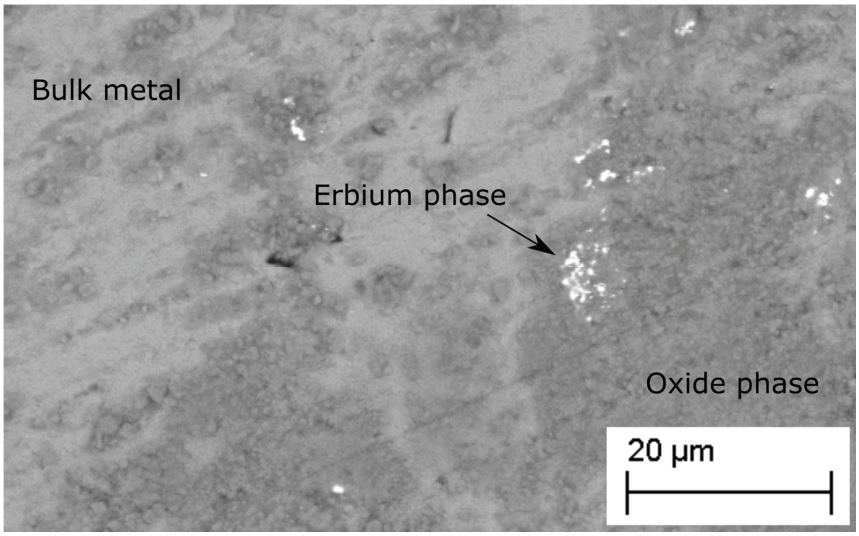

Figure 4-18 Erbium containing sample showing erbium phase in proximity to both metal and oxide after oxidation at 750 °C for 16 hours.

4.5.2.3 Strontium

The cross-section of the strontium sample from 16 hours of oxidation at 750 °C is shown in Figure 4-19. It was found that the oxide layer existed as $MgAl_2O_4$ as was found on the other samples,

however, no clear strontium containing phase was found in either the metal or oxide phase. Small traces of strontium at the lower detection limit of the EDS system were found in the metal phase, however, these could not be confirmed. Examination of the sample from 30 and 90 minutes of oxidation in the tube furnace showed a clear strontium phase in the metal, where the strontium existed as a discrete elongated particles with aluminum just below the oxide layer. These are likely Al_4Sr, based on the phase diagram in Figure 2-30. A large number of pores existed on the surface of both the 30 and 90 minute samples as shown in Figure 4-20. These pores were not present on the yttrium samples as seen in Figure 4-16. The MgO layer on the 30 minute sample measured between 100 and 825 nm, but averaged between 150 and 350 nm. The strontium was found to be primarily associated with the aluminum metal below the surface MgO layer, with no notable change in the Mg:O ratio between regions containing strontium and those that did not. The lack of a strontium phase on the 16 hour sample shows that the strontium that was present in the sample at the start had been completely lost.

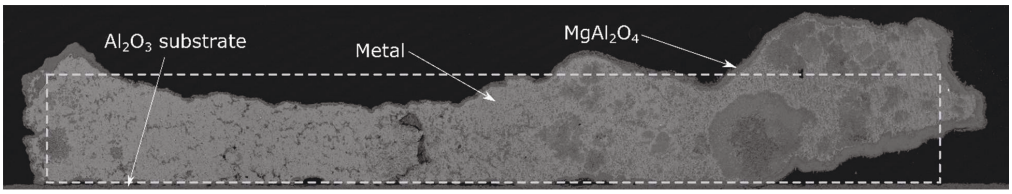

Figure 4-19 Cross-section of 5 % magnesium+strontium sample oxidized at 750 °C for 16 hours in air (dashed line shows the original sample shape of 10x1.5mm).

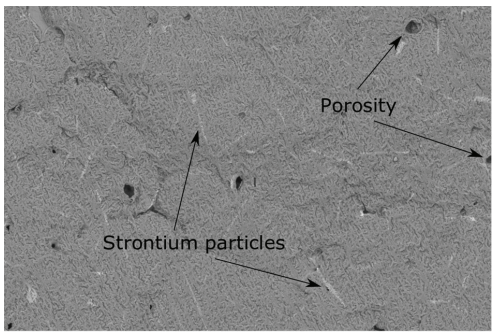

Figure 4-20 Strontium containing sample after oxidation for 90 minutes showing both porosity and strontium particles.

In contrast to the results of this work, Ozdemir et al. (48) and Yuen et al. (49), previously found that the addition of strontium to Al-Mg(Si) alloys resulted in a significant decrease in the oxidation rate and delayed the onset of breakaway oxidation. The reduction in oxidation was attributed to the formation of a protective layer of either Al_4Sr, $SrAl_4O_7$ or $SrSiO_3$ at the oxide-metal interface.

Contrary to Ozdemir and Yuen, Miresmaeili et al. (11) showed that strontium additions caused a larger increase in oxidation than magnesium additions. Further, it was found that 80 % of the strontium was lost during the course of oxidation. The increase in oxidation rate was attributed to SrO only having a Pilling-Bedworth ratio (PBR) of 0.65. This conclusion is questionable as the PBR is not valid for systems where the oxidizing component exists in dilute concentrations.

The large variation amongst results for strontium is puzzling as the addition of strontium appears to have either a strong inhibiting or promoting effect on the oxidation. This effect appears to be dependent on the strontium containing phase formed. With SrO affording no protection to the melt, Al_4Sr, $SrAl_4O_7$ or $SrSiO_3$ where reportedly able to protect the melt. In this work, the strontium was initially found in the metal phase -likely as Al_4Sr, where it formed discrete particles rather than as a layer seen by Ozdemir. With multiple authors showing such vast differences, it may be concluded that strontium can inhibit oxidation if specific conditions are met. However, based on the results of this work, it is concluded that if these conditions are not met, the addition of strontium can have catastrophic effects on the oxidation. What conditions are required to form a protective strontium layer are unclear at this point, however the strontium concentration is likely important.

4.5.3 Discussion of alternate alloying elements

After 16 hours, all the magnesium in the alloy had been oxidized to $MgAl_2O_4$ in all the samples as expected from an Al-Mg alloy. This means that magnesium had the largest influence on the overall oxidation, though yttrium, erbium and strontium all had a minor effect.

In general, the results achieved would indicate that the while both yttrium and strontium were found to form a second phase near the surface, however, this phase was not sufficient to protect the alloy from excessive oxidation. The formation of a second phase near the surface is promising. If the segregation to the surface can be promoted, the concentration may become sufficient to form a uniform layer as is seen in beryllium containing alloys. If all the yttrium in the model alloy

formed a YAl_3 layer at the surface, the resultant layer would be 80 nm thick. A layer of this thickness could be sufficient to protect a melt as it is significantly larger than the protective BeO-$BeAl_2O_4$ layer found on the Al-Mg alloy that contained 2-100 ppm of beryllium.

Examination of the vapor pressure of yttrium, erbium and strontium can offer an explanation for the results seen in this work. Vapor pressures are given in Table 12 for 727 °C and at the melting point of each specific element (66). Strontium in particular has a high vapor pressures over the liquid alloy. This higher vapor pressure leads to the observed loss of strontium from the alloy. The loss of the alloy element results in an increase in the porosity of the oxide layer resulting in an increase in the oxidation rate and an earlier onset of breakaway oxidation.

Table 12 Vapor pressures of select elements at 727 °C and the melting point of each specific element (66).

	Vapor pressure (Pa)	
Element	**727 °C**	**Melting point**
Yttrium	6.6 x 10 -11	0.316 (1527 °C)
Erbium	4.3 x 10 -6	52.5 (1527 °C)
Strontium	121	121 (727 °C)

The higher vapor pressure alone is not sufficient to cause the increase in oxidation as the vapor pressure of magnesium is higher than strontium. However, due to the high oxidation potential of magnesium, a significant portion of the magnesium vapor will be oxidized and deposited on the surface oxide resulting in much of the porosity created by the magnesium vapor being “filled in” by MgO. In contrast, yttrium, erbium and strontium will not oxidize preferentially and the metal vapor will, therefore, be transported out through the oxide layer and into the gas phase. The oxidation enhancing effect caused by the evaporation of elements with a high vapor pressure has previously been noted by Thiele, as translated by Drouzy and Mascré who cited the influence of vapor pressure with respect to the effects of selenium on the oxidation of Al-Mg alloys (9) (38).

4.6 Alternate minor element additions versus beryllium

In terms of finding an alternate route to protect an Al-Mg melt from excessive oxidation, an alternate alloying element to beryllium that has a similar protective effect would be most desirable since addition of alloying elements in the casthouse is a standard practice. Therefore, the addition of a specific element would require minimal technical challenges to implement beyond procuring the new alloying element and determining the minimum amount required to achieve protection.

One of the biggest concerns would be how the alternate element would affect the mechanical properties of the final alloy and complying with the compositional limits for a particular alloy designation. This is especially important as 100 ppm of yttrium, erbium and strontium did not appear to be sufficient to protect the alloy and higher concentrations will likely be required. Yttrium, erbium and strontium are not specifically listed on most alloy designations, and therefore fall into the "others" category. Other elements that are not specifically listed in the alloy designation are typically restricted to a maximum amount between 0.05 and 0.10 % (500 to 1000 ppm) (8). This would act at the maximum amount that could be added to a melt without requiring significant testing to ensure the physical properties of the alloy were sufficient.

4.7 Observations and conclusions on the oxidation protection for Al-Mg alloys

The results of the studies on beryllium and CO_2 have led to a clearer understanding of what is required to protect an Al-Mg alloy from excessive oxidation and provide possible routes forward to replacing beryllium in the casthouse. While beryllium and CO_2 were found to protect the melt in different ways, a number of similarities do exist in in how the oxidation was inhibited.

Both beryllium and CO_2 inhibited oxidation by forming a physical barrier that hindered transport of magnesium and aluminum across the initially formed MgO layer. For beryllium additions, a layer of BeO-$BeAl_2O_4$ was formed at the oxide-metal interface, whereas CO_2 resulted in a diffusion barrier at the oxide-atmosphere interface. Both these layers inhibited the transport of metal out and oxygen inwards. Inhibiting the transport would seem to be the most efficient method of controlling the oxidation.

A general oxidation schematic showing the steps involved in the oxidation is given in Figure 4-21. It is assumed that there exists an initial MgO layer on the surface of the Al-Mg alloy as this will form nearly instantaneously upon exposure to an oxidizing atmosphere and elevated temperatures. In theory, the oxidation could be inhibited by restricting anyone of these steps, however, certain steps are easier to affect than others as will be discussed below.

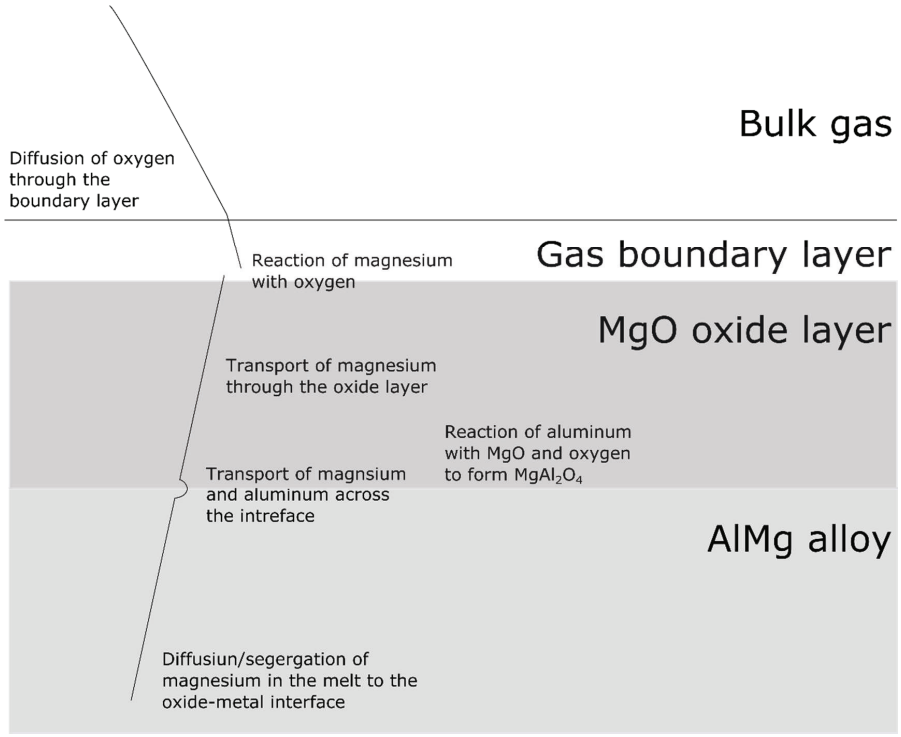

Figure 4-21 General oxidation schematic for an Al-Mg alloy.

4.7.1 Diffusion of oxygen through the boundary layer

Any oxygen near the oxide layer will react with magnesium vapor to form MgO, resulting in a reduced oxygen partial pressure in the boundary layer above the oxide surface. As the nitrogen content will remain nearly constant, a gas boundary layer though which fresh oxygen must diffuse will form. It should be noted that nitrogen can react to form aluminum nitrides, however, the amount is limited in comparison to the total nitrogen content available in the gas atmosphere.

Therefore it is assumed that the nitrogen content can be assumed to be constant. The transport through the boundary layer is determined by air flow conditions and the partial pressure of oxygen in the bulk gas and boundary layer. Given the extremely low oxygen partial pressure required to stop the oxidation of magnesium, managing to slow the transport of oxygen across the boundary layer sufficiently to avoid oxidation seems unlikely.

4.7.2 Reaction of magnesium with oxygen

The most obvious way to inhibit the reaction between magnesium and oxygen would be to make another reaction more thermodynamically favorable. As discussed in the theory section, few elements have a higher affinity for oxygen than magnesium. Coupled with the rapid reaction between magnesium and oxygen, hindering the actual oxidation reaction is unlikely. The most logical way to inhibit the magnesium oxidation reaction would be to inhibit the transport of one of the reactants to the reaction sites.

4.7.3 Transport of magnesium through the oxide layer

Inhibiting the oxidation by slowing the transport of magnesium through the oxide layer is known to be effective, as CO_2 works to inhibit the oxidation this way. CO_2 works by adsorbing onto the MgO layer, forming a “cap” on the oxide layer that acts to prevent the magnesium vapor from leaving the oxide layer. Alternatively, it could be possible to alter the structure of the formed oxide layer, perhaps with the addition of a select alloy element, to make it more resistant to the transport of magnesium vapor out. In paper 4 it was shown that the MgO layer limits oxidation compared to what would be seen on a surface that is free from oxide, however, the calculated diffusion coefficient through the oxide was still several orders of magnitude higher than published values for diffusion through the oxide crystal lattice. If the pores/diffusion channels that act as shortcuts for diffusion out could be closed or minimized, the flux of magnesium out and oxygen inwards would be reduced, resulting in a decrease in oxidation.

4.7.4 Reaction of aluminum with MgO and oxygen

Unlike the reaction of magnesium with oxygen, the reaction of aluminum, oxygen and MgO to form the spinel phase can be restricted. The formation of the spinel phase requires that the magnesium activity be sufficiently low (0.023 at 700 °C (19)). If the magnesium activity can be

held above this critical value, the formation of the spinel phase is inhibited. As formation of the spinel phase directly results in the onset of breakaway oxidation, maintaining a magnesium activity above the critical value in proximity to any aluminum in contact with MgO is critical for inhibiting breakaway oxidation. As magnesium is consumed during oxidation maintaining a specific magnesium activity will be difficult in an alloy. Forming a barrier to separate the metal and MgO would seem to be the most efficient way to inhibit the spinel reaction.

4.7.5 Transport of magnesium and aluminum across the oxide-metal interface

Inhibiting the transport of magnesium and aluminum across the oxide-metal interface is the mechanism by which beryllium inhibits the oxidation. By the formation of a BeO-$BeAl_2O_4$ layer transport of both magnesium and aluminum into the MgO oxide layer is inhibited. By reducing the transport of magnesium into the oxide layer the growth of the oxide layer is subsequently reduced to a rate determined by the diffusion rate across the barrier. Another large advantage of inhibiting the oxidation by forming a barrier at the oxide- metal interface is that the formation of the spinel phase would be controlled by the transport of aluminum across that barrier.

4.7.6 Reduce the segregation of magnesium to the oxide-metal interface

The final option for inhibiting oxidation is to limit the segregation of magnesium in the melt to the oxide layer. This can however, be both positive and negative. If the segregation of magnesium to the oxide-metal interface is slowed, the subsequent oxidation to MgO will be reduced, however, the activity of magnesium may also be reduced quicker as magnesium is lost to the oxide layer. The segregation of magnesium to the oxide-metal interface acts to hold the activity of magnesium above the critical value for spinel formation. If the segregation to the oxide-metal interface is reduced, the magnesium activity will be similarly reduced. The ideal case would be to hold the magnesium activity right above the critical level for spinel formation as this would inhibit breakaway oxidation and minimize the driving force for the diffusion of magnesium through the oxide layer. In the casthouse, the flow in the melt is often controlled in specific ways to allow alloying elements to be distributed and particles to settle, therefore, it is likely that there is little that could be done to effect the segregation of magnesium in the melt to have a positive effect on the oxidation.

4.8 Discussion of proposed alternate alloying additions

Based on the above analysis it can be concluded that the focus on effectively reducing the oxidation of an Al-Mg alloy should be placed on slowing transport of magnesium from the melt into the oxide layer or slowing transport through the oxide layer. The most effective method would seem to be the formation of a protective barrier at the oxide-metal interface as it slows the diffusion of magnesium and aluminum, though the number of alloying options to achieve this are limited.

Based on the new understanding of the mechanism behind beryllium's protective effect and the results of the tests on the proposed alternative alloying elements, three criteria can be established that must be fulfilled in selecting potential elements to replace beryllium. These three criteria are:

- A strong tendency to segregate to the oxide-metal interface (surface active)
- Be stable in the melt/oxide layer (low vapor pressure)
- Ability form solid layer near the oxide metal interface

Tendency to segregate: As the concentration of any alternate alloy element must be kept to a minimum elements that have a strong tendency to segregate to the oxide-metal interface would be required. This segregation would result in a higher effective concentration in the proximity of the oxide-metal interface and enhance the protective effect. This is clearly the case with beryllium where a 100 ppm resulted in a 40 nm thick layer. However, for yttrium and strontium, insufficient segregation occurred to form a protective layer, even though in the case of yttrium the alloy contained sufficient amounts of yttrium to form a Y_2O_3 layer up to 80 nm thick. For this reason, particular focus should be placed on surface active elements.

Stable in the melt: The tests with erbium and strontium showed that the vapor pressure is critical to the protective abilities. Any alternative element must, therefore, have a preference to remain in the melt or oxide layer, where is can influence the transport on magnesium out. The results of Nakajima et al. (36) as shown in Figure 2-17 could be of use here in avoiding those elements which would segregate to the gas phase.

Form a protective layer: Possibly the most important is the selected element must act to form a solid layer in the oxide layer or at the oxide-metal interface. While a tendency to segregate and

stability in the melt/oxide are important criteria, the formation of a barrier is the actual inhibiting mechanism. To this end, elements that have a high solubility in aluminum such as silicon and do not form any intermetallic phases are unlikely to be a suitable candidate to act as a replacement element.

5. Conclusion and Future work

5.1 Conclusions

In this work, the oxidation-inhibiting mechanisms of beryllium additions and CO_2 cover gas for Al-Mg alloys were investigated with the overall goal to better understand and control the oxidation of these alloys. Specifically, the following research questions and goals were set up for this work:

Q1. What is the mechanism behind beryllium's known protective effect?

- Quantifying the effects of beryllium on the rate and extent of oxidation.
- Identifying any beryllium containing phases that form/determine where beryllium reports during oxidation.

Q2. What are the effects of the addition of CO_2 to the atmosphere on the oxidation?

- Quantifying the effects of CO_2 in different atmospheres on the rate and extent of oxidation.
- Characterizing the morphology and composition of the oxide layer formed during oxidation under a CO_2 containing atmosphere.

G1. Develop a broader understanding how to control/minimize the oxidation of Al-Mg alloys

- What specific properties must an alloy element have to inhibit the oxidation of Al-Mg alloys?

G2. Propose and test alternative alloying elements that will potentially give a similar protective effect to beryllium.

- Describe the effects if additions of yttrium, erbium and strontium on the oxidation of Al-Mg alloys.

Research questions Q1-2 were answered with proposed mechanisms for the effects of both beryllium and CO_2 being developed. Completion these research tasks led to a good sense of the broader picture of controlling/minimizing the oxidation to fulfil G1. The work on research goal 2 (G2) did not reveal a directly suitable alloying replacement for beryllium, though useful results

were found on the effects of yttrium, erbium and strontium on the oxidation. These results were used to provide a fuller understanding of how to control the oxidation of an Al-Mg alloy.

5.1.1 Beryllium

Both industrial and model Al-Mg alloys with magnesium concentrations up to 5 % and beryllium concentrations of 2-100 ppm were studied, by carrying out oxidation experiments in a horizontal tube furnace and TGA. Samples surfaces were subsequently characterized using FIB, XPS, SEM and TEM. It was found that the addition of beryllium resulted in the formation of a BeO-$BeAl_2O_4$ layer at the initially formed oxide (MgO) -metal interface. It was proposed that it is this BeO-$BeAl_2O_4$ layer that acted as a diffusion barrier to reduce the diffusion of magnesium and aluminum out through the oxide layer which in turn resulted in a reduction of the oxidation rate.

The formation of this layer lead to the conclusion that two of the key properties of beryllium are:

- High oxidation potential that allowed the formation of a second phase on the oxide-metal interface that was solid.
- Strong segregation to the oxide-metal interface allowed a higher effective concentration at the interface promoting the formation of the BeO-$BeAl_2O_4$ layer. Without this segregation an addition of 2 ppm would likely not be sufficient to form a protective layer.

5.1.2 CO_2

The effects of CO_2 on the oxidation are less well documented in literature than those of beryllium. The significant results in regard to the effects of CO_2 on the oxidation from this work are listed below:

- The addition of as little as 5 % CO_2 to an air atmosphere can protect an Al-Mg alloy containing 5 % magnesium to the same extent as beryllium additions for period up to 420 minutes.
- The effects of CO_2 will remain for a time period after the CO_2 has been removed. The protection time is dependent on the CO_2 exposure time.
- The addition of CO_2 to the atmosphere during the initial stages of breakaway oxidation in pure air will suppress the oxidation rate.

XPS depth profiling showed that the CO_2 had adsorbed onto the initial oxide (MgO) surface. This adsorbed CO_2 is the source of the inhibiting effect. The adsorbed CO_2 will provide a physico-chemical barrier to the diffusion of magnesium vapor out through the oxide layer. With a reduced diffusion of magnesium out, the oxidation rate will be subsequently reduced.

5.1.3 Oxidation protection

Based on the results of the this work it was proposed that the most effective way to control the oxidation of Al-Mg alloys is by limiting the diffusion of magnesium through the initially formed oxide layer. This can be done through both addition of active compounds in the atmosphere and/or through alloy element additions. For alloy additions, ideally, this would be done by creating a barrier at the oxide-metal interface as this would slow the magnesium diffusion out and act to isolate the aluminum from the MgO and serving to delay the formation of the spinel phase and the onset of breakaway oxidation. Yttrium, erbium and strontium were proposed as potential element additions that could achieve such a protective barrier.

5.1.4 Alternate alloy additions

The addition of 100 ppm of yttrium to a 5 % magnesium alloy had mixed results on the oxidation, but on average had a limited impact on delaying the onset of breakaway oxidation, with some samples breaking away earlier and some later than the reference 5 % magnesium alloy. For erbium and strontium additions, a reduction in the time for the onset of breakaway oxidation was found. The yttrium and strontium containing samples were characterized after oxidation exposures of 30 or 90 minutes, it was found that the yttrium and strontium had segregated to a second un-oxidized phase of YAl_3 or Al_4Sr just below the MgO layer. For longer times it was found that both the erbium and strontium concentration had been reduced with no traces of strontium remaining after 16 hours of oxidation. It was proposed that higher vapor pressures of strontium and erbium lead to an increase in porosity in the oxide layer and reduced the time for the onset breakaway oxidation. However, it was proposed that if segregation could be promoted, the discrete particles may form a protective layer.

From this it was concluded that any alternate alloy additions must fulfil three requirements:

1. Strong tendency to segregate to the oxide-metal interface (surface active).

2. Be stable in the melt/oxide layer (low vapor pressure).
3. Ability to form a solid layer near the oxide-metal interface.

5.2 Future Work

There exists potential for further work to be carried out in all the research areas in this work. The proposed oxidation inhibiting mechanism developed for both beryllium and CO_2 gives a good understanding of their respective inhibiting mechanism. If additional experimental data was gathered, more detailed models of the protective mechanism for beryllium and CO_2 could be developed, especially in respect to CO_2. The search for an alternate alloying element is still open with yttrium, erbium and strontium not providing a clear protective effect.

A number of questions remain on the topic of the effects of beryllium. Further work to better understand how beryllium is so efficiently segregated to the oxide-metal interface and forms a uniform layer would be of benefit for the industry. A greater understanding of this could help to better understand how to promote the formation of a protective layer with other alloy additions.

As the results from the tests on the alternate alloys were not successful, it would be beneficial to continue this work and vary a number of experimental parameters including temperature, alloy concentration, surface treatment and surface-to-volume ratio. While the number of alloying elements that are options to be a suitable replacement is limited, binary additives could be tested, as it is possible that a mixture of two or more alloy elements may react to form a protective layer. As the desired properties are now more clearly understood, it may be advisable to carry out initial DFT calculations to see if any positive interactions that are not readily apparent can be identified.

For CO_2, a number of questions still exist on how the adsorbed CO_2 exactly affects the diffusion through the MgO layer. While it is clear that the adsorbed CO_2 layer is the source of the inhibiting effect, it is unclear how this adsorbed CO_2 exactly modifies the MgO layer to inhibit the diffusion through the oxide layer. More detailed characterization of the oxide layer could yield an understanding of the changes to the oxide layer and help determine a more exact mechanism for CO_2's effect.

References

1. Moser C. Furnace Dross - Its Formation and Recovery. In Grandfield J, Eskin DG. Essential readings in light metals: cast shop for aluminum production.: John Wiley & Sons, Incorporated; 2013. p. 150-156.

2. Kvithyld A, Green J. Second International Aluminum Recycling Workshop, Trondheim, Norway. Light Metal Age. 2013; August: p. 30-37.

3. Girard G, Barresi J, Dupuis C, Riverin G. Furnace Operation: "A Gold Mine in your Casthouse. In Aluminium Cast House Technology XI; 2009; Melbourne. p. 77-84.

4. Haginoya I, Fukusako T. Function of CO2 Gas on the suppression of oxidation of molten Al-Mg alloy. Journal Japan Insitute of Light Metals. 1981; 31(11): p. 733-741.

5. Cochran C, Belitskus D, Kinosz D. Oxidation of Aluminum-Magnesium Melts in Air, Oxygen, Flue Gas and Carbon Dioxide. Metalurgical Transactions B. 1977; 8B: p. 323-332.

6. Gauthier G. Improvement of cast Aluminum-Magnesium by additions of beryllium and titanium. Foundry Trade Journal. 1938; 59: p. 373-374.

7. Pilling NB, Bedworth RE. The Oxidation of Metals at High Temperatures. Journal Institute Metals. 1923; 29: p. 529-591.

8. Sigworth G. Best Practices in Aluminum Metalcasting. Schaumburg: American Foundary Society; 2014.

9. Drouzy M, C M. The oxidation of liquid non-ferrous metals in air or oxygen. Metallurgical Reviews. 1969; 131: p. 25-46.

10. Hinton E, Griffiths W, Green N. Comparison of Oxide Thickness of Aluminium and the Effects of Seleceted Alloying Elements. Materials Science Forum. 2013; 765: p. 180-184.

11. Miresmaeili SM. Oxidation of Liquid Al-7Si alloys containing strontium and magnesium. Oxidation of Metals. 2009; 71(1-2): p. 107-123.

12. Haginoya I, Fukusako T. Oxidation of Molten Al-Mg Alloys. Transactions of the Japan Institute of Metals. 1983; 24(9): p. 613-619.

13. Thiele W. Die Oxydation von Aluminium-und Aluminiumlegierungs-schmelzen. Aluminium. 1962; 38: p. 780-786.

14. Wightman G, Fray DJ. The Dynamic Oxidation of Aluminum and Its Alloys. Metallurgical Transactions B. 1983; 14B: p. 625-631.

15. Bartlett RW. Growth Kinetics of Discontinuous Thremal Oxide films; Aluminum. Journal of the Electrochemical Society. 1964; 111(8): p. 903-908.

16. Gullbransen EA, Wysong WS. Thin oxide films on aluminum. The Journal of Physical Chemistry. 1947; 51(5): p. 1087-1103.

17. Cochran CN, Sleppy WC. Oxidation of High-Purity Aluminum and 5052 Aluminum-Magnesium Alloy at Elevated Temperatures. Journal of the Electrochemical Society. 1961; 108(4): p. 322-327.

18. Gaskell D. Introduction to the Thermodynamics of Materials. 4th ed. New York: Taylor and Francis; 2003.

19. Surla K, Valdiveso F, Pijolat M, Soustelle M, Prin M. Kinetic study of the oxidation by oxygen of liquid Al-Mg 5% alloys. Solid State Ionics. 2001; 143: p. 355-365.

20. Young DJ. High Temperature Oxidation and Corrosion of Metals New York: Elsevier Science ; 2016.

21. Sleppy WC. Oxidation of Molten High-purity Aluminum in Dry Oxygen. Journal of the Electrochemical Society. 1961; 108(12): p. 1097-1102.

22. Bradford S. Oxidation: Metal-Gas Reactions. In Corrosion Control. New York: Van Nostrand Reinhold; 1993. p. 292.

23. Kahl W, Fromm E. Examination of the Strength of Oxide Skins on Aluminum Alloy Melts. Metallurgical Transactions. 1985; 16B: p. 47-51.

24. Syvertsen M. Oxide Skin Strength on Molten Aluminum. Metallurgical and materials Transactions B. 2006; 37B: p. 495-504.

25. Beck AF, Pryor MJ, Caule EJ, Heine MA. The Kinetics of the Oxidation of Al in Oxygen at High Temperature. Corrosion Science. 1967; 7: p. 1-22.

26. Smeltzer WW. Oxidation of Aluminum in the Temperature Tange 400°-600°C. Journal of the Electrochemical Society. 1956; 103: p. 209-214.

27. Santos PS, Santos HS, Toledo SP. Standard Transition Aluminas. Electron Microscopy Studies. Materials Research. 2000; 3(4): p. 104-114.

28. Bahk S, Chavez D, Emery B, Wilson B, Stoltzfus J. Protecting aluminum alloy from particle -impact ignition with Al2O3 film. International Journal of Imact Engineering. 1993; 14: p. 61-71.

29. Trunov MA, Schoenitz M, Dreizin EL. Effect of polymorphic phase transformations in alumina layer on ignition of aluminium particles. Combustion Theory Modelling. 2006; 10(4): p. 603-623.

30. Bergsmark E, Simensen CJ, Kofstad P. The Oxidation of Molten Aluminum. Materials Science and Engineering: A. 1989; 120-120: p. 91-95.

31. Tiwari B. Therodynamic Properties of Liquid Al-Mg Alloys Measured by the Emf Method. Metallurgical Transactions A. 1987; 18A: p. 1645-1651.

32. Murray J. The Al−Mg (Aluminum−Magnesium) system. Bulletin of Alloy Phase Diagrams. 1982; 3(1): p. 60-74.

33. Wefers K. Properties and Characterization of surface oxides on aluminum alloys. In 7th International Light Metals Congress; 1981; Leoben and Vienna.

34. Balicki S. Significance of beryllium in the oxidation process of fluid AlMg alloys. Prace IH. 1958; 10: p. 208-213.

35. Lea C, Molinari C. MAgnesium diffusion, surface segregation and oxidation in Al-Mg alloys. Journal of Materials Science. 1984; 19: p. 2336-2352.

36. Nakajima K, Takeda O, Miki T, Mastsubae K, Nakamura S, Nagasaka T. Thermodynamic Analysis of Contamination by Alloying Elements in Aluminum Recycling. Enviromental Science & Technology. 2010; 44(14): p. 5594-5600.

37. Agema K. Aspects of the Oxidation of Liquid Aluminium Alloys PhD Thesis: University of Cambridge ; 1989.

38. Thiele W. Die Oxydation von Aluminium- und Aluminiumlegierungs-Schmelzen. Aluminum. 1962; 38: p. 707-715.

39. Syvertsen M. Oxide Skin strength on Molten AA5XXX Aluminum Alloy-Effect of Beryllium and Alternitives. In Light Metals; 2015; San Diego: TMS Annual Meeting.

40. Murray J. The Al−Be (Aluminum-Beryllium) system. Bulletin of Alloy Phase Diagrams. 1983; 4(1): p. 50-55.

41. Kordis J. The BeO-MgO system. Journal of Nuclear Materials. 1964; 14: p. 322-325.

42. Harrop PJ. Self-Diffusion in Simple Oxides. Journal of Material Science. 1968; 3: p. 206-222.

43. Field DJ, Scamans GM, Butler EP. The Effect of trace alloying additions on the high-temperature oxidation of Al-4.2 wt%Mg and Al-3 wt% Li alloys. In Aluminum-lithium alloys. Warrendale, PA: Metallurgical Society of AIME; 1981. p. 393-405.

44. Degreve F, Figaret R, Laty P. Depth Profiling by Ion Microprobe with High Mass Resolution. International Journal of Masss Spectrometry and Ion Physics. 1979; 29: p. 351-361.

45. Agency for Toxic Substances and Disease Registry. Beryllium Toxicity Patient Education Care Instructions. [Online].; 2011. Available from: https://www.atsdr.cdc.gov/csem/csem.asp?csem=5&po=15.

46. Harmsen A, Hoover M, Seiler F. Health risk implications of using beryllium in fusion reactors. Journal of Nuclear Materials. 1984; 122-123: p. 821-826.

47. Emadi D, Gruzleski JE, Pekguleryuz M. Melt oxidation behaviour and inclusion content in unmodified and Sr-modified A356 alloy Their role in pore nuculation. In AFS transactions; 1996.

48. Ozdemir O, Gruzleski E, Drew A. Effect of low levels of Strontium on the Oxidation Behavior of selected Molten Aluminum-Magnesium Alloys. Oxid Met. 2009.

49. Yuen PK, Dennis K, Drew RAL, Gruzleski JE. Effects of Strontium on the oxidation behavior of Molten Aluminum alloys Containing Silicon and Magnesium. In 6th International AFS Conference, Molten Aluminum Processing; 2001; Orlando.

50. Alcock CB, Itkin VP. The Al-Sr (Aluminum-Strontium) system. Bulletin of Alloy Phase Diagrams. ; 10(6): p. 624-630.

51. Zhang C, Zhang F, Cao WS, Chang YA. Thermodynamic Modeling of the Al-Si-Sr-O quaternary system. Intermetallics. 2010; 18: p. 1419-1427.

52. Risold D, Hallstedt B, Gauckler L. The Strontium-Oxygen System. Calphad. 1996; 20(3): p. 353-361.

53. Ravi Kumar NV, Blandin JJ, Suery M, Grosjean E. The effect of alloying elements on the ignition reistance of magnesium alloys. Scripta materialia. 2003; 49: p. 225-230.

54. Weng X, Zeng X, Wu G, Yao S. The effect of Y-ion implantation on the oxidation of AZ31 magnesium alloy. Materials Letters. 2007; 61: p. 968-970.

55. Gschneidner KA, Calderwood FW. The Al-Y (Aluminum-Yttrium) System. Bulletin of Alloy Phase Diagrams. 1989; 10(1): p. 44-47.

56. Gschneidner KA, Calderwood FW. The Al-Er (Aluminum-Erbium) System. Bulletin of Alloy Phase Diagrams. 1988; 9(6): p. 676-678.

57. Gripenberg H, Forrest D, Bekkevold PB, Solberg E, Lodin J, Stark F, et al. Productivity and Energy Effciency Improvemts at Two Reverberatory Furnaces at Alcoa Norway. In Light Metals 2018; 2018; Phoenix, Az: TMS Annual Meeting.

58. Williams E, Whipple D. Aluminum Melting Furnace Pressure Control. In Light Metals 2018; 2018; Phoenix, Az: TMS Annual Meeting.

59. Stevens D, Kvithyld A, Engh TA. Oxidation of rolled and flash anodized 3000 aluminum in air, nitrogen, oxygen and carbon dioxide atmospheres. Materials Science Forum. 2011; 693: p. 63-70.

60. Lapointe K, Bao S, Kvithyld A. Oxidation of Flash-Anodized Al-Mg Alloy in Dry Atmospheres of N2, CO2, and O2 and Humid Atmosphere of Ar. Met Trans B. 2015; 46(3): p. 1326-1342.

61. Tenório J, Espinosa D. High-Temperature Oxidation of Al-Mg Alloys. Oxidation of Metals. 2000; 3(3/4): p. 361-373.

62. Mason E. Graham's Laws of Diffusion and Effusion. Journal of Chemical Education. 1967; 44(12): p. 740-744.

63. Belitskus DL. Oxidation of Molten Al-Mg Alloy in Air, Air-SO2, and Air-H2S Atmospheres. Oxidation of Metals. 1971; 3(4): p. 313-317.

64. Cashion SP, Ricketts NJ, Hayes PC. Characterisation of protective surface films formed on molten magnesium protected by air/SF6 atmospheres. Journal of Light Metals. 2002; 2(1): p. 37-42.

65. Bao S. Filtration of Aluminum-Experiments, Wetting and Modelling-PhD Thesis Trondheim Norway: NTNU; 2011.

66. Rumble J. Vapor Pressure of metallic elements- data. In CRC handbook of Chemistry and Physics. 992018th ed. Boca Raton Florida: CRC Press/Taylor & Francis; 2018.

Paper I

Paper II

Paper III

The Mechanism Behind the Oxidation Protection of High Mg Al Alloys with Beryllium

NICHOLAS SMITH, ANNE KVITHYLD, and GABRIELLA TRANELL

The addition of beryllium to Al-Mg alloys is known to cause a dramatic decrease in oxidation; however, the mechanism behind this protective effect is not yet fully understood. To aid in finding an alternative to the toxic Be, a fundamental study of Be additions has been carried out. Industrial samples containing 2 ppm Be and a model alloy with 100 ppm Be were oxidized at temperatures between 550 °C and 750 °C in a horizontal tube furnace. The oxide layer and oxide–metal interface were investigated using SEM, FIB, and XPS. It was found that Be forms a uniform oxide layer at the oxide–metal interface which slows the diffusion of Mg and Al from the metal into the oxide layer resulting in a reduced oxidation rate and an increase in the time for breakaway oxidation to occur.

https://doi.org/10.1007/s11663-018-1340-6

I. INTRODUCTION

BERYLLIUM additions in ppm levels have long been used by the aluminum industry as a means of reducing the excessive oxidation that can occur when producing Al alloys with an elevated Mg content. Through TGA experiments, the effects of Be were well documented by Balicki already in 1958, Thiele in 1960, and Cochran in 1976.[1–3] The benefits of Be additions come in reducing the total amount of oxidation over short timeframes, as well as increasing the time until the onset of breakaway oxidation. However, owing to the limited ability of many quantification techniques to detect trace amounts of Be, the mechanism by which Be influences the oxidation has not been fully understood. Due to the significant health risks posed by Be and BeO, especially to the workers in the aluminum casthouses, the use of Be is restricted, and alternative methods are preferred.[4]

The addition of Mg to an Al alloy causes an MgO oxide layer to form, which is further transformed to $MgAl_2O_4$; once all the Mg is oxidized from the melt, these oxides are considered nonprotective in terms of preventing further oxidation. Mg-containing alloys will initially oxidize at a low rate; however, after a period of time ranging from minutes to hours, there will be a sudden and sharp increase in the oxidation rate, known as breakaway oxidation that will continue until all the Mg in the melt is oxidized. The oxidation will result in a notable loss of Mg from the melt. Therefore, extra steps are generally required when producing alloys with a high Mg content to minimize the oxidation. Ppm level additions of Be have been shown to reduce both the amount of oxidation and delay the onset of breakaway oxidation. This results in a reduction of the amount of Mg lost to oxidation and a reduction in the number of oxide inclusions that enter the melt during casting.[1–3,5] The focus of this study will be on describing the formation of the oxide layer in the presence of Be during the incubation period of oxide growth, rather than breakaway oxidation, as the former is the most important time period with respect to industrial Al production—as the primary aim of oxidation control in the casthouse is to remain in the incubation stage and avoid catastrophic breakaway oxidation.

To better understand the mechanism behind how trace Be additions can result in a marked drop in the oxidation of Al-Mg alloys, a series of experiments were undertaken to characterize the oxide layer and the effects of Be on the layer.

II. EXPERIMENTAL

The primary experimental study focused on oxidation experiments conducted in a horizontal tube furnace; however, supplementary metal–oxide reaction and oxide-stability experiments were carried out to support the findings.

A. *Oxidation Experiments*

Figure 1 shows one of the two horizontal tube furnaces and the sample loading system utilized to carry out the oxidation experiments. Ground (22 μm) or polished (1 μm) flat samples measuring approximately

NICHOLAS SMITH and GABRIELLA TRANELL are with the NTNU, Alfred Getz Vei 2, 7034 Trondheim, Norway. Contact e-mail: nicholas.smith@ntnu.no ANNE KVITHYLD is with the SINTEF, Sluppen, P.O. Box 4760, 7465 Trondheim, Norway.
Manuscript submitted February 20, 2018.

Published online: 20 July 2018

$25 \times 15 \times 1.5$ mm were placed in an alumina boat suspended in the furnace and held for a set time and temperature under an air atmosphere in the furnace as shown in Figure 1. This method gives samples that can be analyzed from various oxidation times, showing how the oxide morphology evolves with time. The samples were removed from the furnace after the required holding time and analyzed by means of a scanning electron microscope (SEM), dual-beam focused ion beam miller (FIB), and X-ray photoelectron spectroscopy (XPS). Table I shows the experimental matrix for the experiments done in the tube furnace.

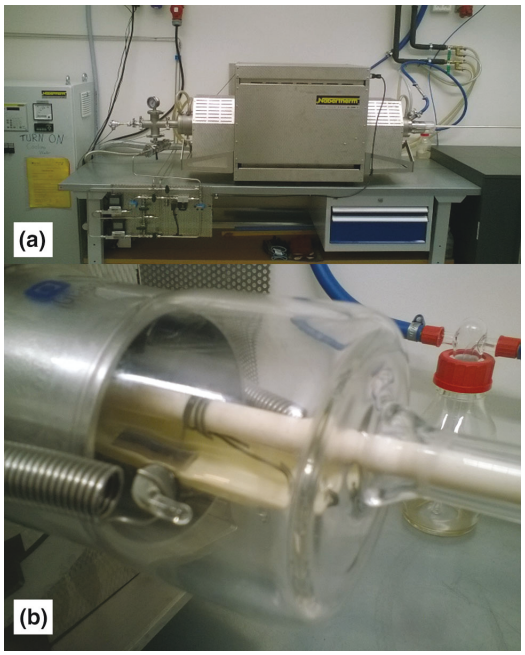

Fig. 1—(*a*) Horizontal tube furnace used for oxidation tests of 100 ppm Be samples. (*b*) Sample loading system for the horizontal tube furnace with sample in alumina boat.

The first series of experiments were carried out on industrially produced 5XXX series Al alloys. Two different alloys were used: one containing 2 ppm of Be and the other being Be free. Besides the Be content, both alloys were of the same grade and had a similar Mg content (4.7 pct). Samples were cut with a SiC abrasive saw and ground to 22 μm with SiC paper on all sides. To minimize oxidation at room temperature, the sample was placed in the furnace within 30 minutes of the final grinding. Samples were held at temperatures between 550 °C and 750 °C for 10, 30, or 120 minutes with the mass of each sample measured before and after oxidation to find the percentage mass gain due to oxidation.

To enhance the effects of Be, a second set of experiments was carried out on a model alloy with an elevated Be content over what is typically found in industrial alloys; this alloy consisted of 100 ppm of Be and 4.5 pct Mg in pure Al. It was assumed that the higher level of Be would only act to enhance the effects and aid in the detection of Be without changing the overall oxidation protection mechanism. The alloy was made from 99.999 pct pure Al from Puratronic, 99.98 pct pure Mg from Sigma Aldrich, and 99 pct pure Be from Alfa Aesar. First, a 0.5 pct AlBe master alloy was made in an arc melter that passed an electrical current through a tungsten electrode, creating an arc that rapidly melted the metal. The sample was then rapidly cooled on a water-cooled copper plate. This process was repeated several times to ensure a homogeneous alloy. The master alloy plus Al and Mg was charged into an alumina crucible and heated in an induction furnace to 850 °C and held for 15 minutes. It was then sectioned to size, polished to a 1 μm finish using a SiC abrasive saw and standard sample polishing techniques, to allow generation of the best possible chemical composition and depth profile.

B. *Sample Analysis*

A FEI Helios NanoLab DualBeam FIB was used to examine the surface of the samples after oxidation. After examination of the surface, the gallium ion beam was used to cut vertically down through the surface of the oxide and into the bulk metal. This allows a cross section of the oxide layer to be examined and the thickness of the layer to be measured.

Table I. Experimental Matrix for Oxidation Experiments of an Al 4.5 Pct Mg Alloy Containing Beryllium

	Time (Min)						
Temp (°C)	10	30	45	60	90	120	360
2 ppm Be							
550	X	X				X	
700	X	X				X	
750	X	X				X	
100 ppm Be							
550		X	X	X	X		X
700							X
750		X		X		X	

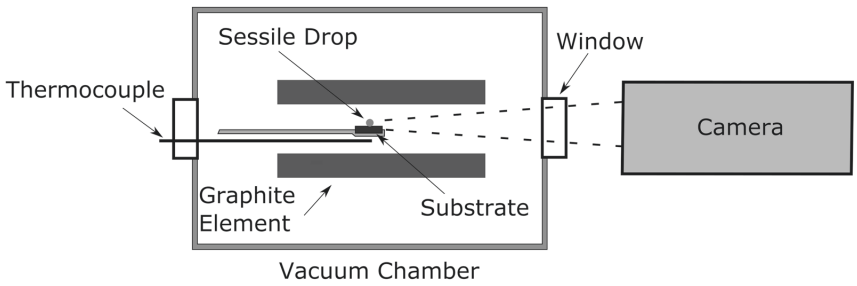

Fig. 2—Sessile drop furnace setup used to study the reaction and contact angle between oxide substrates and AlBe alloys under a high vacuum at 1100 °C.

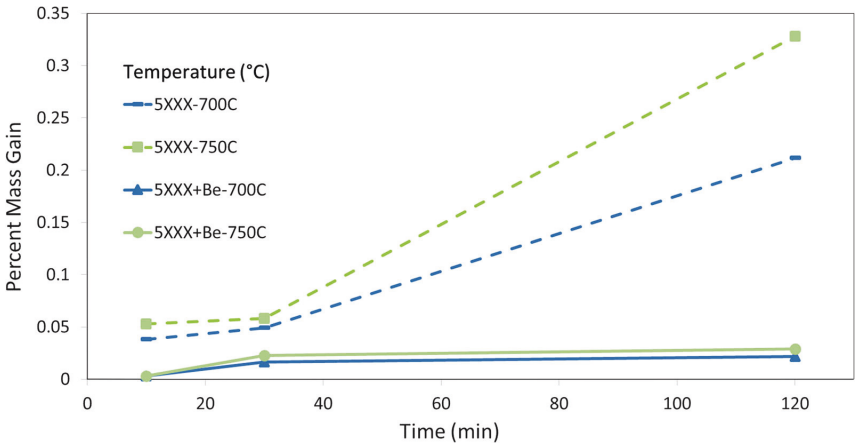

Fig. 3—Percentage mass gains in samples with and without 2 ppm Be oxidized in synthetic air for 10, 30, or 120 min at 700 °C and 750 °C showing a significant decrease in the total amount of oxidation with the addition of 2 ppm Be.

A Thermofisher Thetaprobe XP Spectrometer was used to create a XPS composition depth profile from the top surface through the oxide layer into the base metal. To create the depth profile, argon sputtering was used with an estimated sputtering rate of 8 nm per analysis cycle (120 seconds of sputtering time).

C. *Metal–Oxide Reaction*

The effects of Be on an Al drop in contact with Al_2O_3 and MgO substrates was measured using a sessile drop furnace as seen in Figure 2. This setup allowed observation of any reactions between the metal and substrate, as well as measuring the metal–substrate contact angle.

Pure Al with 0, 30, or 60 ppm of Be was tested on both Al_2O_3 and MgO substrates. In order to test the contact angle between the metal droplet and the substrate without interference of the oxide skin on the Al drop, the oxide skin was removed under a high vacuum/low oxygen partial pressure. Under a high vacuum, the Al_2O_3 skin will become less stable, and there is a decrease in thickness of the skin as the flux of oxygen away as AlO gas will exceed the flux of oxygen into the skin. The rate of this evaporation is temperature dependent, and, at temperatures over 1100 °C, the oxide skin can be completely removed in a short time.[6] Once the skin has been removed, a stable contact angle can be measured. In the experiments, the samples were held for two hours under a 1.5×10^{-5} mbar vacuum at 1100 °C.

D. *Oxide Stability*

Experiments to better understand the stabilities of BeO, MgO, and Al_2O_3 when mixed were carried out by mixing these three oxides in powder form in a 1:1:1 and a 1:1:2 ratio (BeO:MgO:Al_2O_3) and placed in Mo crucible and held at 1100 °C for 7 hours. The samples were subsequently analyzed using a D8 Focus powder X-ray Diffractometer (XRD) to see which phases had formed. The XRD scan was completed with a two theta angle ranging from 15 to 105 deg. This range captured all the major known peaks associated with the ternary BeO-MgO-Al_2O_3 system.

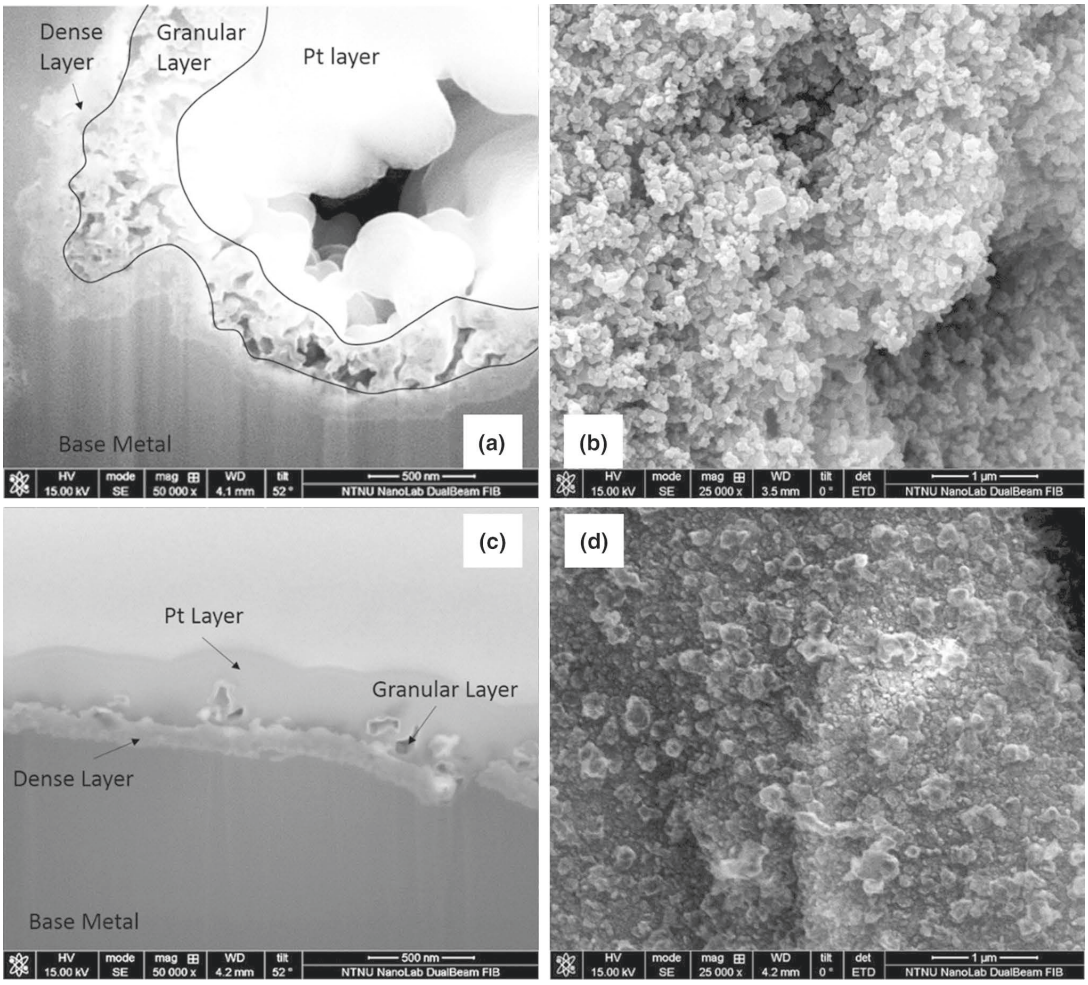

Fig. 4—Samples from oxidation experiments in synthetic air in the horizontal tube furnace shown in (*a*). Cross section of sample without Be from 120 min at 700 °C showing large amounts of granular growth on the top of the oxide layer. (*b*) Top surface of sample without Be from 120 min at 700 °C with granular growth covering the entire sample surface. (*c*) Cross section of sample with 2 ppm Be from 120 min at 700 °C with only minor granular growth being visible. (*d*) Surface of sample with 2 ppm Be from 120 min at 700 °C showing only minimal coverage of the granular layer.

III. RESULTS

A. *Beryllium in Industrial Al-Mg-Be Samples*

1. *Mass gain*

The addition of 2 ppm of Be was found to have a significant impact on the total amount of oxidation/sample mass gain. Figure 3 shows the percentage mass gain of the samples with and without 2 ppm Be. The addition of Be resulted in up to a tenfold decrease in the mass gain.[7] These results are in agreement with previous mass gain and TGA analysis conducted on Be in Mg-Al alloys.[1–3]

2. *Surface and cross-sectional morphology*

The addition of Be had a clear impact on the morphology of the oxide layer. Figures 4(a) through (d) shows the top surface and cross section of samples oxidized at 700 °C. In Figures 4(a) and (b), two distinct oxide layers can be seen on the sample without Be: a dense layer adjacent to the metal, and a granular layer on top of the dense layer. The platinum layer above the granular layer in the cross-section figures was deposited by the FIB during the process of making the cross section to protect the integrity of the granular layer from the ion beam. With the addition of Be, the thickness of

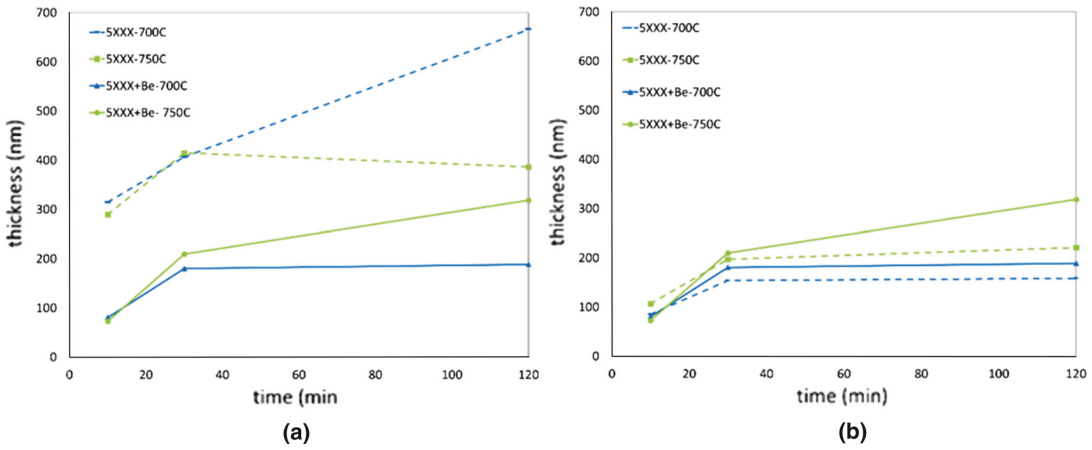

Fig. 5—Measured oxide layer thicknesses of samples oxidized in air at 700 °C and 750 °C. (*a*) The thickness of the entire oxide layer. (*b*) The thickness of only the dense oxide layer.

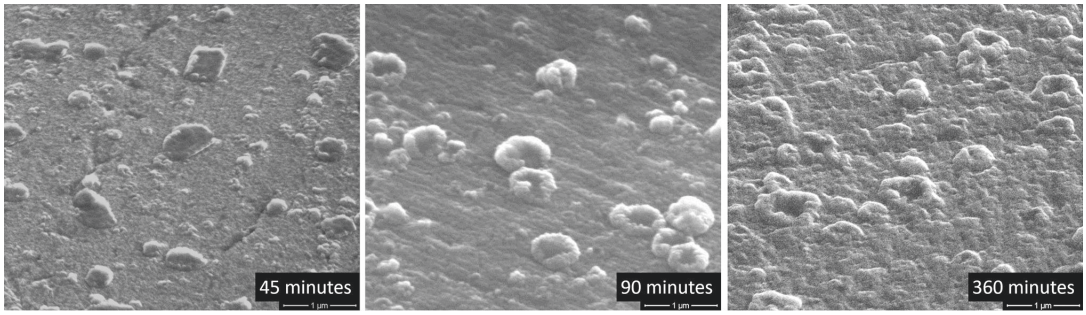

Fig. 6—FIB images from 45, 90, and 360 min of oxidation in air at 550 °C on sample with 100 ppm Be, showing the rapid formation of growths on the surface and envelopment of the growths by the surrounding oxide layer with time.

the granular layer is significantly reduced as can be seen in Figures 4(c) and (d) where the amount of granular layer can be seen to be reduced to near zero, whereas the dense layer has a nearly consistent thickness between the two alloys. The granular layer is made up of many small, often faceted granules that grow out of the dense oxide layer creating an open network of oxide.[7] This layer is similar in appearance to MgO oxide layer found by other researchers on Al-Mg alloys.[3,8,9]

Figure 5(a) shows the thickness of the entire oxide layer measured from the FIB cross sections. Exact measurement of the granular layer thickness was not possible due to the uneven nature of the layer, and therefore, the thickness of this layer should be taken as an indication of the approximate thickness, not the exact thickness. Figure 5(b) shows the thickness of just the dense layer. A comparison of the thickness of the oxide layers shows that the thickness of the dense layer is similar between the samples with and without Be.[7] The significant difference between the Be-containing and Be-free alloys is the granular layer thickness.

B. *Model 100 ppm Al-Mg-Be Samples*

1. *Surface and cross-sectional morphology*

Examination in the FIB of samples with 100 ppm Be oxidized at 550 °C for 45, 90, and 360 minutes showed that within the first 45 minutes, the surface of the sample was covered in growths measuring up to 0.5 μm across. These growths appeared to remain nearly constant in size for longer oxidation times, as illustrated by Figure 6. The oxide surrounding these growths was seen to grow and began to envelop the growths after 360 minutes of oxidation time. These growths are not present on a reference sample that was oxidized under the same conditions, but contained no Be as shown in Figure 7; rather the surface was covered in large granular MgO growths.[10]

The formation of the growths was not uniform across the entire sample surface with the number of growths varying from region to region. Grain boundaries particularly appeared to be nucleation sites for the growths as seen in Figure 8.[10]

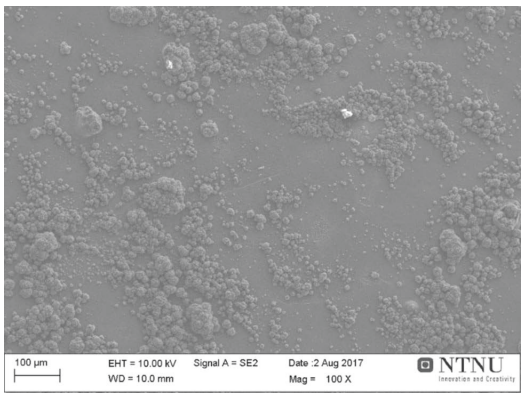

Fig. 7—Surface of reference sample without Be oxidized for 240 min at 550 °C in air showing the large granular MgO growths on the surface, but no smaller, dense growths, as seen on the Be-containing sample (Fig. 6).

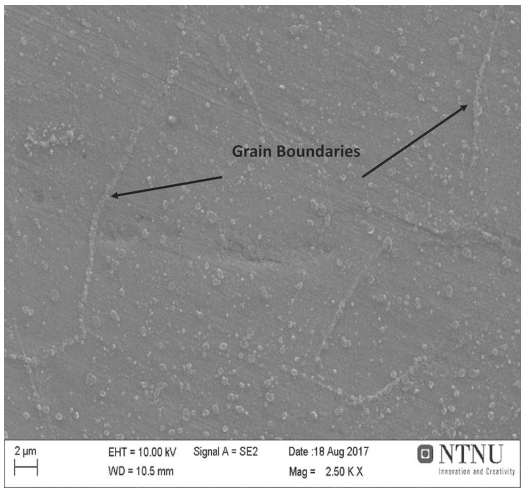

Fig. 8—100 ppm Be sample oxidized for 360 min at 550 °C in air showing preferential growth along the grain boundaries.

2. *Composition*

Samples for the XPS were sectioned from the 100 ppm sample oxidized at 550 °C for 60 and 360 minutes. The results of the XPS are given in Figures 9 and 10.[10] In these figures, an increase in sputtering time indicates an increase in depth taking the top surface of the oxide to be the top and moving downward towards the bulk aluminum metal. Due to the growths that formed on the surface and the uneven sputtering rate that resulted from these growths, it was not possible to accurately calculate depth from sputtering time. A corresponding oxygen ion curve exists for each of the metal oxide curves given in Figures 9 and 10, however, these have been omitted from the figures for simplicity. It can be seen that for both oxidation times the top surface of the oxide layer is MgO (far left in Figures 9 and 10). Downwards towards the metal the amount of Al oxide increases followed by an increase in the metallic Al concentration. Further downward, a clear BeO signal forms, and the MgO signal decreases to zero. There is little difference between the 60 and 360 minute samples with exception of the thickness of each layer and the ratio of the Be oxide to Al oxide signals. Both XPS curves show that the Mg metal content in the top part of the metal phase is well below the nominal 4.5 pct, indicating a large loss due to oxidation and evaporation.

Figures 11(a) and (b) shows SEM images of the surface of the 360 minute sample before and after sputtering. Before sputtering, the surface can be seen to have the rough granular appearance typical of MgO, but additionally growths on the top surface that are confirmed to be MgO by the XPS, are found. After sputtering for 3000 seconds, two distinct phases appear as seen in Figure 11(b). A bright phase on the surface that corresponds with the location of growths on the surface seen in Figure 11(a) and a darker background phase. An Energy Dispersive X-ray Spectroscopy (EDS) scan showed the bright phase is the only oxygen-containing phase present after sputtering. As the XPS shows the BeO-Al_2O_3 phase is the only oxygen-containing phase remaining after sputtering, it should correspond with this bright phase, while the dark phase is the Al metal. This is shown schematically in Figure 12 for both the 60 and 360 minute samples.[10]

For the samples oxidized at 700 °C, no large growths were visible on the surface. Rather an uneven surface with a number of small cracks as seen in Figure 13(a). This sample had too much surface topography to allow an XPS analysis. The sample was characterized in the FIB and compared to the 550 °C sample to help understand the means of oxidation protection on molten samples. Figure 13(b) shows a cross section of the 700 °C sample where a thin layer ranging from 15 to 50 nm in thickness exists between MgO oxide layer and bulk metal. Given the location of this layer in comparison with the samples from 550 °C it can logically be assumed that this is a BeO-Al_2O_3 layer that formed as a uniform layer across the entire oxide metal interface rather than as the clusters seen with oxidation below the melting point.[10]

It is difficult to directly measure the amount of $MgAl_2O_4$ and $BeAl_2O_4$ phase present from the XPS. It is known that for the $MgAl_2O_4$ phase to form the activity of Mg must be below 0.023 which corresponds to 2.7 at. pct and that Al_2O_3 cannot form until after all MgO has been transformed to $MgAl_2O_4$.[5] Therefore, any Al oxide ions found would predominately be associated with the $MgAl_2O_4$ or $BeAl_2O_4$ spinel phases. The XPS scans clearly show the presence of Al oxide ions indicating that the spinel phase is present. As the Al oxide signal increases before the Be signal, the $MgAl_2O_4$ phase is implied. However, at sputtering times over 1600 seconds the Mg oxide ion signal has decreased to zero, but a strong Al oxide signal remains indicating the presence of $BeAl_2O_4$. The Al oxide:Be oxide ratio shows

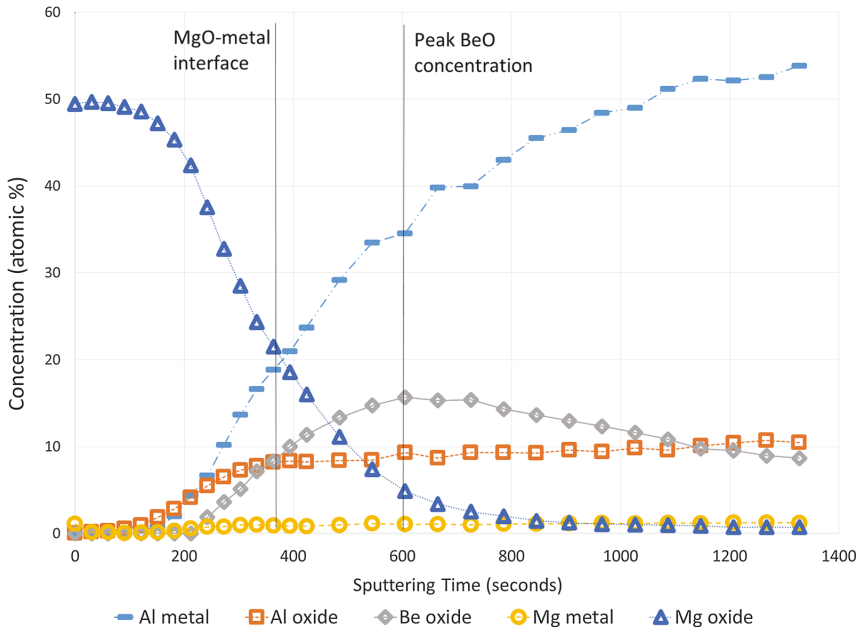

Fig. 9—XPS depth profile of the oxide layer for the sample after 60 min of oxidation time in air at 550 °C.

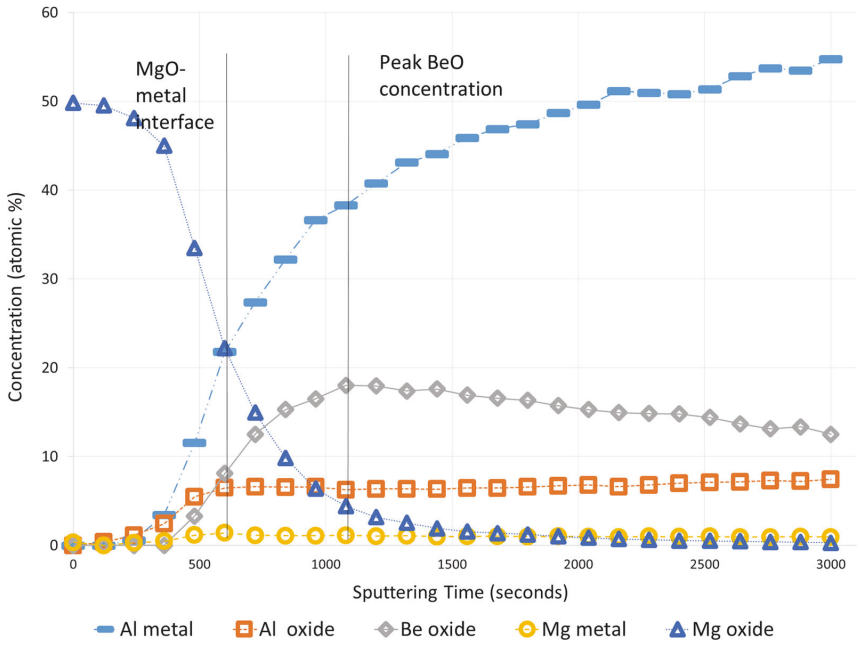

Fig. 10—XPS depth profile of the oxide layer for the sample after 360 min of oxidation time in air at 550 °C.

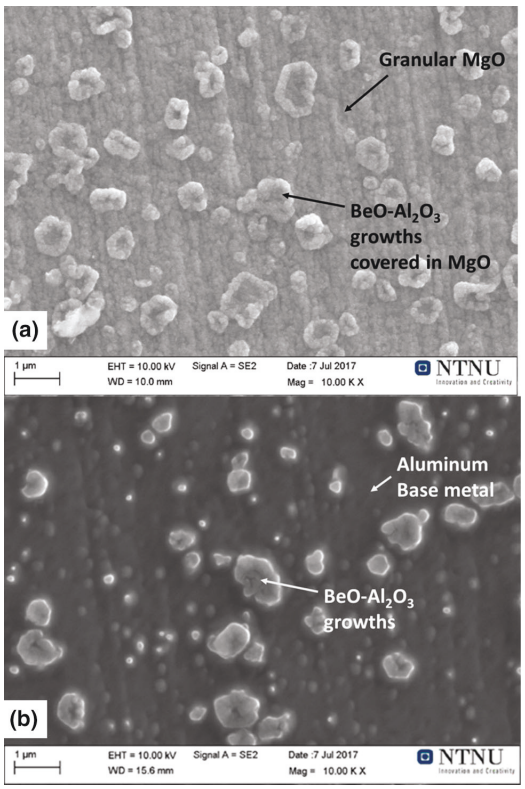

Fig. 11—(*a*) 100 ppm Be sample oxidized for 360 min at 550 °C before sputtering, showing surface covered by MgO. (*b*) Same sample only after sputtering/XPS analysis showing 2 distinct phases: a bright oxide phase and a dark metal phase.

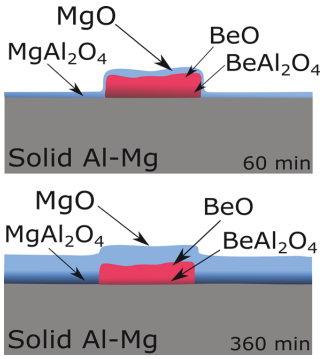

Fig. 12—Schematic showing a cross section of the oxide layer formed on the solid sample after 60 or 360 min of oxidation based on the results of the XPS depth profile and the morphological analysis in the FIB.

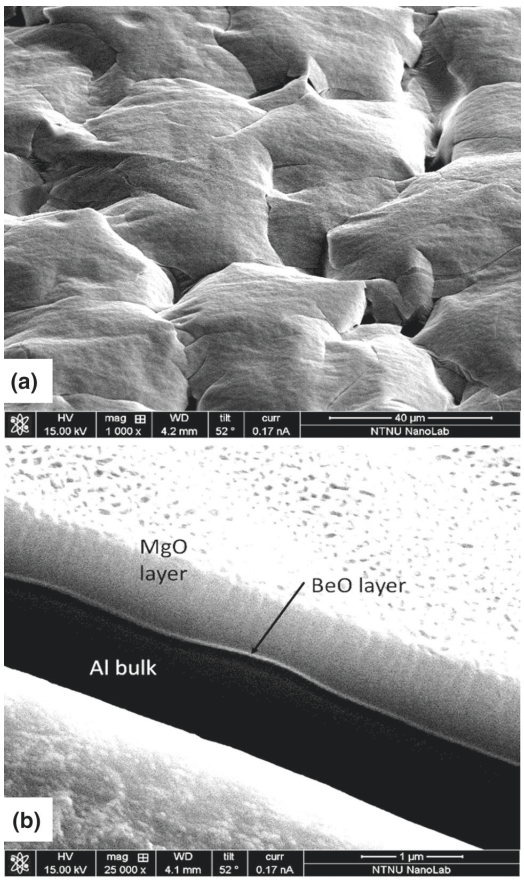

Fig. 13—Sample with 100 ppm Be from 360 min of oxidation at 700 °C in air. (*a*) Surface showing uneven surface with small cracks. (*b*) Cross section through oxide layer showing a thin BeO layer that was found between the MgO layer and Al base metal.

that both BeO and $BeAl_2O_4$ must be present after the entire Mg oxide layer has been removed by sputtering as both a Be oxide and an Al oxide signal remain. For the entire layer to be made up of $BeAl_2O_4$, the Al oxide:Be oxide ratio must be 2:1. If the ratio is higher than this, then a $BeAl_2O_4$-Al_2O_3 layer would exist. If the ratio is below 2:1 the layer must be $BeAl_2O_4$-BeO. As the ratio does not reach 2:1 at any point in the depth profile, both BeO and $BeAl_2O_4$ must be present in the oxide layer.

The Al oxide:Be oxide ratio increases as the depth increases for both the 60 and 360 minute oxidation samples with a higher ratio seen for the 60 minute sample which exceeds unity for the last 200 seconds. The higher Al oxide:Be oxide ratio for the shorter oxidation time indicates that the formation of the BeO layer is

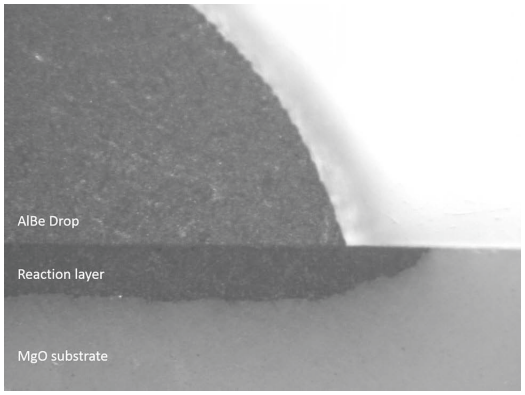

Fig. 14—Sample from Sessile drop furnace showing an Al drop with 60 ppm Be on MgO substrate after holding for 15 min in vacuum at 1100 °C. $MgAl_2O_4$ reaction layer between the substrate and drop can be seen.

Table II. Contact Angles Measured on MgO and Al_2O_3 with 0, 30, or 60 ppm Be in Al

	Al_2O_3		MgO
	15 Min	60 Min	15 Min
0 ppm Be	85	54	
30 ppm Be	88	56	77
60 ppm Be	90	62	97

time dependent on the transport of Be from the metal to the oxide layer, with longer times allowing for more concentration and oxidation of Be in the oxide layer. The Al oxide:Be oxide ratio would be further reduced if the oxidation occurs above the melting point as the transport of Be to the oxide–metal interface is faster in the liquid phase.

C. *Metal–Oxide Reaction*

Table II shows the contact angles measured for pure Al with 0, 30 or 60 ppm Be on Al_2O_3 and MgO substrates for a temperature of 1140 °C. It was not possible to measure the contact angle at times longer than 15 minutes for the samples on the MgO substrate. This is due to the strong reaction of the Al with the substrate. At low pressures, the $MgAl_2O_4$ spinel phase is the stable oxide phase. This reaction occurs rapidly resulting in a reaction layer in the substrate and gassing of Mg vapor that is deposited on the furnace walls and windows: this reaction can be written as shown in Eq. [1]. The sessile drop sample with the reaction layer is shown in Figure 14. Due to this reaction the angle measured on the MgO is not stable and is not reliable, but is presented here for thoroughness.

$$4MgO + 2Al = MgAl_2O_4 + 3Mg \qquad [1]$$

D. *Oxide Stability*

An excerpt of the XRD scans for both the 1:1:1 and 1:1:2 mixing ratios are shown together in Figure 15, and were obtained after analysis of the two different oxide powder mixing ratios. The same peaks were seen in both of the scans. The most significant peaks are the oxides BeO, MgO and Al_2O_3. The major peaks all vary significantly due to the higher Al_2O_3 content in the 1:1:2 sample. Both $BeAl_2O_4$ and $MgAl_2O_4$ were found in the samples. A number of overlapping peaks exist for this system, but at least 3 distinct peaks existed for each $BeAl_2O_4$ and $MgAl_2O_4$. The peaks at 22.15, 27.54 and 56.88 deg are unique to $BeAl_2O_4$ and 31.26, 44.79 and 65.78 deg are unique to $MgAl_2O_4$.

IV. DISCUSSION

From the morphology studies of the 2 and 100 ppm Be alloys, it can clearly be seen that the growth of the granular layer with time accounts for the bulk of the oxidation occurring on Be-free samples. This oxide growth is rate controlled by the transport of Mg through the dense oxide layer. The effect of Be reducing the granular MgO layer formation is clearly visible on the industrial samples where the thickness of granular layer was reduced to near zero with the addition of 2 ppm of Be. This means the addition of Be must slow the transport of Mg through the oxide layer. This can also be shown by looking at the samples from oxidation at 550 °C (Figure 6) where the oxide layer surrounding the growths increases in thickness faster than the growths—resulting in the growths being enveloped in the MgO. This indicates that the growths inhibit the oxidation. Further, as seen in Figure 7, the oxidation on a Be-free sample at 550 °C occurs at preferential sites resulting in large clusters of MgO. The BeO growths found on the samples containing Be were found at preferential sites such as grain boundaries; it is believed that the BeO growths form at the preferential sites for Mg oxidation resulting in a reduction of the large oxide clusters seen on Be-free samples.

The minor increase in the contact angle seen with increasing amounts of Be, *i.e.* increased wetting is negligible when compared to the error seen with this setup $\pm$ 5 deg. The contact angle results for pure aluminum are in good agreement with those found by Bao.[6] Syvertsen carried out measurements of the oxide skin strength on a liquid Al-Mg melt and found that additions of 2 ppm Be had no impact on the skin strength. This offers a confirmation of the wetting results obtained here as the skin strength is partially a measure of the surface tension between the oxide and metal.[11]

The rapid reaction of the Al drop with the MgO substrate shows that even with Be additions MgO will react strongly with liquid aluminum forming the $MgAl_2O_4$ spinel unless the MgO layer and Al metal are separated by a protective layer.

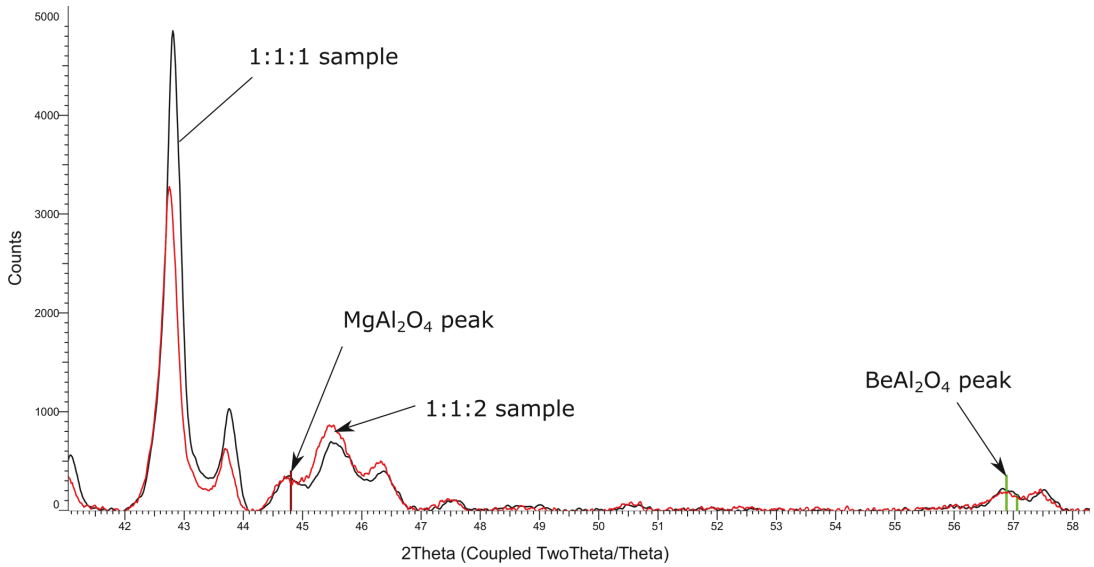

Fig. 15—A portion of the XRD patterns from oxide mixing experiments showing both the 1:1:1 and 1:1:2 mixing ratios. Both $BeAl_2O_4$ and $MgAl_2O_4$ are seen to form in similar amounts (same peak intensity) where the binary oxides show different amounts. Unlabeled peaks correspond to the binary MgO, BeO, or Al_2O_3 oxides phases.

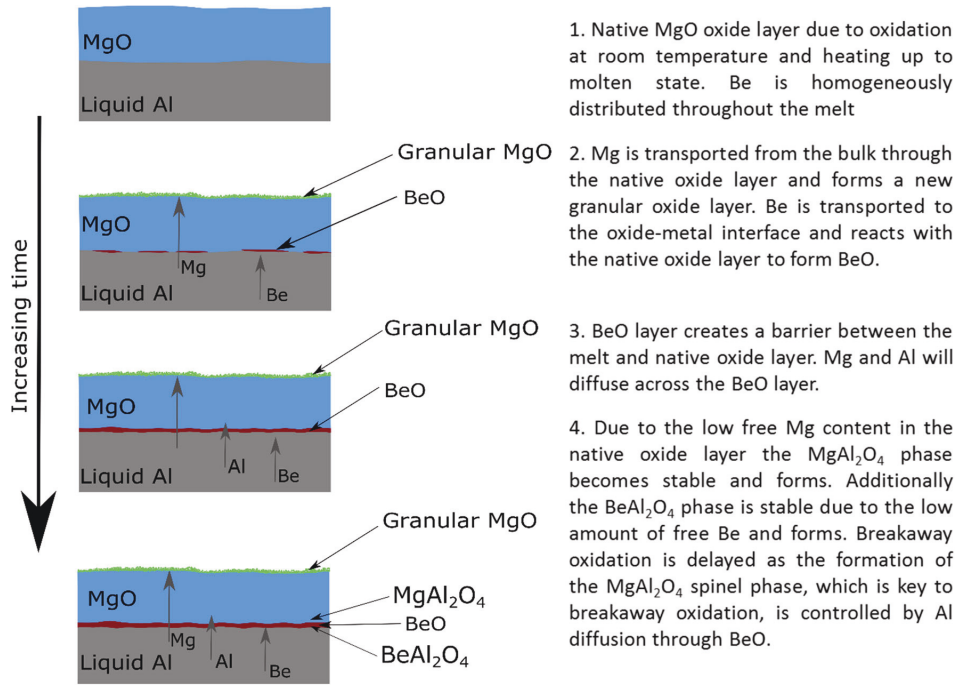

Fig. 16—Proposed mechanism behind the protective effect of Be on Mg-containing Al melts.

For the oxide stability tests, the similar heights of the $BeAl_2O_4$ and $MgAl_2O_4$ peaks for both oxide mixing ratios indicates a similar amount of the phases in both samples regardless of the initial mixing ratio. This means that both the $BeAl_2O_4$ and $MgAl_2O_4$ spinel phases exist and can form simultaneously in a system containing Mg, Be, Al, and O.

Based on the results and discussion above the proposed reaction and protection mechanism of an Al-Mg alloy containing Be is given in Figure 16. The proposed steps in the oxidation are:

1. The starting point of this model is taken as a liquid Al-Mg alloy with a layer of MgO. The MgO layer will form as a result of oxidation at room temperature, heating, and melting. While BeO is a more stable oxide than MgO, the initial oxide layer is found to be MgO as the activity of Mg is significantly higher than the Be at ppm levels. Any Be present on the surface will have reacted to form BeO; however, given the small amounts of Be that would be present at the surface, any BeO formed is neglected at this stage.
2. As metallic Be interacts with the MgO layer, it will react to form BeO and Mg per Eq. [2] rather than the direct oxidation with oxygen through Eq. [3]. Due to the rapid diffusion of Be in the liquid alloy, an elevated concentration of Be compared with the bulk alloy will form resulting in a higher Be activity at the oxide–metal interface. This higher Be activity will help to drive the oxidation of Be to BeO. The diffusion of Be to the oxide–metal interface will happen rapidly given the small atomic radius of the Be atom as the diffusion coefficient is inversely proportional to the atomic radius. With the atomic radius of Be at 1.12 Å compared to 1.60 Å for Mg and 1.43 Å for Al, the Be should diffuse rapidly through the liquid Al allowing for significant and rapid Be concentration at the oxide–metal interface.[12]

$$MgO + Be = BeO + Mg \quad [2]$$

$$Be + O = BeO \quad [3]$$

3. As holding time in the liquid state increases, a continuous BeO layer will begin to form at the oxide–metal interface since the primary source of oxygen for the oxidation of Be is the MgO layer. The areas on the BeO layers that are the thinnest will have the highest access to oxygen and see the most growth. This results in a relatively uniform layer of BeO covering the entire oxide–metal interface. While this BeO layer is forming, Mg from the metal and as a byproduct from Be oxidation, will continue to diffuse outward and cause the granular oxidation on the surface of the oxide.

   Once the BeO layer has formed and covered the entire oxide–metal interface, a barrier between the metal and oxide has been established, and diffusion across this BeO layer is required for any further oxidation of Be, Mg, or Al to occur.

   For the 100 ppm Be samples, the BeO layer ranges from 15 to 50 nm thick and an average of around 40 nm after 6 hours at 700 °C. The layer for the 2 ppm samples could not be observed on the FIB, and therefore must be at least one order of magnitude thinner. If the entire Be content in the sample was oxidized to BeO, the thickness of the layer would be approximately 250 nm for the 100 ppm sample and 5 nm for the 2 ppm sample based on the sample size used. Based on the average BeO layer thickness, 16 pct of the Be in the 100 ppm sample was oxidized at 700 °C indicating a strong tendency to segregate to the oxide layer. Regardless of the thickness of this layer, it must act as an effective barrier to the diffusion.
4. The MgO layer will be nearly free of metallic Mg and Al, and thus, a diffusion gradient will be established and flux of these elements across the BeO layer will develop. The diffusion coefficients of Mg and Al through the hexagonal BeO layer are not available at this momemt, rendering the calculations of the actual rates of Mg and Al diffusion across this layer as not possible. The smaller atomic size of Be compared with Mg should significantly reduce the ability of Mg to diffuse outward through the BeO layer compared with the initial MgO layer. In addition, the MgO layer is generally considered to be a noncontinuous layer and acts as a poor transport barrier. The smaller diameter and higher concentration of Al compared with Mg means Al will have a higher flux across the BeO layer than Mg. Given the limited supply of both Mg and Be to the system, it is assumed that the $MgAl_2O_4$ and $BeAl_2O_4$ phases will be the most stable and form *via* Eqs. [1] and [4]. The oxide-stability experiments show that both these phases can exist under nonequilibrium conditions. It is well established that the $MgAl_2O_4$ phase only becomes stable after the metallic Mg activity has dropped below 0.023. This has not been shown for the $BeAl_2O_4$ spinel, but given the similar oxidation characteristics, it is assumed the same is also true for the $BeAl_2O_4$ phase.

$$4BeO + 2Al = BeAl_2O_4 + 3Be \quad [4]$$

Breakaway oxidation is delayed as the formation of the $MgAl_2O_4$ phase is now diffusion controlled. Before the BeO layer formed, the MgO was in direct contact with Al. This allowed rapid transformation of MgO to $MgAl_2O_4$. The BeO layer now acts as a barrier separating the Al from the MgO causing the $MgAl_2O_4$ reaction rate to become tied to the diffusion of Al across BeO.

Based on the proposed mechanism above suggestions for alternative alloying additions can be made. An alternate element should react to form a diffusion barrier at the oxide metal interface. To encourage the formation of this layer an alternative element would need to have a strong tendency to segregate to the oxide–metal interface and readily react to from a protective layer. From this several candidates can be proposed, such as other group 2 elements or rare earth elements. In regards to the group 2 elements, Sr seems to

be the obvious candidate as it oxidizes preferentially to magnesium. Previous studies on the effects of Sr on the oxidation have shown mixed results with its effectiveness for inhibiting oxidation.[13,14] Rare earth elements stand out as a potential alternative as they are surface active and will readily react. Yttrium has seen usage as an alloying element to reduce the oxidation of solid Mg alloys at 500 °C and may prove effective in controlling the oxidation of liquid AlMg alloys.[15–17] The effect of both Sr and rare earth elements on the oxidation will be the subject of further research.

V. CONCLUSION

Industrial (2 ppm Be) and model (100 ppm Be) Al-Mg alloys have been oxidized in air at temperatures between 550 °C and 750 °C in order to establish the mechanism by which Be provides oxidation protection to Al-Mg alloys. Based on the results from FIB and XPS studies of the oxidized surface, a protection mechanism has been proposed, and the following conclusions have been made:

- On samples below the melting point, Be forms as $BeO\text{-}Al_2O_3$ growths on the surface in combination with MgO.
- The composition of these growths does not correspond to a $BeAl_2O_4$ phase, but rather a $BeO\text{-}BeAl_2O_4$ phase. The ratio of Al oxide:Be oxide increases with depth in the growth.
- On samples below the melting point, the surface growths form predominantly in areas most prone to oxidation such as grain boundaries, and thus act to slow the oxidation as a network of MgO continues to form and grow around the $BeO\text{-}BeAl_2O_4$ growths.
- On molten samples, the BeO forms a uniform layer of 15 to 50 nm thickness under an initial MgO surface layer for a sample with 100 ppm Be and 4.5 pct Mg.
- This BeO layer acts as a barrier to Mg and Al diffusion into the oxide thus slowing MgO and $MgAl_2O_4$ formation.

In addition, the stability of the $MgO\text{-}BeO\text{-}Al_2O_3$ ternary oxide system and the formation of $MgAl_2O_4$ or $BeAl_2O_4$ were studied along with the metal–oxide reaction of an Al drop with trace Be amounts on Al_2O_3 and MgO, and experiments have been carried out where the following were found:

- Both $MgAl_2O_4$ and $BeAl_2O_4$ will form in the ternary $MgO\text{-}BeO\text{-}Al_2O_3$ oxide system after a holding time of 7 hours at 1100 °C.
- Addition, of 30 and 60 ppm of Be to Al will have negligible impact on the wetting angle on a Al_2O_3 substrate. The same alloys on an MgO substrate will rapidly react to form an $MgAl_2O_4$ reaction layer.

ACKNOWLEDGMENTS

This paper has been funded by the SFI Metal Production (Centre for Research-based Innovation, 237738). The authors gratefully acknowledge the financial support from the Research Council of Norway and the partners of the SFI Metal Production. Further, the authors would like to thank Ingeborg-Helene Svenum, Martin Fleissner, Per Erik Vullum, and Christian Simensen of SINTEF for their help in the analysis of the samples, and the University of Pittsburg especially Prof. Brian Gleeson for the kind permission to use the laboratory space and fruitful discussions.

REFERENCES

1. S. Balicki: *Prace Inst.*, 1958, vol. 10, pp. 208–13.
2. W. Thiele: *Aluminium*, 1962, vol. 38, pp. 780–86.
3. C. Cochran, D. Belitskus, and D. Kinosz: *Metall. Mater. Trans. B*, 1977, vol. 8B, pp. 323–32.
4. G. Sigworth: *Best Practices in Aluminum Metalcasting*, American Foundry Society, Schaumburg, IL, 2014.
5. K. Surla, F. Valdiveso, M. Pijolat, M. Soustelle, and M. Prin: *Solid State Ionics*, 2001, vol. 143, pp. 355–65.
6. S. Bao: Ph.D. Thesis, NTNU, Trondheim, Norway, 2011, pp. 4–80.
7. N. Smith: *Light Metals 2017*, TMS2017, San Deigo, pp. 1465–74.
8. I. Haginoya and T. Fukusako: *Trans. JIM*, 1983, vol. 24 (9), pp. 613–19.
9. K. Wefers: *Aluminum*, 1981, vol. 57, pp. 722–26.
10. N. Smith: *Light Metals*, TMS2018, Phoenix, 2018, pp. 913–19.
11. M. Syvertsen: *Light Metals*, TMS2017, San Diego, 2015, pp. 1451–55.
12. T. Engh: *Principles of Metal Refining*, 1st ed., Oxford University Press, New York, NY, 1992, pp. 114–17.
13. O. Ozdemir, E. Gruzleski, and A. Drew: *Oxid. Metals*, 2009, vol. 72, pp. 241–57.
14. S. Miresmaeili: *Metal*, 2005, vol. 2005, pp. 223–31.
15. X. Wang, X. Zeng, G. Wu, and S. Yao: *Appl. Surf. Sci.*, 2006, vol. 253, pp. 2437–42.
16. X. Wang, X. Zeng, G. Wu, S. Yao, and Y. Lai: *Appl. Surf. Sci.*, 2007, vol. 253, pp. 3574–80.
17. X. Wang, X. Zeng, G. Wu, and S. Yao: *Mater. Lett.*, 2007, vol. 61, pp. 968–70.

Paper IV

Mechanism behind the inhibiting effect of CO_2 on the oxidation of Al-Mg Alloys

Nicholas Smith[a], Brian Gleeson[c], Wissam A. Saidi[c], Anne. Kvithyld[b], Gabriella. Tranell[a]

[a] *Department of Material Science, NTNU, Trondheim, Norway*
[b] *SINTEF Industry, Trondheim, Norway*
[c] *Department of Mechanical Engineering and Materials Science, University of Pittsburgh, Pittsburgh, PA 15216, USA*

Abstract: Al-Mg alloys are known to suffer from problematic oxidation during melting, refining and casting. The use of a CO_2/air cover gas is known to minimize this oxidation; however a mechanistic understanding of the beneficial inhibiting effect is lacking. A series of thermogravimetric experiments were conducted under a variety of different CO_2-containing atmospheres at 750 °C to elucidate the inhibiting effect. Characterization of the oxide layer was done by surface and cross-sectional analysis in the electron microscope and XPS depth profiling. It was found that additions of as little as 5% CO_2 to air delayed the onset of breakaway oxidation for at least 7 hours and gave a notable reduction in the mass gain compared to exposure to pure air at 750 °C. The XPS depth profile showed a carbon-containing layer due to adsorbed CO_2 at the surface of the oxide layer. It was inferred that this carbon-containing layer slowed the transport of Mg vapor from the metal through the oxide layer resulting in a reduction in the amount of Mg vapor available for oxidation.

1 INTRODUCTION

Al-Mg alloys are known to exhibit excessive oxidation rates, with corresponding melt losses in the casthouses. The addition of Mg to an Al melt has a significant impact on the oxidation rate, as Mg oxidizes preferentially to Al to form an MgO or $MgAl_2O_4$ oxide layer, depending on the Mg content of the alloy (1). Magnesium is known to segregate to the surface, giving a higher effective Mg content at the metal-oxide interface. Further, it has been shown that the evaporation of Mg from an Al-Mg alloy at elevated temperatures is significant (2), showing that the vapor pressure of Mg over an Al-Mg allow is appreciable. Wightman and Fray (3) deduced that it was Mg transport through the oxide layer that was rate controlling for the oxidation. By contrast, it has also been proposed that the transport of oxygen through the oxide layer is rate controlling (4). Whether the oxide grows outwards (Mg diffusion) or inwards (O_2 diffusion), i.e., regardless of which diffusing species is rate controlling, the gas diffusion rate across the oxide layer is of importance.

The oxidation of Al-Mg alloys are known to undergo three distinct stages of oxidation: incubation, breakaway and passivation. The incubation stage is an initial period of low oxidation that is controlled by diffusion through the MgO layer. After a period ranging from a few minutes to hours, depending on alloy composition and oxidation conditions, the MgO layer will rupture, initiating breakaway oxidation, resulting in a dramatic increase in the oxidation rate and a significant loss of Mg from the alloy due to its vaporization and subsequent oxidation to MgO or $MgAl_2O_4$. The oxidation rate will remain high until most of the Mg in the alloy has been depleted, at which point the rate will decrease to near zero (1). Gases typically considered to be inert, such as argon or nitrogen, tend to have little effect on the rate of liquid Al-g alloy oxidation, as these gases at standard laboratory purity have sufficient amounts of oxygen to allow oxidation to occur

unless additional steps are taken to remove all traces of oxygen from the gas (5). Oxygen partial pressures below ~10^{-45} and ~10^{-51}mbar are required to prevent Al and Mg, respectively, from oxidizing at 750 °C (6). While ppm additions of beryllium to the alloy has been used by the aluminum- producing industry to suppress oxidation, its use presents potential health risks (7). To that end, reactive cover gases have shown promise as a potential replacement.

CO_2 is one such reactive gas that has been shown to reduce the oxidation of Al-Mg alloys (3) (4) (8) (9). Air-based atmospheres containing as little as 5% CO_2 have been shown to suppress the oxidation of Al-Mg alloys and delay breakaway oxidation. Cochran *et al.* (8)found that the minimum amount of CO_2 required to protect an Al-Mg melt from excessive oxidation is proportional to the magnesium content. Haginoya *et al.* (4) carried out a detailed study, to date only published in Japanese, on the effects of CO_2 on the oxidation and confirmed that CO_2 additions to the atmosphere could slow the oxidation kinetics. Moreover, it was proposed that the inhibiting effect was due to the adsorption of CO_2 onto the MgO surface slowing the transport of oxygen to the melt; however, conclusive proof of this was not reported.

1.1. Thermodynamic considerations. From a thermodynamic viewpoint, the minor addition of CO_2 to an air atmosphere would not be expected to affect the oxidation of an AlMg melt, as both Mg and Al are able to reduce CO_2 at the temperature range in question. With the CO_2 first being reduced to CO per equations 1 or 3 below, the CO may also be further reduced to C per equation 2 or 4. Magnesium will oxidize preferentially to Al, however, once all Mg has been oxidized to MgO, the alloy will continue to oxidize to $MgAl_2O_4$ (10).

$$\frac{1}{2}Mg + \frac{1}{2}CO_2 = \frac{1}{2}MgO + \frac{1}{2}CO \qquad \Delta G = -296.8 \text{ kJ/mol oxygen at } 750°C \qquad (1)$$

$$Mg + CO = MgO + C \qquad \Delta G = -288.4 \text{ kJ/mol oxygen at } 750°C \qquad (2)$$

$$\frac{1}{3}Al + \frac{1}{2}CO_2 = \frac{1}{6}Al_2O_3 + \frac{1}{2}CO \qquad \Delta G = -257.4 \text{ kJ/mol oxygen at } 750°C \qquad (3)$$

$$\frac{2}{3}Al + CO = \frac{1}{3}Al_2O_3 + C \qquad \Delta G = -249.0 \text{ kJ/mol oxygen at } 750°C \qquad (4)$$

In an atmosphere not containing any free oxygen, the maximum CO partial pressure in the system is controlled by the Boudouard reaction given in equation 5. The equilibrium CO fraction ($CO/CO+CO_2$) is calculated to be 0.78 at 750 °C and will increase as the temperature increases. As CO is only generated from equations 1 and 3, it will take time for the CO partial pressure to reach the level required for it to react in this system either by equation 2, 4 or 5, unless the total amount of gas is limited in relation to the reactant surface area. Under a flowing gas the amount of CO build-up will be limited, which suggests that deposition of elemental carbon on the surface should not be expected. The addition of oxygen to the system will drive the CO partial pressure down as the CO will be oxidized back to CO_2 in accordance with equation 6.

$$CO = \frac{1}{2}C + \frac{1}{2}CO_2 \qquad (5)$$

$$\frac{1}{2}CO + \frac{1}{4}O_2 = \frac{1}{2}CO_2 \qquad \Delta G = -193.8 \text{ kJ/mol oxygen at } 750°C \qquad (6)$$

In a mixed CO_2/air atmosphere, any free oxygen in the system should react with Mg to form MgO per equation 7 or, in the absence of Mg or very low mg chemical activity, with Al per equation 8. Based on Graham's law (11) which states that the diffusion rate of a given gas constituent is inversely proportional

to the square root of its molecular weight, the flux of O_2 from the bulk gas to the oxide layer should occur faster than CO_2 for a similar bulk-gas content of these two constituents. Specifically, under a CO_2/air atmosphere the sample will have an N_2 containing boundary layer which O_2 and CO_2 must diffuse through before reacting. It is calculated using Graham's law that the O_2 flux through this boundary layer will be 1.2 times higher than that of CO_2 if the gradients of the two oxidants are the same.

$$Mg + \frac{1}{2}O_2 = MgO \qquad \Delta G = -676.9 \text{ kJ/mol oxygen at } 750°C \qquad (7)$$

$$\frac{2}{3}Al + \frac{1}{2}O_2 = \frac{1}{3}Al_2O_3 \qquad \Delta G = -451.3 \text{ kJ/mol oxygen at } 750°C \qquad (8)$$

Based on the analysis above it can be surmised that the oxidation inhibiting effect of CO_2 is neither thermodynamically nor directly kinetically dictated. Thus, a fundamental understanding of the mechanism and kinetic effects, explaining how CO_2 reduces the oxidation is still lacking. The purpose of this work was to elucidate on this mechanism.

2 EXPERIMENTAL PROCEDURES

2.1. Materials. A model aluminum alloy with a targeted 5 wt. % Mg was prepared by combining appropriate amounts of 99.999 % pure Al and 99.98 % Mg to give a total mass of 147 grams. The mixture was then placed in an alumina crucible and induction melted in an argon atmosphere. The alloy melt was held at 850 °C for 15 minutes to ensure homogenization. The alloy composition was analyzed by ICP-MS and found to contain 4.85 ± 0.16% Mg. Oxidation samples measuring 10 mm in diameter and 1.5 mm thick were made using a SiC abrasive saw to cut the as-cast alloy to 1.5 mm thick slices, which were then punched to 10 mm discs. Prior to oxidation, samples were polished to a 1 μm finish and stored in ethanol.

To complement the oxidation tests on the model alloy additional tests were carried out in a horizontal tube furnace with a 6063 series alloy that contained 0.72 % Mg and 0.52 % Si, provided by an industrial partner. Samples measuring 12.5 x 25 x 1.5 mm and polished to a 1μm finish were prepared using the same method as above for testing in the tube furnace.

2.2. Oxidation Testing. A Linseis STA 2400 thermogravimetric analysis (TGA) system with a 10 μg sensitivity was used for the main series of oxidation experiments. A schematic of the system is shown in Figure 1. For a given test, a sample stored in ethanol was dried, weighed, and placed in the TGA and exposed to a variety of different gas atmospheres. Samples were heated to the oxidation temperature of 750 °C under an argon environment with a heating time of 35 minutes. Once the sample reached 750 °C, the chosen reactant gas was introduced into the chamber and exposure continued for up to 420 minutes. Table 1 outlines the experimental matrix for the main study. An exception to the standard procedure were experiments 16-20, where the reactant gas was started at the beginning of heating. A standard total gas flow of 0.2 liters per minute was used for all experiments.

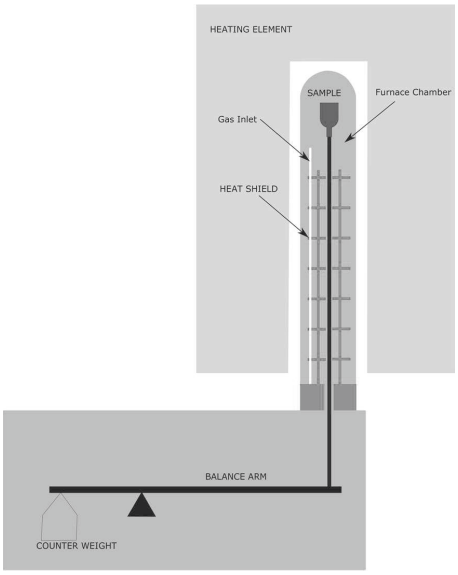

Figure 1. Schematic of the TGA used for this work.

The supplementary tests on the 6063 alloy in a horizontal tube furnace were carried out to give additional insight onto the effects of CO_2 and CO on the oxidation. The prepared samples were oxidized in an atmosphere of $5CO_2$/95Ar, 5CO/95Ar or 100 Ar for 90 minutes at 550 °C. Samples were placed in an alumina boat and slid into a preheated alumina tube furnace and held for 90 minutes before being removed.

2.3. Sample Analyses. After oxidation, the percent mass gain vs. time was plotted by dividing the mass change by the initial mass. Mass gain provides clear information about effects of different conditions on the oxidation rate, however, to best understand the mechanism behind the inhibiting effect of CO_2, a detailed characterization of the oxide layer morphology was required. This was achieved by analyzing the samples using an FEI Helios NanoLab DualBeam focused ion beam (FIB) miller in which a cross section was cut through the oxide layer into the base metal such that the morphology and thickness of the oxide layer could be evaluated. Selected samples were analyzed in a Joel JEM ARM200F TEM with TEM samples being prepared using the FIB. Finally, to locate any carbon-containing regions on and/or within the oxide layer, a Kratos Axis Ultra DLD X-ray photoelectron spectrometer (XPS) coupled with argon sputtering was used to generate a depth profile through the oxide layer. The surfaces of the 6063 alloy were examined in the SEM after oxidation to characterize the effects of the different atmosphere on the oxide morphology.

2.4. Density functional theory calculations. To supplement the experimental work, density functional theory (DFT) simulations were conducted using the Vienna ab-initio simulation package VASP (12) (13) employing Perdew-Burke-Ernzerhof (PBE) exchange-correlation functional in all calculations (14). The electron-nuclear interactions were described using the projector augmented wave (PAW) in which the wave functions are expanded using plane waves with an energy cutoff of 350 eV. The Al(111) surface was modeled using a (3x3) surface supercell based on conventional unit cell (lattice constant 4.04 Å) , and eight layers in the non-periodic direction. A vacuum of more than 15 Å was used to mitigate fictitious interactions in the non-periodic direction. A 4x4x1 k-grid was used to sample the Brillouin zone. The energy relaxation

was iterated until the forces acting on all of the atoms were less than 1 meV/ Å, with a convergence in the total energy of 10^{-6} eV. During optimization of the substrate structures, the four layers from the bottom of the slab were fixed, whereas the other four layers were fully relaxed to their lowest energy configurations with respect to all of the remaining degrees of freedom. The fixed layers were set to their bulk positions using their optimized lattice constants. Validation of the computational framework was done by checking that the energy cutoff, k-grid, energy tolerances were sufficient to converge energy differences to less than 1 meV.

3 RESULTS

3.1. TGA mass gain results. Results of the experiments are summarized in Table 1. Mass gain was calculated by taking the mass difference of the sample between 405 minutes and 5 minutes of oxidation at 750 °C. No traces of deposited Mg vapor were visually observed on the crucible or furnace walls after a given oxidation test. Any mass loss due to Mg evaporation was hence assumed minimal and could be neglected. Breakaway time was defined by the point where the mass gain departed from a linearity, and was defined by the following criterion:

$$mass_t - mass_{t-1min} > 0.02$$

The time for breakaway oxidation to begin was generally found to be between 175 and 185 minutes at temperature, but varied between 133 and 310 minutes for oxidation in 100 % air.

The calculated thickness of the oxide layer was based on the total mass gain from the oxidation exposure and the assumption of the oxide layer being pore-free crystalline MgO with a density of 3.58 g/cm^3. The surface area was calculated to be the area of the top, bottom and side of the sample. To that end it was confirmed from FIB examination that the oxide layer had a similar thickness on both the top and bottom surface of the sample. Multiple backgrounds tests, where the crucible had an MgO sample that would not react, were conducted and showed that the change in airflow at the start of oxidation would take up to 180 minutes to fully stabilize. Due to such a large buoyancy effect versus the small overall mass gain, on the samples that did not breakaway, the mass gain used to determine the thickness was calculated by taking the mass from 405 minutes of oxidation minus the mass at 195 minutes of oxidation, and extrapolating back to the start of oxidation. This minimized any buoyancy effect. For experiments 16-20, where there was no increase in gas flow at the start of the isothermal period, the mass gain was calculated from 5 minutes to 405 minutes at temperature.

Table 1. Results of TGA experiments

	Stage 1			Stage 2			Notes	Mass gain (mg)	%mass gain	mass gain (mg/cm2)	Breakaway time	calculated thickness (nm)
EXP #	Gas 1	Gas 2	time	Gas 3	Gas 4	time						
1	100 Air		420					15.03	6.23	30.69	175	
2								2.2	0.86	4.49	310	
3	20 CO	80 Ar	420					0.31	0.13	0.63	>420 min	424
4	5 CO_2	95 air	420					0.06	0.02	0.12	>420 min	82
5	20 CO_2	80 air	420					0.25	0.08	0.51	>420 min	342
6								0.25	0.10	0.51	>420 min	342
7	50 CO_2	50 air	420					0.32	0.12	0.65	>420 min	438
8	20 CO_2	80 Ar	420					0.38	0.18	0.78	>420 min	520
9	20 CO_2	80 air	30	100 air		390		0.77	0.32	1.57	378	
10								1.35	0.58	2.76	303	
11	20 CO_2	80 air	60	100 air		360		0.32	0.13	0.65	>420 min	438
12	100 air		60	20 CO_2	80 air	360		0.21	0.09	0.43	>420 min	287
13	100 air		till break away	20 CO_2	80 air			3.16	1.68	6.45	175	
14								5.63	2.91	11.50	184	
15								2.63	1.44	5.37	133	
16	20 CO_2	80 air	420				from start	0.17	0.08	0.35	>420 min	233
17	20 CO_2	80 air	420				Not flowing	0.46	0.22	0.94	>420 min	629
18								0.28	0.14	0.57	>420 min	383
19	20 CO_2	80 Ar	420				Not flowing	0.89	0.33	1.82	>420 min	1217
20								0.5	0.27	1.02	>420 min	684

Figures 2-6 show the effect of different flow conditions on the percent mass gain. In all the figures the zero point for % mass gain is set to five minutes after the reactant gas has been switched on, as a significant proportion of the instability in the mass balance had stabilized within that time. Figure 2 shows the mass gain of the alloy for increasing amounts of CO_2 in air ranging from 5 to 50 % CO_2, compared to pure air (experiments 4-7). It can be seen that while there is a variation in the length of the incubation period for the samples in pure air, the samples oxidized under a CO_2-containing atmosphere remained in the low mass-gain incubation region for all 7 hours. It can also be seen that additions of 5% CO_2 to air protected the alloy equally as well as 50CO_2/50air, as the variation in the mass gain between the samples is less than one standard deviation. This is in disagreement with the work by Haginoya et al. (4) who found that the amount of CO_2 was important. This may be due to the higher Mg content used in that work requiring a higher amount of CO_2 to protect the melt.

Figure 3 shows that the mass gain in CO_2/Ar (experiment 8) was very similar to CO_2/air. This figure also compares the percent mass gain curves for CO_2/Ar vs. CO/Ar, where it can be seen that CO provides a similar protective effect when compared to air.

In experiments 9-11 the samples were initially oxidized in a CO_2-containing environment for an initial period after which the CO_2 was turned off and oxidation continued in pure air. It was found that 30 minutes of CO_2 was not sufficient to protect the sample for the entire 7 hours, as those samples exposed initially to CO_2 for 30 minutes began to breakaway near the end of the oxidation cycle. However, 60 minutes of initial exposure to CO_2 was sufficient to protect the sample for 7 hours, as shown in Figure 4.

Figure 5 shows the results of samples that were initially oxidized in only air for a short period followed by oxidation in CO_2/air (experiments 12-15). Addition of CO_2 to the atmosphere shortly after the onset of breakaway oxidation (experiments 13-15) was found to provide a protective effect and resulted in the suppression of breakaway oxidation. The ability to suppress breakaway oxidation is time dependent, in that

if CO_2 is not introduced in the early stage of breakaway oxidation it appears to have a limited effect on the oxidation (experiment 14), as can be seen in Figure 5. Oxidation in pure air for 60 minutes followed by $20CO_2$/80air (experiment 12) showed similar mass gain to samples oxidized for the entire holding period in a CO_2 atmosphere.

Experiments 1-16 were done under an atmosphere that was flowing, and therefore had a constant CO_2 and CO partial pressures over the sample surface. In experiments 17-20, the furnace was filled with $20CO_2$/80air and sealed for the duration of the experiment, thus allowing the CO_2 and CO partial pressures to vary with time. The results from these experiments are shown in Figure 6, where it can be seen that the mass gain was slightly higher in the experiments where the gas was not flowing. Further, the $20CO_2$/80Ar samples had an average mass gain of 1.42mg/cm^2 versus 0.76 mg/cm^2 for $20CO_2$/80Air.

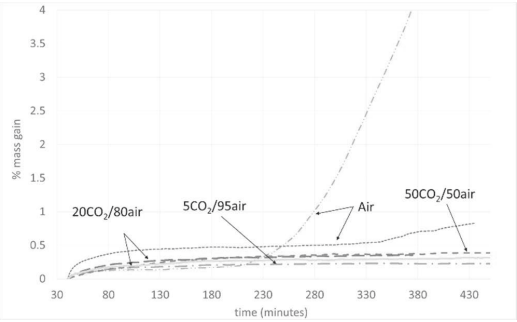

Figure 2. Effects of varing CO_2 amounts in air compared to oxidation in pure air, experiment numbers 1-2, 4-7.

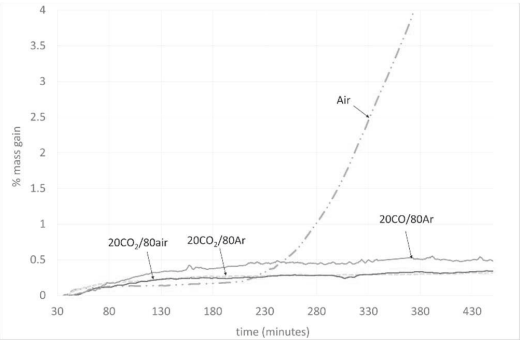

Figure 3. Similarities of $20CO_2$/80air and $20CO_2$/80Ar and 20CO/80Ar, experiment numbers 1, 3, 5, 8.

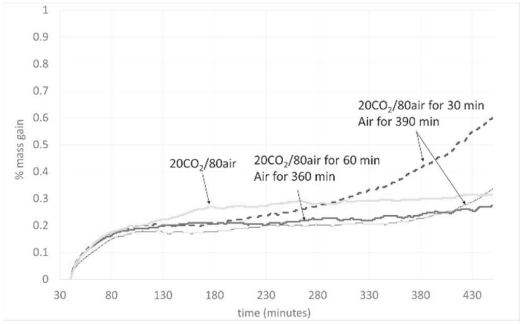

Figure 4. Effects of CO_2 for a short period at start of the oxidation cycle followed by air only, experiment numbers 5, 9-11.

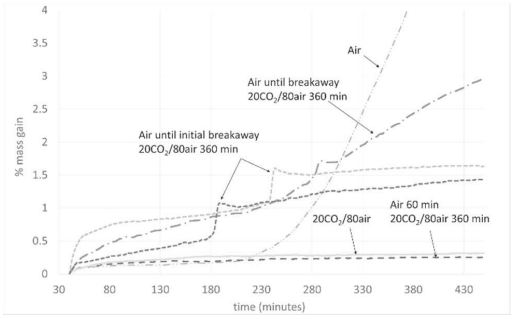

Figure 5. Effects of CO_2 additions after a period of oxidation in an air only atmosphere, experiment numbers 1, 5, 12, 13-15.

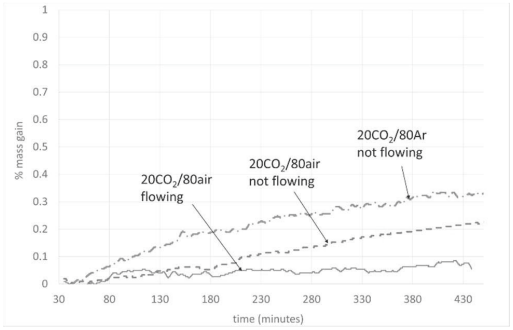

Figure 6. Effects of a non-flowing atmosphere on the mass gain, experiment numbers 16-20.

3.2. Oxide Layer Morphology. As a reference, a sample heated in argon and then held at 750 °C for 1 minute was found to have a 60 nm thick oxide layer, indicating that an appreciable amount of oxidation occurred during the 35 minutes required to heat and melt the samples. Examination in the FIB showed that cracks in the oxide layer were present for all the samples after oxidation. In general, the cracks appeared to be covered by an oxide layer under 10 nm thick, as indicated in Figure 7 showing a cross-section of a crack after oxidation in $20CO_2$/80Air at 750 °C for 60 minutes. For samples that were oxidized in CO_2 for a short

period followed by oxidation in pure air (experiments 9-11), many of the oxide cracks were filled completely with oxide, as shown in Figure 8. It is inferred that these cracks formed when the alloy melted and that subsequent oxidation in the cracks was limited by the presence of CO_2, resulting in an oxide layer of approximately 10 nm thick.

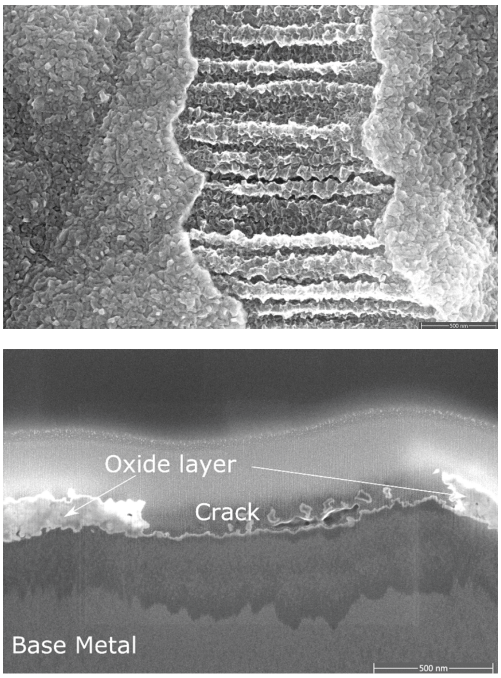

Figure 7. Top surface and cross-section of crack on sample oxidized for 60 min in $20CO_2/80Air$ at 750 °C.

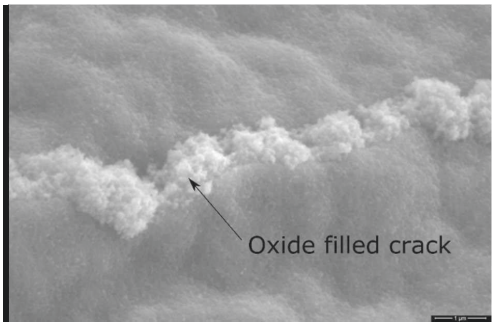

Figure 8. Crack filled with oxide after 30 min with $20CO_2/80air$ followed by 390 min in pure air at 750°C.

For samples oxidized in $20CO_2/80air$, an increasing amount of porosity was found at the oxide-metal interface with longer holding times; as indicated in Figure 9 a-b, which shows two samples oxidized in $20CO_2/80Air$ at 750 °C for 60 minutes (a) or 420 minutes (b). By comparison, only a trace amount of porosity was evident in the oxide layer formed after oxidation in $20CO_2/80$ air for 60 minutes followed by

360 minutes in pure air (Figure 10). These results suggest that the porosity formation is dependent on the presence of CO_2 for longer periods.

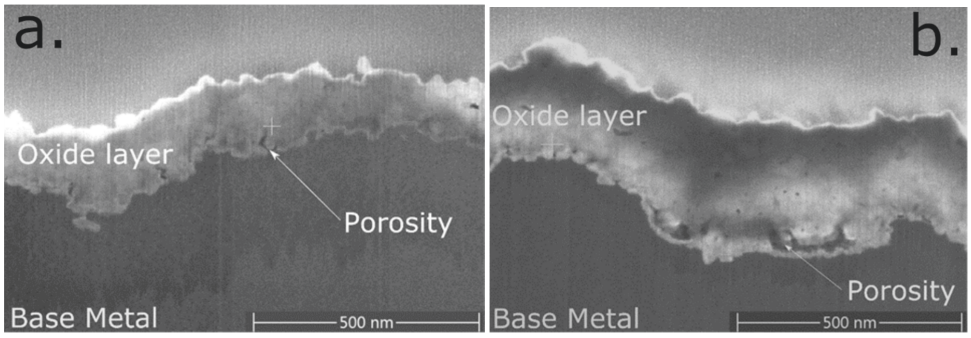

Figure 9. Sample oxidized in $20CO_2$/80air at 750°C for a) 60 min b) 420 min with porosity at oxide-metal interface.

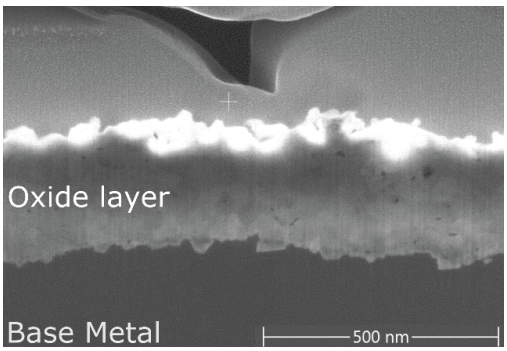

Figure 10. Sample oxidized in $20CO_2$/80air at 750°C for 60 min followed by 360 min in air with no significant porosity.

Cross-sectional TEM examination of samples oxidized under a CO_2 containing atmosphere showed that the oxide layer is comprised of small grains measuring 35 nm ±20 nm in size. Electron energy loss spectroscopy (EELS) revealed that the oxide layer consisted of 100% MgO with no indication of aluminum oxide, spinel or carbon present. This was confirmed by the TEM diffraction pattern that showed the oxide layer to be FCC-MgO, as seen in Figure 11.

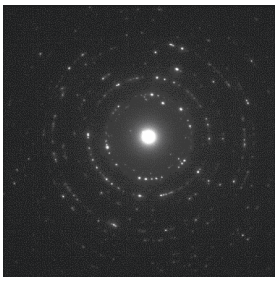

Figure 11. Diffraction pattern from the oxide layer on the sample oxidized at 750°C in $20CO_2$/80air for 420 min showing the layer is FCC-MgO.

The thickness of the oxide layer formed in experiment 5 was 316 nm, based on measurements taken from Figure 9b; whereas, the thickness calculated based on the mass gain is 342 nm. This equates to a discrepancy of only 0.02 mg between calculated and measured thickness. Similarly, for the other samples that did not undergo breakaway oxidation it was found that the measured and calculated oxide thicknesses were of the same order of magnitude.

While the mass-change results showed little difference between samples oxidized in $20CO_2$/80air and $20CO_2$/80Ar, a minor difference in the morphology of the layers was found. The layer on the sample oxidized in CO_2/Ar had a granular layer at the gas-oxide interface in select areas, as seen in Figure 12. The majority of the sample did not appear to form this granular layer, as seen in Figure 13, but instead formed a similar-structured oxide layer as found on samples oxidized in CO_2/Air as seen in Figure 9.

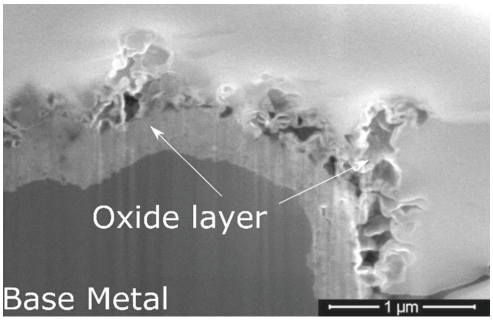

Figure 12. Cross-section of sample with a dense layer covered by a granular layer after oxidization in $20CO_2$/80Ar for 420 min at 750 °C.

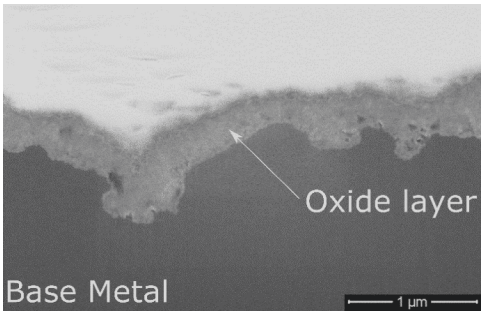

Figure 13. Sample oxidized in $20CO_2$/80Ar for 420 min at 750°C with no granular layer preset (same sample as Figure 12).

3.3. XPS depth profile. The high amount of topography of the samples oxidized at 750 °C resulted in less than ideal conditions for an XPS depth profile. To overcome this, a sample was oxidized at 550°C for 420 minutes in $20CO_2$/80Ar with the aim of creating a smooth surface for XPS. However, an Mg-rich phase existed in the sample and at 550 °C this phase exhibited extensive oxidation, resulting in a granular oxide layer that was 3 µm thick on average as shown in Figure 14, but was up to 10 µm thick in selected locations.

It is deduced that at 550°C the oxygen partial pressure in the Ar was not sufficient to form a dense oxide layer like that seen on samples exposed at 750 °C. Due to the thickness of the oxide layer formed at 550 °C, it was not possible to sputter through the entire oxide layer into the base metal. As a result only the top 2 µm of the oxide layer were examined. The overall profile is shown in Figure 15. Here it can be seen that the oxide layer is primarily MgO, however, increasing amounts of Al and $MgAl_2O_4$ can be found with increasing depths. The oxygen signal was interpreted to be comprised of three peaks: oxygen associated with MgO; oxygen associated with $MgAl_2O_4$; and oxygen associated with carbon. The ionic Mg and Al peaks stemming from the oxides were clear and well defined, allowing the amount of oxygen associated with those oxides to be subtracted, leaving a clear peak showing the oxygen that must be associated with the carbon. Analysis of the carbon peak showed that the carbon signal was comprised of four peaks, as shown in Figure 16. Figure 17 shows the depth profile from the carbon signal and the associated oxygen signal. The peak at 291.5 eV is at a similar position to the one reported by Onishi et al. (15)after exposure of MgO to CO_2 at room temperature. It was suggested by these authors that this is the magnesium carbonate peak; however, thermodynamic calculation shows that magnesium carbonate should not form on samples at the temperatures used in this work. It is speculated that this carbonate formed when the sample cooled after the isothermal exposure. The oxygen signal is believed to be primarily associated with the peak at 286.4 eV. Initially a 2:1 ratio is seen between the oxygen and C 286.14 eV signal, which would strongly indicate the presence of adsorbed CO_2. The oxygen signal decreases as the depth into the oxide layer increases, and the O:C ratio at the end of the profile becomes 1:1. This decrease in oxygen is likely due to the adsorbed CO_2 being reduced to CO by Mg inside the oxide layer. The two unknown carbon peaks are at too high of binding energies to be elemental carbon or a carbide phase (16) and their source is currently unknown. An XPS profile from a sample oxidized at 750 °C was generated, but as explained above, the topography made it difficult to obtain an accurate depth profile. The carbon signal from the 750 °C sample is shown in Figure 18. Here it can be seen that the general shape of the curve is the same as that of the 550 °C sample. Therefore, it can be assumed that similar carbon species will exist on a sample from 750 °C as was found at 550 °C.

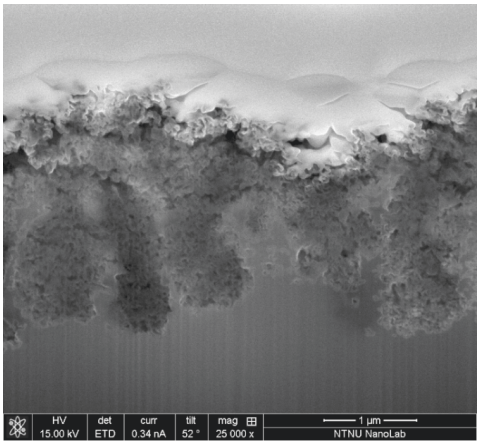

Figure 14. Oxide layer on sample oxidized at 550°C in $20CO_2/80Ar$ for 420 minutes and analyzed by the XPS.

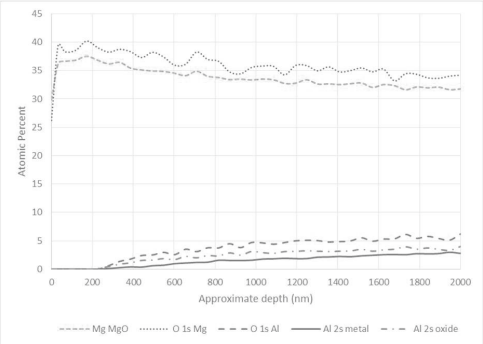

Figure 15. XPS depth profile of Mg and Al for sample from oxidized at 550°C.

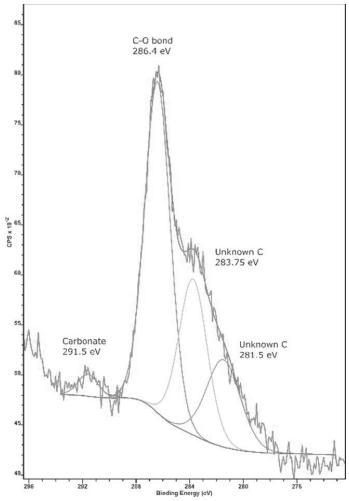

Figure 16. Carbon peak from 172 nm depth of 550 °C sample.

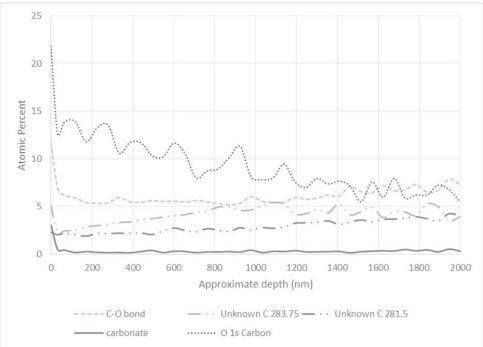

Figure 17. Depth profile of carbon and the associated oxygen signal from sample oxidized at 550°C in air.

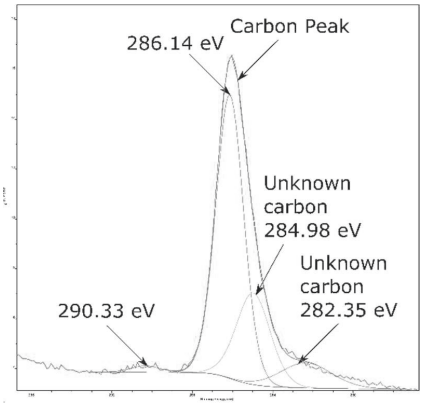

Figure 18. Carbon peak from oxidation at 750 °C XPS scan at after 90 seconds of sputtering

3.4. 6063 series alloy experiments. The oxidation of the wrought 6063 alloy showed that 5%CO_2/Ar inhibited oxidation significantly more effectively than 5%CO/Ar, as can be seen by comparing Figures 19 and 20. The sample oxidized in a CO_2-containing environment showed no significant visible oxidation as opposed to the sample exposed to CO, where a notable amount of oxide was present on the surface. Exposure of the alloy to a 100% Ar atmosphere led to oxide clusters, which are inferred to be the result of the oxidation of Mg vapor with the impurity oxygen present in the argon. This shows that the addition of CO_2 to an Ar atmosphere has a significant inhibiting effect even when only trace amounts of oxygen are present and can suppress the oxidation or formation of Mg vapor. While CO in Ar showed the highest amount of oxidation, the total amount of oxidation was negligible, as no measurable increase in the sample mass was recorded after 90 minutes of oxidation.

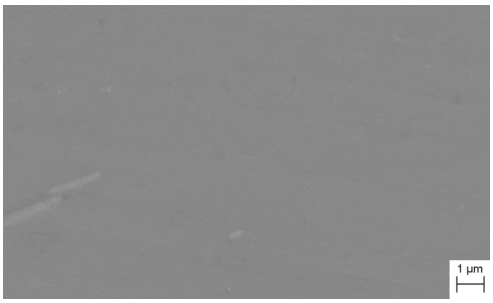

Figure 19. 6063 alloy showing a surface with no visible oxidation after exposure in 5CO_2/95Ar for 90 min at 500°C.

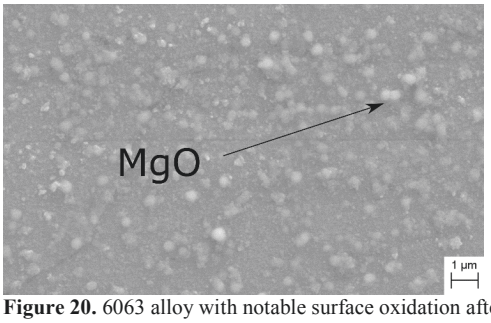

Figure 20. 6063 alloy with notable surface oxidation after exposure in 5CO/95Ar for 90 min at 500 °C

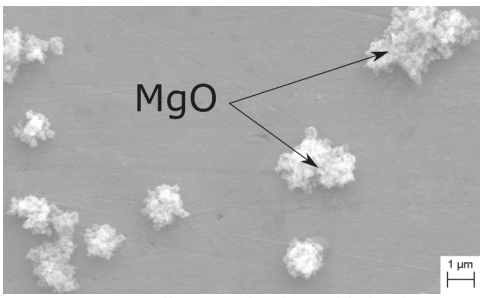

Figure 21. 6063 alloy sample after oxidation in 100 Ar showing oxide clusters that are the result of oxidation in the gas phase followed by deposition on the surface.

4 DISCUSSION

A mixed CO_2/air atmosphere was found to have a strong inhibiting effect on the oxidation of a 5%Mg-Al alloy compared to a pure air atmosphere. This inhibiting effect did not appear to depend on the CO_2 concentration, as partial pressures corresponding to between 5 and 50 % showed similar results. The addition of CO_2 appeared to reduce the flux of Mg through the oxide layer, thus increasing the time to breakaway oxidation.

To better understand how CO_2 inhibits the oxidation, it is informative to consider the interaction of the CO_2 with Al and Mg and how it differs from O_2 and CO. Accordingly, DFT calculations were conducted to provide a more detailed examination of the interaction between CO_2, O_2, and CO with crystalline Mg and Al.

Without going in to detail, the calculations were in agreement with previous results (2) in that they showed a strong segregation enthalpy of 0.3 eV for Mg from subsurface layers to the outermost layer. Further, the calculations show that CO_2 can interact with a Mg-doped Al(111) surface either molecularly or dissociatively with exothermic energies of 0.08 eV and 1.41 eV, respectively. In the CO_2 dissociated state, both oxygen and CO are released, where O binds to the Mg site and the CO is unbound in the gas phase. On the other hand, on the pristine Al(111) surface, CO_2 only weakly binds via van der Waals interactions. This shows that Mg-doping acts as an oxygen attractor to the surface, as indicated in Figure 22. Further, the DFT calculations reveal that CO does not dissociate on either pristine Al(111) or Mg-doped Al(111), but adsorbs weakly via van der Waals interactions.

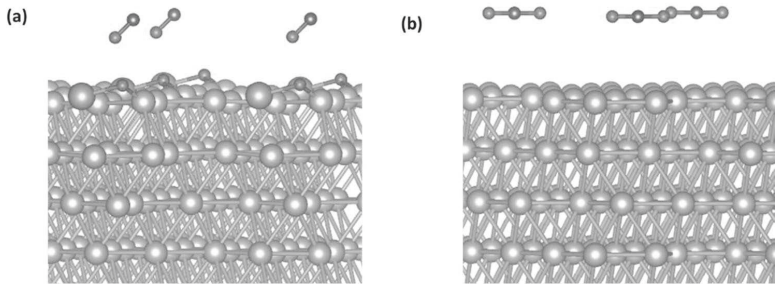

Figure 22. Interaction of CO_2 with Mg doped (a) and pristine Al(111) (b). Al, Mg, O, C are shown as turquoise, orange, brown, and red spheres, respectively.

The DFT calculations also showed that oxygen dissociates on both the pristine Al(111) and Mg-doped Al(111) surfaces. The exothermic dissociation energy on the pristine Al(111) surface was calculated to be 4.47 eV/oxygen. On the Mg-doped surface, oxygen can dissociate on Al or Mg sites with exothermic dissociation energies of 4.21 and 4.5 eV/oxygen, respectively. The stronger interactions of Mg with oxygen compared to Al is consistent with their oxidation enthalpies.

In summary the DFT calculations, in agreement with thermodynamic predictions, show that the interactions of oxygen with either pristine or Mg-doped Al(111) surface is a significantly more favorable with O_2 than with CO_2. This indicates that directly preferential reaction/adsorption of CO_2 on the metal surface is not likely unless the CO_2 sticking probability is greater than that of oxygen. Previous studies have showed that the oxygen sticking probability on Al(111) is very low despite strong adsorption energies. This is due to spin selection rules associated with the triplet spin state of O_2 (g), which results in a highly nonadiabatic behavior in the oxygen/Al(111)interactions (17). On the other hand, CO_2 is in a singlet spin arrangement in its ground state and hence is not affected by the spin selection rules as it dissociates on the Mg-doped Al(111) surface.

4.1. TGA and morphology considerations. The results from the TGA experiments were found to generally agree with those of Haginoya and Fukusako (4). From a comparison between the oxide layers on the samples oxidized in a CO_2-containing atmosphere and those in pure air, it has been observed that the addition of CO_2 limits the formation of a granular layer at the surface of the oxide layer. This granular layer has previously been seen to form as a result of the oxidation of AlMg alloys at elevated temperatures (7). As the effect was clear in both CO_2/air and CO_2/Ar atmospheres (Figure 3), the inhibiting effect of CO_2 must act independent of the oxygen partial pressure.

For the oxidation of the 6063 series alloy, the lack of oxide clusters that were found on the sample oxidized in CO_2/Ar, as opposed to CO/Ar or pure Ar, indicates that the addition of CO_2 acts to reduce the amount of Mg vapor at the oxide surface. Since the localized growths found on the surface of Figure 21 after testing in 100% Ar can only occur if Mg is transported from the alloy through the oxide-gas interface, this provides strong evidence that in the absence of CO_2 a notable amount of Mg vapor exists at the oxide-gas interface. With the addition of CO_2 this Mg vapor is no longer present as CO gas lacks the ability to significantly reduce the Mg vaporization through the oxide layer as notable amounts of MgO are present on the surface of this sample. A possible explanation for this can be deduced from the results of Onishi *et al*. (15), who found that CO_2 was able to absorb onto MgO surface at room temperature while both O_2 and CO were not.

4.2. Effects of CO. The effects of a CO_2/Ar atmosphere gave similar results to a CO_2/Air atmosphere, as shown in Figure 3. In experiments 17-20 where the gas was held static over the sample, a slightly higher mass gain was recorded in CO_2/Ar than in CO_2/Air. While the average difference is small it does indicate that the oxidation is dependent on the CO partial pressure. When the oxidation occurs in a CO_2/air environment, any formed CO will be oxidized back to CO_2 in the gas phase per equation 6, thus maintaining a low CO partial pressure; however, for oxidation in a CO_2/Ar atmosphere the CO partial pressure will increase.

This is likely due to differences in how CO interacts with the oxide surface. However, CO must interact with the surface in a way that will inhibit the oxidation, as the overall mass gain in CO was still lower than air. The work by Wightman et al. (3) showed that oxidation in CO_2 is independent of CO_2 concentration, but the reaction of CO with Mg (equation 2) is dependent on the CO concentration. This would support the conclusion from this work that the CO partial pressure is important to the oxidation rate.

4.3. Mass transport considerations. To better understand the effects of CO_2 on the diffusion of Mg vapor through the oxide layer, the diffusion coefficient was calculated based on the TGA results. The diffusion coefficient for the flux of Mg vapor through the oxide layer was calculated from equation 9.

$$J_{Mg} = \frac{D_{Mg}(p^1_{Mg} - p^2_{Mg})}{\delta RT} \quad (9)$$

where J_{Mg} is the mass flux of Mg vapor, D_{Mg} is the diffusion coefficient, P is the Mg pressure at the oxide-metal (1) and the oxide-gas (2) interface, δ is the oxide layer thickness, R is the gas constant and T is the temperature.

J_{Mg} can be calculated from the TGA mass gain curves by taking the mass gain per unit area divided by the time. Doing this, an average diffusion coefficient of 4.0×10^{-5} cm^2/s is calculated for experiments 4-7. A predicted diffusion coefficient of 1.54 cm^2/s at 750 °C is estimated from the Chapman-Enskog equation for gaseous diffusion (18). The large discrepancy between the predicted and the measured values indicates that the diffusion of Mg vapor out through the oxide is, as expected, significantly limited compared with what would be expected for unhindered Mg vapor diffusion. The diffusion coefficient calculated during breakaway oxidation from experiment 1 is 5.3×10^{-3} cm^2/s. This value is still several orders of magnitude lower than the Chapman-Enskog value, suggesting that even during breakaway oxidation the oxide layer provides a considerable hindrance to the outward transport of Mg vapor. The published value for the diffusion of Mg through crystalline MgO is 1.71×10^{-11} cm^2/s at 1429 °C (19). This is significantly lower than the measured value from this work, showing that the diffusion out is faster than diffusion through the crystal lattice, but also restricted in comparison to free evaporation.

4.4. Proposed Mechanism. The thermodynamic calculations cannot clearly explain the inhibiting effect that CO_2 has on the oxidation, as the reaction between metal and O_2 should be occurring preferentially. As argued before, CO_2 is a singlet spin state compares to O_2 that is a tripled state, and hence there could be a preferential sticking of the CO_2 to the initially formed MgO surface compared to O_2. This differentiates the CO_2 from oxygen and is aligned with the results of Onishi et al. (15). In order to understand the mechanism by which CO_2 reduces the oxidation rate, we consider the physical evidence gathered in this work:

- The O:C ratio at the MgO surface corresponds to that of CO_2
- The O:C ratio decreases throughout the MgO oxide layer towards the oxide/metal interface

- CO_2 quickly reduces oxidation when added to the atmosphere prior to the onset of breakaway
- The effect of CO_2 in the atmosphere "lingers" when removed

If the assumption that, in agreement with literature, CO_2 molecules are adsorbed on the MgO surface, the oxidation process may be described as follows and shown schematically in Figure 23:

1. An AlMg alloy with an oxide layer of MgO is formed due to oxidation that occurs at low temperatures and melting, including any transformation from the amorphous to crystalline structure. As the alloy is heated from room temperature to its melting point the oxide undergoes rapid further oxidation to form a crystalline layer of MgO around 60 nm thick.
2. When CO_2 enters the system, it will adsorb on to the formed MgO surface and pores, creating a carbon- containing layer.
3. Mg vapor will continue to diffuse outward through the adsorbed CO_2 layer.
4. Due to a limited supply of oxygen below the oxide surface the CO_2 will be reduced to CO trapped in MgO and forming Mg-C-O bonds.

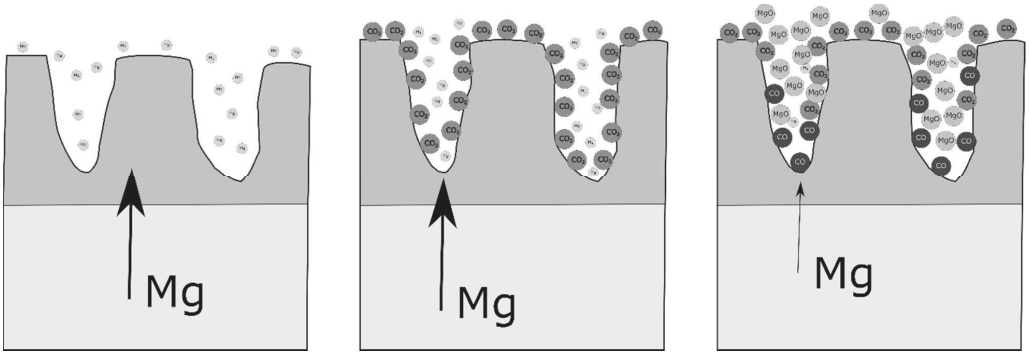

Figure 23. Oxidation schematic showing how CO_2 inhibits oxidation.

It is proposed that the barrier created by the adsorbed CO_2 can reduce diffusion of magnesium out in one of two ways given below. Regardless of how the layer inhibits the diffusion of Mg, it is clear, from the XPS profiles, that a layer of adsorbed CO_2 does form at the oxide-gas interface and provides a physical barrier to the diffusion of Mg vapor out, resulting in the loss of a granular layer that has previously been seen on the oxidation of AlMg alloys in air (7).

1. The formation of an MgO layer that contains adsorbed CO_2 and CO modifies the physical structure of the MgO layer to form a "cap" at the surface of the oxide layer that reduces the rate of Mg diffusion out. As the oxide layer grows around the adsorbed CO_2 the oxygen partial pressure will decrease and the adsorbed CO_2 will react with the Mg to form an Mg-O-C phase that has a different structure to the MgO formed in the absence of CO_2 and is more resistant to the diffusion of Mg out.
2. The CO_2 adsorbs onto the MgO to form a monolayer that inhibits the diffusion of Mg out. The evaporative protection of a surface monolayer is a well-documented phenomenon for the evaporation of water at lower temperatures and a similar mechanism could be at play here (20).

To work as an effective physical barrier to Mg evaporating from the metal, the CO_2 molecules must bind strongly both to the MgO surface and to each other. The former seems more likely as the XPS clearly showed that the CO_2 is reduced as the O:C ratio decreases down towards the metal surface. This indicates that CO_2 reacts with Mg vapor inside the oxide film, creating Mg-O-C bonds in the structure, and possible C deposition as the atmosphere becomes enriched in CO.

The immediate observed effect of adding CO_2 means that the adsorption is fast. Further evidence of the rapid adsorption can be taken from Figure 7, where oxidation thickness in cracks was significantly reduced compared to un-cracked oxide, showing any fresh metal that is exposed will be quickly passivated by the CO_2 before significant oxide growth can occur. The lingering effect is likely due to the slow oxidation of the carbon atoms in the structure as oxygen is allowed to diffuse into the structure, gradually opening pores in the oxide layer again and forming a layer that is more open to diffusion, allowing Mg vapor to escape.

4.5. CO_2's effect on breakaway oxidation. The ability of CO_2 to stop the initial stages of breakaway oxidation can be explained by a lack of available oxygen for the spinel formation. By application of Graham's law it can be concluded that the diffusion of oxygen from the gas phase into and through the oxide layer must be slowed to a similar extent as the Mg vapor diffusion out was slowed. If the diffusion of oxygen inward is restricted, the only other source of oxygen for the spinel phase formation is via equation 10 below, with the existing MgO layer. However, the Gibbs energy for this reaction is positive at 750 °C, and therefore the spinel phase cannot form via the reaction between Al metal and MgO. Further, as the Mg metal will be trapped in the oxide layer by the carbon layer, the Mg activity in the oxide layer increase. As the activity of Mg must be below 0.023 for the spinel phase to form (10), any increase in the activity will inhibit the spinel formation. If the CO_2 is added too late in the breakaway period the spinel phase will have already resulted in damage to the oxide layer allowing the direct flux of oxygen into the melt, which will cause the spinel phase to form via equation 11.

$$MgO + \frac{1}{2}Al = \frac{1}{4}MgAl_2O_4 + \frac{3}{4}Mg \qquad \Delta G = 22.1 \text{ kJ/mol oxygen at } 750°C \qquad (10)$$

$$\frac{1}{4}MgO + \frac{1}{2}Al + \frac{3}{8}O_2 = \frac{1}{4}MgAl_2O_4 \qquad \Delta G = -485.6 \text{ kJ/mol oxygen at } 750°C \qquad (11)$$

The formation of the porosity at the oxide-metal interface is likely due to the buildup of Mg vapor in the oxide layer. As the amount of Mg builds in the oxide layer, it may become large enough to allow porosity to form in the oxide layer.

5 CONCLUSION

The effects of an atmosphere containing CO_2 on the oxidation of an Al-Mg alloy was investigated experimentally and through DFT calculations to better understand the mechanism behind the previously-observed inhibiting effect. It was confirmed that CO_2 provides a significant inhibiting effect on the oxidation of Al-Mg alloys with the addition of CO_2 delaying the onset of breakaway oxidation and reducing the overall mass loss due to oxidation.

This inhibiting effect is attributed to the presence of an adsorbed CO_2 layer on the thermally grown MgO layer. The resulting carbon-containing layer acts as a physical barrier to the diffusion of Mg vapor out. The exact physical changes to the oxide layer are yet to be confirmed, however, it was proposed that the adsorbed CO_2 reacts with Mg vapor in the oxide layer and forms a layer that is more resistant to the diffusion of Mg. Further, it was found that:

- Increased CO_2 partial pressures over 5% did not provide more protection for the same Mg content.
- Under a non-flowing atmosphere the CO_2/Ar resulted in a higher mass gain than CO_2/air, meaning that a low CO partial pressure aids in inhibiting the oxidation.
- The diffusion coefficient for the diffusion of Mg vapor out was found to be 1000 times lower than what would be expected from diffusion of an oxide free surface and over 100 times lower than the diffusion coefficient during breakaway oxidation.
- CO_2 will preferentially adsorb to MgO.
- Breakaway oxidation could be suppressed if CO_2 is added to during the initial stage of breakaway.
- CO/Ar atmosphere is not as effective as CO_2/Air, but still provides an inhibiting effect over pure air.

ACKNOWLEDGEMENTS

This paper has been funded by the SFI Metal Production, (Centre for Research-based Innovation, 237738). The authors gratefully acknowledge the financial support from the Research Council of Norway and the partners of the SFI Metal Production. The computational work is supported by the University of Pittsburgh Center for Research Computing through the resources provided.

REFERENCES

1. I. Haginoya, T. Fukusako, Oxidation of Molten Al-Mg Alloys, Transactions of the Japan Institute of Metals, 24(9) (1983) 61-619. https://doi.org/10.2320/matertrans1960.24.613

2. C. Lea, C. Molinari, Magnesium diffusion, surface segregation and oxidation in Al-Mg alloys, Journal of Materials Science 19 (1984) 2336-2352. https://doi.org/10.1007/BF01058110

3. G. Wightman, D. Fray, The Dynamic Oxidation of Aluminum, Metallurgical Transactions B. (1983) 625-631. https://doi.org/10.1007/BF02653948

4. I. Haginoya, T. Fukusako, Function of CO_2 Gas on the suppression of oxidation of molten Al-Mg alloy, Journal Japan Insitute of Light Metals 31 (1981) 733-741

5. S. Bao, Filtration of Aluminum-Experiments, Wetting and Modelling Trondhiem Norway: NTNU; 2011. PhD Thesis

6. D. Gaskell, Introduction to the Thermodynamics of Materials. 4th ed. New York: Taylor and Francis; 2003.

7. N. Smith, B. Gleeson, A. Kvithyld, G. Tranell, Effects of 2 ppm Beryllium on the Oxidation of a 5XXX Aluminum Alloy at Temperatures Between 500 and 750 °C, In Light Metal 2017 (2017), San Diego. https://doi.org/10.1007/978-3-319-51541-0_175

8. C. Cochran, D. Belitskus, D. Kinosz, Oxidation of Aluminum-Magnesium Melts in Air, Oxygen, Flue Gas and Carbon Dioxide, Metalurgical Transactions B. 8B (1977) 323-332. https://doi.org/10.1007/BF02657663

9. J. Tenório, D. Espinosa, High-Temperature Oxidation of Al-Mg Alloys, Oxidation of Metals 3 (2004) 361-373. https://doi.org/10.1023/A:1004549522648

10. K. Surla, F. Valdiveso, M. Pijolat, Soustelle M, Prin M. Kinetic study of the oxidation by oxygen of liquid Al-Mg 5% ALLOYS, Solid State Ionics 143 (2001) 355-365. https://doi.org/10.1016/S0167-2738(01)00861-X

11. E. Mason, Graham's Laws of Diffusion and Effusion, Journal of Chemical Education 44 (1967) 740-744.

12. P.E. Blochl, Projector Augmented-Wave Method. Phys. Rev. B. 50 (1994) 17953-17979. https://doi.org/10.1103/PhysRevB.50.17953

13. J.P. Perdew, K. Burke, M. Ernzerhof, Generalized Gradiant Approximation Made Simple, Phys. Rev. Lett. 77 (1996) 3865-3868. https://doi.org/10.1103/PhysRevLett.77.3865

14. G. Kresse, D. Joubert, From ultrasoft pseudopotentials to the projector augmented-wave method, Phys. Rev. B. 59 (1999) 1758. https://doi.org/10.1103/PhysRevB.59.1758

15. H. Onishi, C. Egawa, T. Aruga, Y. Iwasawa, Adsorption of Na atoms and oxygen-containing molecules on MgO(100) and (111) surfaces, Surface Science 191 (1987) 497-491. https://doi.org/10.1016/S0039-6028(87)81192-5

16. T. Barr, S. Sea, Nature of the use of adventitious carbon as a binding energy standard, J. Vac. Sci. Technol. A. 13(3) (1995) 1239-1246. https://doi.org/10.1116/1.579868

17. J. Behler, B. Delley, S. Lorenz, K. Reuter, M. Scheffler, Dissociation of O2 at Al(111): The Role of Spin Selection Rules, Physical review letters 94 (2005) https://doi.org/10.1103/PhysRevLett.94.036104

18. D.R. Poirier, G.H. Geiger, Transpoort Phenomena in Materials Processing Warrendale : The Minerals, Metals & Materials Society, (1994)

19. R. Linder, G. Parfitt, Diffusion of Radioactive Magnesium in Magnesium Oxide Crystals, The Journal of Chemical Physics 26 (1957) 182-185. https://doi.org/10.1063/1.1743247

20. R.J. Archer, V. La Mer, The Rate of evaporation of water through fatty acid monolayers, The Journal of Physical Chemistry 59 (1959) 200-208.

Paper V

Effects of CO_2 cover gas and yttrium additions on the oxidation of AlMg alloys

Smith N.[1], Gleeson B.[3], Saidi W.[3], Kvithyld A.[2], Tranell G.[1]

[1]NTNU Alfred Getz Vei 2, 7034 Trondheim, Norway
[2]SINTEF P.O.Box 4760 Sluppen, 7465 Trondheim, Norway
[3]University of Pittsburgh 3700 O'Hara Street Pittsburgh PA 15261

Corresponding Author: Nicholas Smith Nicholas.Smith@ntnu.no

Keywords: aluminum magnesium oxidation beryllium CO_2 yttrium

Abstract

AlMg alloys are known to suffer from problematic oxidation that can result in significant dross formation and loss of Mg from the melt. Historically, beryllium has been used to minimize the oxidation as it forms a protective BeO layer at the oxide-metal interface that inhibits further oxidation of the Mg. Alternative protection agents to beryllium are desired due to its strong negative health impacts. The purpose of this paper is to summarize findings in respect to the effectiveness of CO_2 cover gas and yttrium additions as alternatives to beryllium; by examining the rate and product of oxidation using thermogravimetric analysis, electron microscopy and EDS. It was found that additions of as little as 5% CO_2 to air atmosphere can reduce the oxidation of a 5% Mg alloy to nearly the same extent as beryllium additions, while the addition of 100 ppm of yttrium was found to have a limited impact on the oxidation.

Introduction

The addition of select elements to an AlMg alloy in ppm levels is known to have a significant impact on the oxidation characteristics, with beryllium being the most well-known example in literature. The addition of 2 ppm beryllium to a 5000 series alloy was previously found to result in up to a tenfold decrease in the oxidation (1). Further, beryllium additions were found to delay the onset of breakaway oxidation by up to 170 hours (2). The inhibiting effect of beryllium has been attributed to the formation of a BeO layer at the oxide-metal interface. This BeO layer acts as a barrier between the MgO layer and the alloy, limiting the diffusion of magnesium and aluminum metal from the alloy through the oxide layer and thus slowing the oxidation. The use of beryllium brings with it inherent health risks to casthouse operators who breathe or come into contact with beryllium dust (3). The aluminum industry, therefore, desires alternatives to beryllium that provide a similar inhibiting effect, but without the health risks. Two of the options that exist to replace beryllium are reactive cover gases or an alternative alloying element that has a similar effect to beryllium.

The effects of a mixed CO_2/air atmosphere on the oxidation have been previously shown by Cochran et al. (4) and Haginoya et al. (published in Japanese) (5). Cochran proposed that the amount of CO_2 required to protect a specific alloy was a function of the magnesium content. Haginoya showed conclusively that CO_2 additions can effectively delay the onset of breakaway oxidation if added from the start of oxidation. Further, the negative effects of breakaway oxidation can be minimized if CO_2 is added to the atmosphere after an initial period of oxidation in pure air. It was proposed by Haginoya that the adsorption of CO_2 onto

the oxide surface was critical to the inhibiting mechanism. Despite this (single) previous work, a clear understanding of the mechanism behind how CO_2 inhibits the oxidation is not known.

The formation of a protective layer at the oxide-metal interface, as is the case for beryllium, is a viable method to reduce the excessive oxidation. To that end, it has been proposed that additions of yttrium may inhibit the oxidation of AlMg alloys by formation of such a layer. Yttrium is a lantanoid-a strong oxide former that is known to be surface active. Furthermore, it may react to form the Al_3Y intermetallic phase which has a melting point above what is typically seen in aluminum industrial furnaces. An yttrium concentration of 5.5 at% is required to form the Al_3Y phase at 750 °C. The Al_3Y phase is solid at temperatures below 960 °C (6). If sufficient segregation occurs, the formation of this solid phase at the oxide-metal interface, with an associated melt-protective effect, may be possible. Yttrium has previously been shown to suppress the ignition of a magnesium alloy via the formation of Y_2O_3 at cracks that had formed in the MgO layer, thus preventing the burning of the metal at temperatures up to 730 °C (7).

The aim of the current paper is to summarize our findings of the respective effects of CO_2 in the gas atmosphere and yttrium-alloy additions to the melt in terms of suppressing melt oxidation.

Experimental

Two model alloys were used in this work a 5 % magnesium and a 100 ppm yttrium-5 % magnesium alloy. To produce the model alloys, 99.999 % pure aluminum from Puratronic, 99.98 % pure magnesium from Sigma Aldrich and 99.9 % yttrium from Alfa Aesar were used as raw materials. To generate the 100 ppm yttrium-5 % magnesium alloy, first, a master alloy containing 5 % of yttrium in aluminum was made in a tungsten arc melter under an argon atmosphere. The master alloy plus aluminum and magnesium in proportions to give the desired alloy composition, were charged in to an alumina crucible. The alumina crucible was heated to 850 °C under an argon atmosphere and held for 15 minutes to ensure a homogenous alloy.

To quantify the effects of CO_2 and yttrium on the oxidation, a Linseis PT 2400 a thermogravimetric balance (TGA) with a sensitivity of 10 µg was used to measure the mass change over time at a constant temperature. The model alloys were sectioned to 1.25 mm thick slices using a SiC abrasive saw. The slices were then punched to discs measuring 10 mm in diameter. One side of the sample was ground to a 1 µm finish (CO_2) or 22 µm (Y) finish and washed in ethanol. The sample was weighed and placed in the furnace within 30 minutes of final grinding.

Various CO_2 containing environments were tried, with CO_2 percentages ranging from 5-50 % CO_2 in air with both gasses provided by AGA, the effects were measured over a 7 hour time period at 750 °C. The generated oxide layers were characterized in a DualBeam Focused Ion Beam miller (FIB) and Transmission Electron Microscope (TEM). No special sample preparation was required to examine both the top surface and cross-section in the FIB. TEM samples were selected and prepared in the FIB.

For the tests on the yttrium containing alloy, a standard oxidation program was used across all experimental runs, which consisted of heating from room temperature to 750 °C in 35 minutes under a flowing argon atmosphere, followed by holding of the sample for 16 hours at 750 °C under an atmosphere of flowing air (supplied by AGA). Cooling from 750 °C to room temperature took approximately one hour and was done under an argon atmosphere. The furnace was vacuumed and filled with argon prior to the start of heating and a total gas flow rate of 0.05 liter per minute was maintained at all times. Characterization was carried out in the Scanning Electron Microscope (SEM) equipped with Energy–Dispersive X-ray Spectroscopy (EDS) and the FIB. As a reference a 5% magnesium alloy without yttrium was tested to the same procedure to provide a baseline for comparison.

To investigate the morphology of the oxide layer on the yttrium samples from shorter oxidation times, a horizontal alumina tube furnace was employed. The furnace was vacuumed and filled with dry air two times to ensure a similar atmosphere to the TGA experiments. A sample measuring 24 x 14 x 1.5 mm was prepared with the same method used for the TGA experiments. The prepared sample was placed in an alumina boat that was then slid into the preheated furnace at 750 °C and held for 30 or 90 minutes before removal. This allowed the oxide layer to be examined for shorter time periods than were possible in the TGA, due to the longer heating and cooling time of the TGA.

Results

CO_2 atmosphere

TGA curves

In agreement with previous studies (4) (5), the addition of CO_2 to an air atmosphere was found to inhibit the oxidation of an AlMg alloy to a similar extent as beryllium additions as shown in Figure 1 as both CO_2 and beryllium resulted in a low percent mass gain and delay in the onset of breakaway oxidation. Tests in pure air generally broke away after 210-220 minutes from the start of heating, whereas, the samples oxidized in CO_2 did not breakaway after 7 hours at temperature. Varying the CO_2 percentages between 5-50 % did not have a notable impact on the oxidation. The onset of breakaway oxidation was determined by the criterion below, to determine the point where the mass change over 1 minute departed from linear.

$$mass_t - mass_{t-1min} > 0.02$$

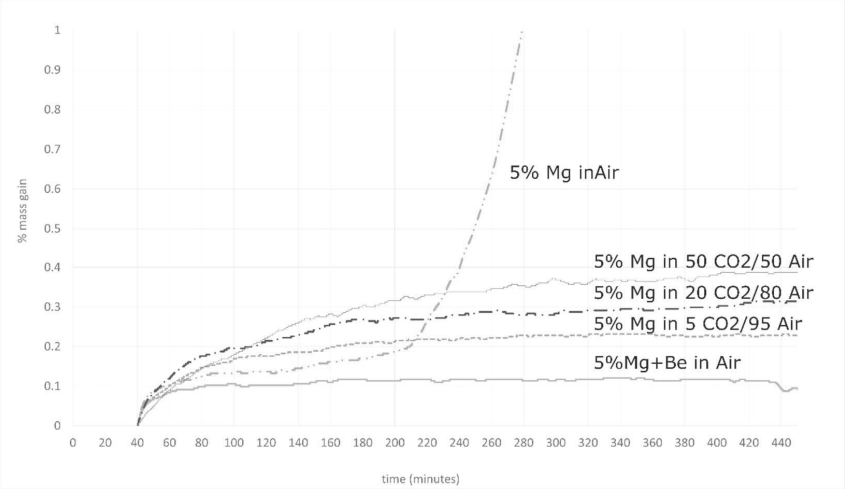

Figure 1 TGA curve showing the effects of CO_2 on the oxidation at 750 °C.

Morphology and composition

Examination of the generated oxide layer in the FIB showed an oxide layer with a uniform thickness of 300-400 nm that was composed of small grains of MgO as confirmed by the diffraction pattern and EDS scan in the TEM. The grains averaged 35 nm across as shown in Figure 2-Figure 3. This oxide layer is similar to what was found on the beryllium containing samples from previous work (1).

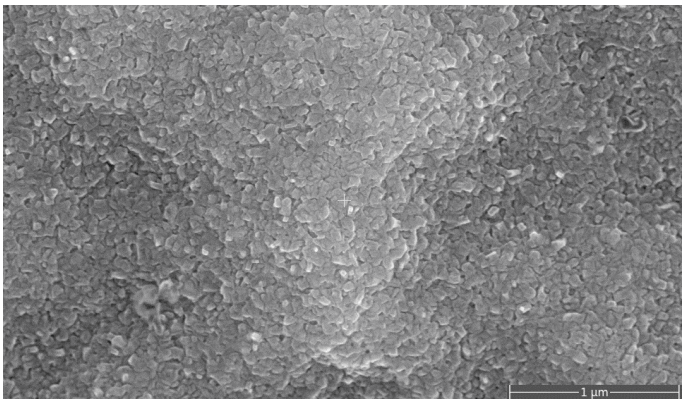

Figure 2 Top surface of sample oxidized in 20CO_2/80 Air for 7 hours at 750 °C showing small grains of MgO.

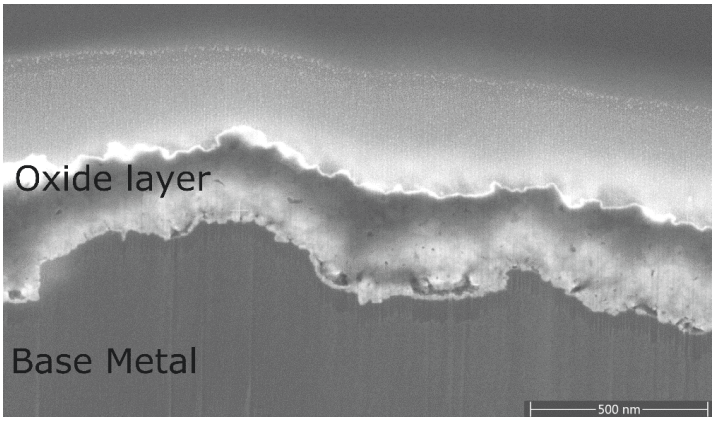

Figure 3 Cross-section of oxide layer on sample oxidized at 750 °C in 20CO_2/80Air for 7 hours.

Yttrium addition

TGA curves

The summarized results for yttrium samples that were oxidized to completion (oxidation of all Mg to $MgAl_2O_4$) are given in Table 1 with the mass gain curves shown in Figure 4. For comparison the results of a baseline containing a 5 % magnesium alloy is also included. The time for breakaway oxidation to begin after the isothermal period had been reached was calculated to determine the effectiveness compared to a 5 % Mg alloy that was free of yttrium. A sample with 100 ppm of beryllium and 5 % magnesium was tested to the same procedure as the yttrium containing samples, and it did not break away after 16 hours of oxidation.

Yttrium additions on average had a limited impact on the oxidation compared to a 5 % Mg alloy, however, significant variation was found amongst the samples as shown in Figure 4 with breakaway times varying from 170 to 328 minutes. The total sample mass gain is determined by the magnesium content as the oxidation will essentially stop once all the magnesium is oxidized to $MgAl_2O_4$. As the total percent mass

gain for Y3 was less than Y1 and Y2 it would indicate the magnesium content in the samples varied. However, this did not seem to affect the breakaway time for this alloy significantly as Y1 had a higher Mg content than Y3, yet it broke away later as can be seen in Table 1.

Table 1 Mass gain and breakaway time for oxidation tests for yttrium samples that were oxidized to completion.

Test	Mass gain (mg)	% Mass gain	Breakaway time (min)
Y1	43.7	15.6	328
Y2	42.2	15.6	186
Y3	31.2	12.9	170
5% Mg reference	30.5	13.6	209

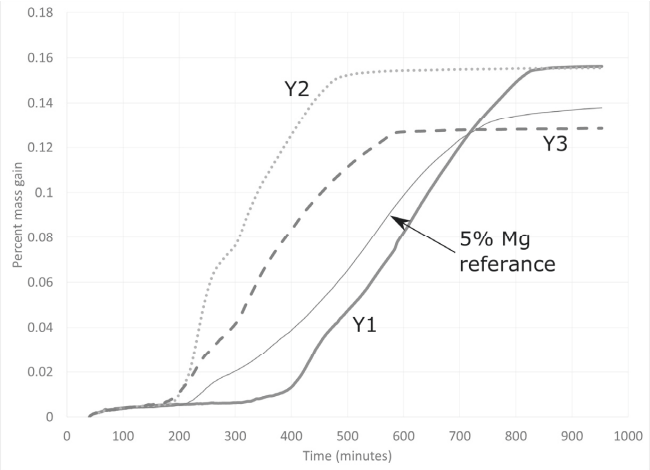

Figure 4 TGA curves for yttrium containing alloy oxidized in air at 750 showing a large variation between breakaway times in comparison to a 5% magnesium reference that did not contain yttrium.

Morphology and composition

After oxidation for 16 hours the samples were found to be significantly distorted from their original disk shape and were covered with a black oxide layer. Cross-sectional images from the SEM are shown in Figure 5-Figure 6, with the dashed rectangle showing the outline of the original sample shape (10 mm diameter x 1.25 mm). EDS scans showed that the samples were covered in a layer of $MgAl_2O_4$ spinel with no traces of yttrium in the oxide layer. The presence of the spinel phase was determined from the Mg:O ratio, where a 1:1 ratio indicated MgO and a 1:4 ratio indicated $MgAl_2O_4$. Towards the center of the sample, un-oxidized aluminum was found. An yttrium containing phase was found in the aluminum metal where the yttrium had segregated out into a second phase where the primary component was aluminum. This phase existed as discrete particles spread throughout the aluminum. The exact composition of the yttrium phase was not determined as the particle size is less than the analysis volume of the EDS. The measured yttrium content was found to be between 3-5 atomic percent. Given that the yttrium content in the second phase was less

than 5 atomic percent it is likely that it was the Al_3Y phase as this is the intermetallic phase with the lowest yttrium content.

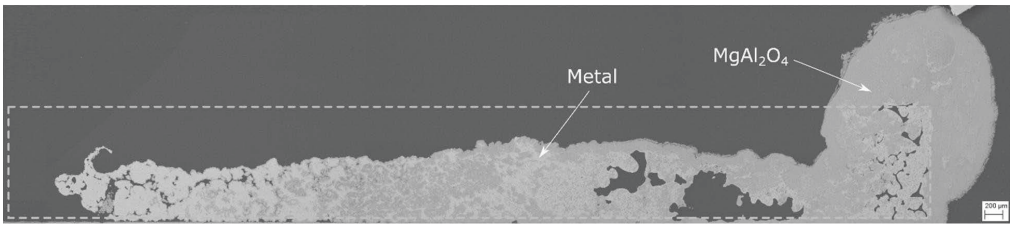

Figure 5 Cross-section of 5 % Mg sample oxidized at 750 °C for 16 hours in air with the dotted line representing the original sample shape.

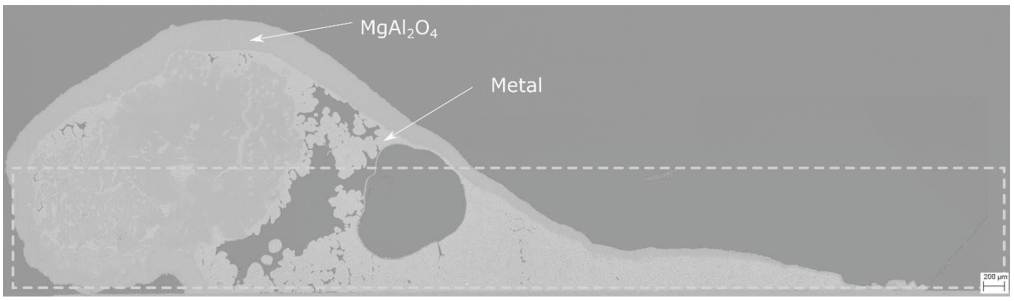

Figure 6 Cross-section of 5 % Mg +Y sample oxidized at 750 °C for 16 hours in air with the dotted line representing the original sample shape.

Investigation of the yttrium containing sample oxidized for thirty minutes in the tube furnace showed that the yttrium had segregated to the oxide layer as discreet particles as shown in Figure 7. The oxide layer was found to be a thin layer of MgO measuring between 130-600 nm thick, but generally was 200-470 nm thick. Backscatter electron images show that the yttrium existed just below the oxide layer. No variation in the magnesium and oxygen EDS signal was seen between the regions containing yttrium and those without, but a variation in the aluminum signal was found, indicating that the yttrium was in the un-oxidized state just below the MgO oxide layer. After 90 minutes of oxidation, the yttrium phase was no longer visible with the backscatter detector due to a thickening of the MgO layer, but was still detectable with EDS.

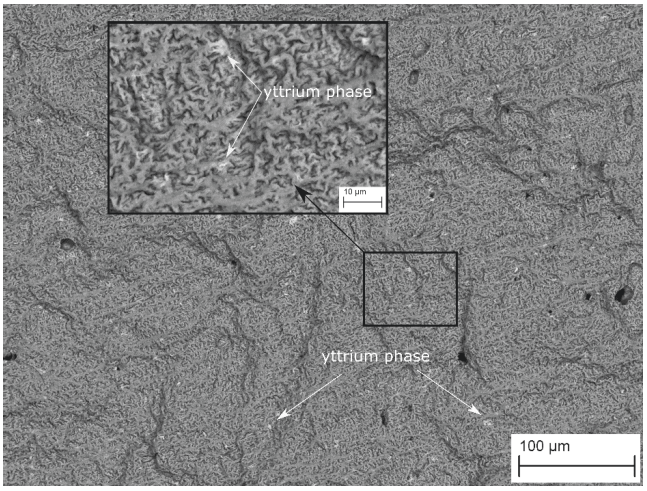

Figure 7 Surface of 100 ppm yttrium sample after 30 minutes of oxidation in air at 750 °C showing MgO layer with yttrium phase underneath.

Discussion

From a thermodynamic standpoint, the addition of limited amounts of CO_2 to an air atmosphere should have a no effect on the oxidation, as magnesium will react preferentially with oxygen. However, it is clear from the TGA results that this is not the case. The addition of CO_2 appeared to have a similar effect on the oxidation as beryllium additions, in that the growth of the granular oxide layer on the surface of the dense oxide layer was notably reduced. The granular oxide layer on top of a dense oxide layer was found after the oxidation of an AlMg alloy in air for time periods before the onset of breakaway oxidation. The addition of beryllium resulted in a loss of this granular layer. The loss of the granular layer was the result of reduced diffusion of magnesium vapor through the oxide layer caused by a BeO layer (1). This would indicate that the addition of CO_2 to the atmosphere modified the oxide layer, inhibiting the diffusion of magnesium out compared to an oxide layer formed in pure air. In an expanded explanation (8), it was concluded that a carbon-containing diffusion barrier is formed on top of/in the MgO layer, limiting the amount of magnesium vapor escaping from the alloy, resulting in a reduced oxidation rate.

The average effect of yttrium additions was limited with respect to the time breakaway oxidation began, with some samples showing an increase and some a decrease in time compared to an yttrium free 5% magnesium alloy. The formation of discrete Al_3Y particles near the oxide layer can be considered promising as it suggests that the segregation and nucleation conditions were sufficient to form an yttrium containing phase even with an initial concentration of only 100 ppm. However, these particles did not grow into a protective layer as was desired. The lack of a clear protective effect such as was seen in previous work on ignition proof magnesium alloys (7) is likely the result of having insufficient yttrium to form a protective layer. The Y:Mg ratio was only 1:500 as opposed to the 1:25 seen in the ignition proof magnesium alloy, therefore, it is possible that higher yttrium concentrations could inhibit oxidation.

Based on the results of the tests with CO_2 and yttrium, further insights can be made into potential replacements for beryllium. Both beryllium and CO_2 reduced the oxidation by minimizing the diffusion of magnesium from the melt and out through the oxide layer. The diffusion of magnesium out through the oxide layer can then be taken as the rate controlling step in the oxidation process. Therefore, reducing the

diffusion of magnesium out from the bulk metal and/or oxygen in from the atmosphere to the reaction site is the ideal method to controlling the oxidation. In terms of a cover gas, CO_2 seems to be ideally suited for this as it readily available, relatively safe and effective. Any alternative cover gas would be required to react with the oxide surface to modify it in a way which prevents the diffusion of magnesium out. As it is not known exactly how the CO_2 modifies the existing layer, it is difficult to conclude which specific properties that would be required of a cover gas.

In terms of alternative alloying additions to beryllium, any alternative addition would be required to have the following properties at the very minimum:

- Strong tendency to segregate to the oxide-metal interface (surface active)
- Be stable in the melt/oxide layer (low vapor pressure)
- Ability to form a solid layer near the oxide metal interface

A strong segregation tendency is required as it will allow smaller quantities of the alloying element to be used. If the addition of a particular alloy element that is not specifically listed in the alloy designation is often restricted to a concentration as low as 0.5 % (500 ppm), this would be the absolute maximum limit any specific alternate would have (3). The high tendency of beryllium to segregate is a prime of example of this as only 2 ppm is required to protect a 5 % magnesium alloy, as after a short time the concentration near the oxide layer will be notably higher in beryllium than the bulk. A tendency to segregate will increase the effective concentration near the oxide layer and increase the likelihood of a diffusion barrier forming. Particular focus should, therefore, be placed on known surface active elements.

Any added element must be stable in the melt. If the element has a high vapor pressure any positive effects may be lost as the concentration will decrease with time and/or result in an increase in porosity of the oxide layer. The negative effects of elements with a high vapor pressure was noted by Thiele as translated by Drouzy and Mascré (9) (10).

Most importantly, the added alloying element must be able to react to form a solid layer at the oxide-metal interface that acts as a barrier to the diffusion of magnesium out and/or oxygen in. This layer could be within the oxide layer or just beneath the oxide layer. Given that the elements that have a higher preference for oxygen than magnesium do not appear to meet the other criteria listed above, it is unlikely that another oxide forming element, like beryllium, will be identified. Thus, the focus should be on finding an alloying element that forms a solid intermetallic phase at the oxide-metal interface.

Yttrium additions would appear to fulfill these requirements with the exception that it forms as discrete particles rather than as a layer at the oxide-metal interface. The formation of a second phase near the surface is promising, if the segregation to the surface can be further promoted the concentration may become sufficient to form a uniform layer as seen in beryllium containing alloys. If all the yttrium in the model alloy formed an Al_3Y layer at the surface the resultant layer would be 80 nm thick. A layer of this thickness could be sufficient to reduce magnesium diffusion through the oxide layer as it is two times thicker than the protective BeO layer found on the 100 ppm beryllium-5% magnesium alloy (1). This would indicate that sufficient amounts of yttrium existed in the melt, but it was not distributed in a manner that allows the desired results to be achieved.

Conclusion

The addition of CO_2 to an air atmosphere was shown to reduce the oxidation of an AlMg alloy to a similar extent as beryllium additions. It was proposed that the addition of CO_2 modified the surface of the oxide

layer in a way that reduced the transport of Mg out of the oxide layer resulting in a decrease in the oxidation and an increase in the time for breakaway oxidation to begin.

Yttrium additions were found to on average have little effect on the oxidation, but for individual experiments the time for breakaway oxidation to begin varied from 170 to 328 minutes compared to 209 minutes for an yttrium free alloy. Oxidation for shorter times showed that after 30 minutes of oxidation yttrium existed as a second un-oxidized phase of discrete Al_3Y particles just below the MgO oxide layer.

Based on the results of this work it was proposed three requirements for any future alternative alloying elements to beryllium must have. These are: tendency to segregate, stable in the melt, forms a solid layer at the oxide-metal interface.

Acknowledgement

This paper has been funded by the SFI Metal Production, (Centre for Research-based Innovation, 237738). The authors gratefully acknowledge the financial support from the Research Council of Norway and the partners of the SFI Metal Production. The computational work is supported by the University of Pittsburgh Center for Research Computing through the resources provided.

References

1. Smith N, Wissam S, Gleeson B, Kvithyld A, Tranell G. (2018) The Mechanism Behind the Oxidation Protection of High Mg Al Alloys with Beryllium. Met. Trans B. doi: 10.1007/s11663-018-1340-6

2. Thiele W (1962) Die Oxydation von Aluminium-und Aluminiumlegierungs-schmelzen. Aluminium 38:780-786.

3. Sigworth G (2014) Best Practices in Aluminum Metalcasting Schaumburg. American Foundary Society, Schaumburg IL.

4. Cochran C, Belitskus D, Kinosz D (1977) Oxidation of Aluminum-Magnesium Melts in Air, Oxygen, Flue Gas and Carbon Dioxide. Met Trans B. 8B:323-332.

5. Haginoya I, Fukusako T (1981) Function of CO2 Gas on the suppression of oxidation of molten Al-Mg alloy. Journal Japan Insitute of Light Metals 31(11):733-741.

6. Gachneidner KA, Calderwood FW (1989) The Al-Y (Aluminum-Yttrium) System. Bulletin of Alloy Phase Diagrams 10(1):44-47.

7. Ravi Kumar NV, Blandin JJ, Suery M, Grosjean E (2003) The Effect of alloying elements on the ignition reistance of magnesium alloys. Scripta materialia 49:225-230.

8. Smith N, Gleeson B, Saidi W, Kvithyld A, Tranell G. (submitted 2018) Mechanisim behind the inhibiting effect of CO2 on the oxidation of AlMg alloys. unpublished.

9. Thiele W (1962) Die Oxydation von Aluminium- und Aluminiumlegierungs-Schmelzen. Aluminum 38:707-715.

10. Drouzy M, C M. (1969) The oxidation of liquid non-ferrous metals in air or oxygen. Metallurgical Reviews 131:25-46.